# Modeling the Impact of Atmospheric Moisture Transport on Global Ice Volume

by

Kerim Hestnes Nisancioglu

Submitted to the Department of Earth, Atmospheric, and Planetary Sciences
in partial fulfillment of the requirements for the degree of

Doctor of Philosophy

at the

MASSACHUSETTS INSTITUTE OF TECHNOLOGY

June 2004



Author . . . . . .
Department of Earth, Atmospheric, and Planetary Sciences
April 30th, 2004

Certified by . . . . . .
Peter H. Stone
Professor of Climate Dynamics
Thesis Supervisor

Accepted by . . . . . .
Maria Zuber
Department Head and E.A. Griswold Professor of Geophysics

# Modeling the Impact of Atmospheric Moisture Transport on Global Ice Volume

by

Kerim Hestnes Nisancioglu

Submitted to the Department of Earth, Atmospheric, and Planetary Sciences
on April 30th, 2004, in partial fulfillment of the
requirements for the degree of
Doctor of Philosophy

## Abstract

Following Milankovitch's original hypothesis most model studies of changes in global ice volume on orbital time scales have focused on the impact of ablation on ice sheet mass balance. In most cases, poleward moisture flux is fixed and accumulation of snow only depends on local temperature. In this study, a simple coupled atmosphere-ice process model is introduced. An improved representation of the atmospheric hydrological cycle is included, and accumulation is related to the meridional flux of moisture by large scale baroclinic eddies. The ice sheets in the Northern Hemisphere respond to both precession and obliquity frequencies when the model is forced with seasonal insolation. Obliquity variations are introduced by the impact of earth's tilt on the meridional temperature gradient and the poleward flux of moisture, whereas precession governs surface melting by regulating summer temperatures. The response of the ice sheet to obliquity and precession is comparable, and significantly smaller than what is observed in the oxygen isotope record of the late Pliocene and early Pleistocene (2.7 - 0.8 Ma BP). This suggests that in order to successfully reproduce the strong 41 Ka periodicity observed in the record, other mechanisms must be involved such as nonlinear self-sustained, or stochastic processes, or alternatively the obliquity dominated signal originates from Antarctica. In Antarctica the seasonal cycle is damped due to the large thermal mass of the southern ocean, and surface melt is insignificant. Both of these factors reduce the influence of precession in regulating ice volume. Instead, the mass balance is dominated by accumulation and calving, thereby enhancing the role of obliquity in controlling ice volume.

Thesis Supervisor: Peter H. Stone
Title: Professor of Climate Dynamics

# Contents

# Acknowledgments

I would like to thank my thesis committee members Ed Boyle, Maureen Raymo, Peter Stone and Eli Tziperman as well as my office mates Baylor Fox-Kemper, Veronique Bugnion, Peter Huybers and Jeff Scott for stimulating discussions throughout the course of my studies at MIT. At the same time, I am grateful to the many people I got to know at MIT and in Cambridge during the past several years. In particular I would like to thank Mary Elliff, the BAD coop, the Green Monkeys, the PAOC lunch gang, and the unofficial MIT telemark club. Without you, my stay at MIT would have been no fun! Last, but not least, I am deeply in debt to Sussie who very patiently and lovingly supported me and kept me going throughout the hardest parts of these past years.

This work was in part funded by the Paleoclimate Program of the National Science Foundation with the award "Collaborative Research: Modeling the Role of Obliquity and Insolation Gradients in Controlling Global Ice Volume".

# Chapter 1

# Introduction

The glacial cycles observed in proxy records of the past $\sim 2.8$ Ma, represent some of the largest and most significant changes in past climate. Explaining these changes would greatly advance the understanding of the climate system and its future response to man-made forcing. However, the physical mechanisms driving the cycles in ice volume are not well understood. After data supporting the early work of *Milankovitch* (1941) was presented by *Hays et al.* (1976), the prevalent theory has been that major fluctuations in global climate, associated with the ice age cycles, are caused by variations in insolation at critical latitudes and seasons. In particular, ice sheet growth and retreat is thought to be sensitive to high northern latitude summer insolation.

Variations in summer insolation at high latitudes are dominated by the precession of the equinoxes at periods of 19 Ka and 23 Ka, combined with a minor contribution due to changes in obliquity of the Earth's axis at a period of 41 Ka. In contrast, changes in global ice volume and deep sea temperatures are dominated by cycles of $41$ Ka and $\sim 100$ Ka, with a smaller contribution by cycles at 19 Ka and 23 Ka. Although *Hays et al.* (1976) found a statistical association between the ice volume record and high latitude summer insolation, a physical explanation for the cause of the glacial cycles is still missing.

Numerous studies have tried to explain the large $\sim 100$ Ka cycles dominating the records of global ice volume during the past $\sim 0.8$ Ma. However, relatively few have investigated the origin

of the smaller amplitude $41$ Ka cycles, which have been found to dominate records older than $\sim 0.8$ Ma (*Pisias and Moore*, 1981; *Ruddiman et al.*, 1986). As for the $\sim 100$ Ka ice volume cycles, the $41$Ka cycles are left unexplained by the currently accepted Milankovitch theory. At the same time, no existing climate model has been able to successfully reproduce the $41$ Ka cycles in ice volume.

The main objective of this study is to investigate the possible physical mechanisms responsible for the 41 Ka cycles observed in the ice volume record. A hypothesis is presented where variations in the insolation gradient between high and low latitudes play an important role in controlling the poleward flux of heat and moisture by the atmosphere. Under favorable orbital configurations, the flux of moisture to high latitudes is enhanced, and the accumulation of snow on the continents increases. Combined with a strong ice-albedo feedback this could lead to growth of ice sheets.

Climate models are valuable tools in the search for physical explanations of the questions posed by the proxy record. However, existing coupled atmosphere-ocean General Circulation Models (GCMs) require too much computing power to simulate climate on orbital time scales ($> 10$ Ka). Instead, it has been common to use Energy Balance Models (EBMs) to study changes in climate in response to variations in insolation. These types of models can be grouped into four categories: 1) annual mean atmospheric models; 2) seasonal atmospheric models with a mixed layer ocean; 3) Northern Hemisphere ice sheet models; and 4) coupled climate-ice sheet models, which in some cases include a representation of the deep ocean.

Examples of studies with the first type of models include the early work by *Budyko* (1969); *Sellers* (1969); *North* (1975), who investigated the sensitivity of climate to changes in annual global mean insolation. However, changes in the Earth's orbital parameters result in a redistribution of insolation with latitude and time of the year, with a negligible impact on annual global mean insolation. Therefore, annual mean models are not adequate when investigating the impact of orbital insolation on climate, as they cannot capture the parts of the insolation variations which are seasonal and translate them into long term climate change.

The second type of models include a representation of the seasonal cycle, and have been used to investigate the orbital theory of Milankovitch (e.g. *Schneider and Thompson* (1979); *Suarez and*

*Held* (1979)). In this case, the seasonal variations in orbital insolation are resolved. However, as for the first type of models, past changes in ice cover are assumed to follow the simulated variations in the extent of perennial snow. This approach assumes that ice cover and the powerful ice-albedo feedback are governed only by temperature, as the extent of snow in these models is fixed to the zero degree isotherm. In reality the growth and decay of land based ice sheets is governed by the balance of accumulation and ablation. Therefore, when investigating changes in ice cover, it is necessary to include an appropriate representation of the dynamics and mass balance of ice sheets in the model.

The third type of models improve upon this by focusing on modeling past changes in mass balance and size of typical Northern Hemisphere ice sheets, such as the Laurentide. This type of studies was initiated by *Weertman* (1964, 1976) and later improved by *Oerlemans* (1980); *Birchfield et al.* (1981); *Hyde and Peltier* (1987); *Clark and Pollard* (1998), who used simple ice sheet models, forced by a prescribed distribution of accumulation minus ablation, to predict ice thickness versus latitude. These models do not calculate the atmospheric energy balance in order to estimate snowfall and surface melt, instead changes to the prescribed distribution of net accumulation follow variations in mean summer insolation.

The fourth type of models include zonal mean seasonal climate models coupled to the simple *Weertman* (1964) type ice sheet model (e.g. *Pollard* (1978, 1982)), as well as intermediate complexity climate models coupled to a dynamic ice sheet (e.g. *Gallee et al.* (1991); *Deblonde et al.* (1992); *Berger et al.* (1999)). These models give a more realistic representation of the climate as compared with the simpler models. However, it should be noted that none of the models described here take into account the influence of changes in meridional atmospheric moisture flux on accumulation of snow on the ice sheet. Even in the more sophisticated climate models it has been common to parameterize accumulation by relating it to local temperature, thereby neglecting any impact by changes in atmospheric moisture transport.

Partly due to the lack of good data on variations in global ice volume older than about half-million years, most model studies have focused on understanding the more recent records domin-

ated by the $\sim 100$ Ka glacial cycles (see reviews in *Imbrie et al.* (1993) and *Paillard* (2001)). All of these models respond with periods close to the precession and obliquity periods of the insolation forcing. However, the amplitude of the response is in most cases significantly smaller than what is observed in the proxy records. At the same time, the dominant $\sim 100$ Ka cycles of the ice volume record, characterized by rapid deglaciations, are only found when including a time lag in the response of the model. Such an internal time lag can be produced by taking into account bedrock depression under the load of the ice (e.g. *Oerlemans* (1980); *Birchfield et al.* (1981); *Hyde and Peltier* (1987)), or by adding a parameterization of ice calving into proglacial lakes or marine incursions at the margin of the ice sheet (*Pollard*, 1982). Alternatively, the $\sim 100$ Ka cycles have been explained as free, self-sustained oscillations (e.g. *Letreut and Ghil* (1983); *Saltzman and Sutera* (1984); *Ghil* (1994); *Gildor and Tziperman* (2001)), which might be phase-locked to oscillations in orbital insolation (e.g. *Saltzman et al.* (1984); *Gildor and Tziperman* (2000)).

One of the very few model studies which has investigated variations in ice volume before the $\sim 0.8$ Ma transition, is the study by *Berger et al.* (1999). In this study, a zonal mean atmospheric model coupled to an ocean mixed layer and continental ice sheets (*Gallee et al.*, 1991) is forced with seasonal insolation for the past $3$ Ma. Under conditions of increased atmospheric $CO_2$, the simulated ice volume responds to the main periods of obliquity and precession in the interval $2-1$ Ma, whereas no significant periodicity is observed in the interval $3-2$ Ma BP. There is no clear dominance of obliquity as observed in the proxy records $\sim 3-0.8$ Ma BP, and during most of the simulation there is a relatively strong eccentricity signal with a period of $400$ Ka, which is not observed in the record. At the same time, during the early part of the simulation ($3.0-1.0$ Ma BP), ice-free conditions dominate, inter-spaced by brief intervals of ice advance paced by these longer period oscillations of eccentricity.

As is the case for all the models discussed above, the possible influence of changes in atmospheric moisture flux has not been taken into account, possibly neglecting an important feedback between changes in insolation and ice volume on orbital time scales. With this concern in mind, a seasonal atmosphere-ice process model is formulated in chapter 3 which is as simple as pos-

sible, while including a dependence of accumulation on atmospheric moisture flux, as well as an improved representation of the ice-albedo feedback. Keeping the model simple, ensures that the physical processes and feedbacks involved can be understood, and that multiple experiments forced with insolation reconstructions covering periods of up to $1$ Ma can be carried out in a reasonable amount of time.

The sensitivity of the model climate to changes in insolation is investigated in chapters 4 and 5. The perturbations applied will be of three different characters: 1) variations in solar constant, which applies a uniform change in insolation at all latitudes and seasons similar to the effect of changing atmospheric $CO_2$ levels; 2) variations in earth's obliquity, which principally changes the relative amount of insolation received at high and low latitudes, and 3) variations in orbital precession, which redistributes the amount of insolation received during each season, without affecting the latitudinal insolation distribution.

In chapter 6, the atmosphere-ice model is used to investigate the physics governing the oscillations in ice volume observed in the proxy record, with emphasis on the glacial cycles of the Late Pliocene and Early Pleistocene ($\sim 3.0 - 0.8$ Ma BP). Finally, a summary of the results is given in chapter 7. Before introducing the model, the following chapter (chapter 2) gives an introduction to the paleoclimate record as well as a discussion of the present understanding of the original orbital theory due to *Milankovitch* (1941).

# Chapter 2

# The Paleoclimate Record

Over the past years a tremendous amount of data on past climate has been collected from deep sea sediment cores, ice cores, and terrestrial data. However, at present, several of the most fundamental questions posed by this data remain unanswered. A few examples are as follows: it is not known what triggered the onset of enhanced glaciations $\sim 2.8 - 2.6$ Ma BP; why the initial oscillations in ice volume were dominated by a period of $41$ Ka; or why larger oscillations in ice volume with a duration of approximately $100$ Ka dominated after $\sim 0.8$ Ma BP.

Following the original work of *Milankovitch* (1941) most scientists would agree that on orbital time scales, variations in ice volume are related to oscillations in high latitude insolation. However, most work in the field has focused on the last $0.8$ Ma of the record. In this chapter, it will be argued that when considering the full ice volume record of the past $3$ Ma, current understanding of the relation between insolation changes and glacial cycles is not adequate. Instead, an alternative hypothesis is tested which relates changes in ice volume to the impact of obliquity on the meridional flux of moisture to high latitudes. Part of the work presented here has been published by *Raymo and Nisancioglu* (2003), and the reader is referred to appendix A for further reading.

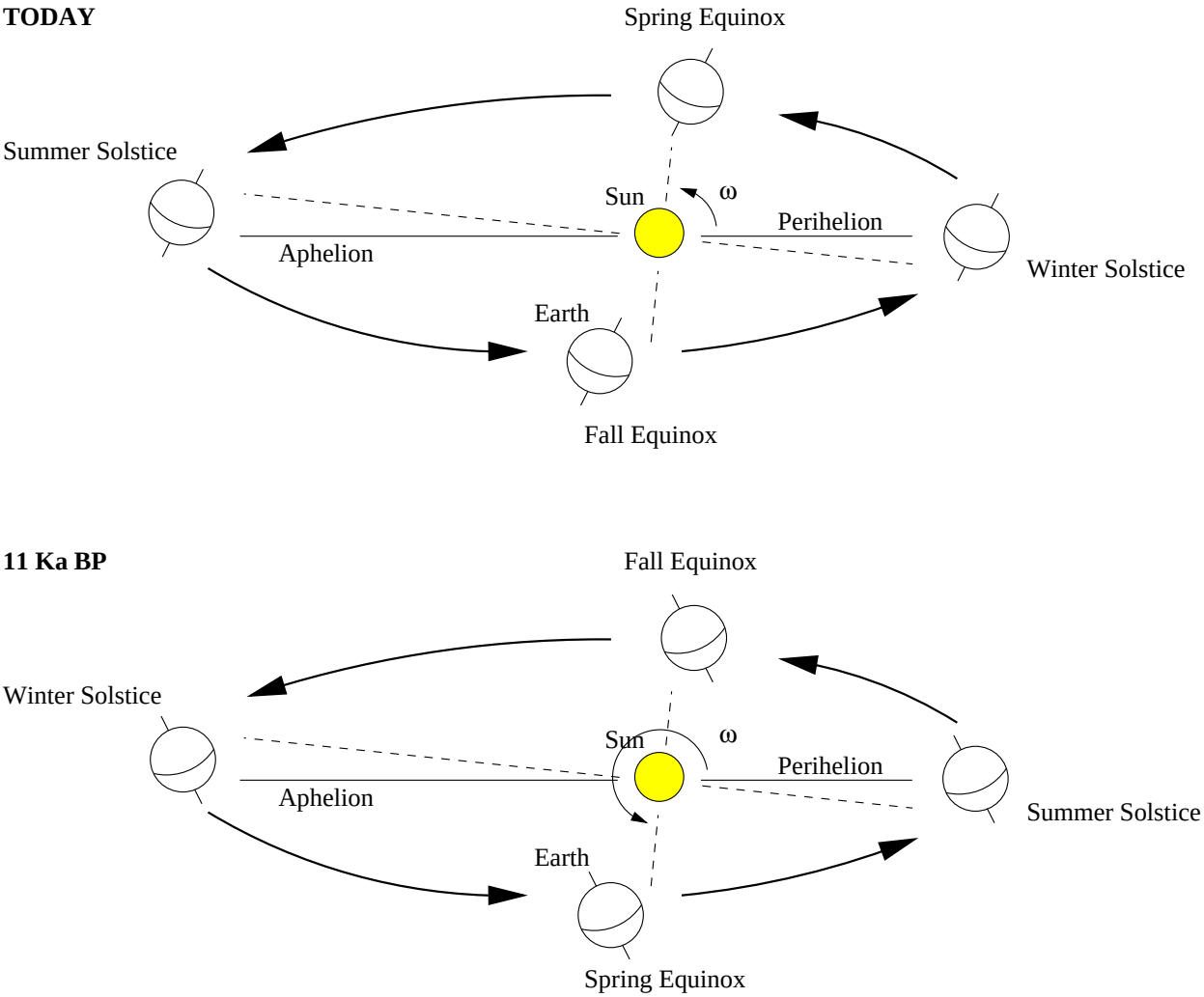


Figure 2-1: Sketch of the Earth's orbit around the sun today (0 Ka BP) and at the last glacial termination (11 Ka BP), showing the positions of the solstices and equinoxes relative to perihelion. The longitude of perihelion ($\omega$) is measured as the angle between the line to the Earth from the Sun at spring equinox and the line to the Earth at perihelion.

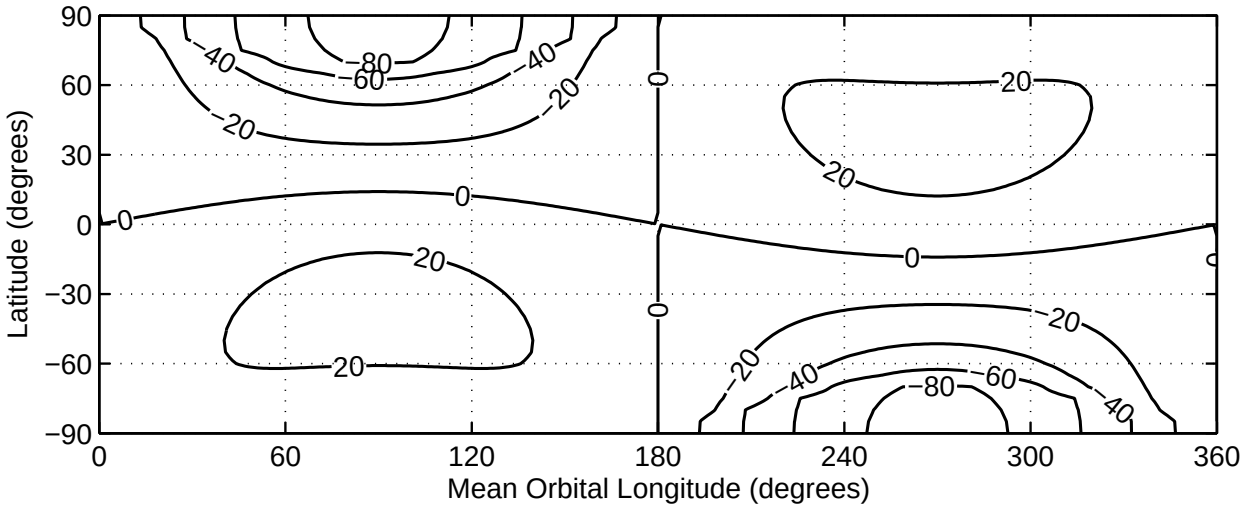


Figure 2-2: Insolation difference in units of $W/m^2$ as a function of latitude and season for a decrease in obliquity from $25°$ to $21°$ in the case of a perfectly circular orbit ($e = 0$). The start of the year is fixed at the spring equinox and the year is divided into $360$ degrees, where $90°$ is summer solstice. A detailed description of the calendar adopted in this study is given in section 3.1.1 on page 37.

## 2.1 Orbital Parameters and Insolation

The Earth's orbit around the sun is an ellipse where the degree to which the orbit departs from a circle is measured by its eccentricity ($e$). The point on the orbit closest to the sun is called the perihelion, and the point most distant from the sun the aphelion (figure 2-1). If the distance from the Earth to the Sun is $r_p$ at perihelion, and $r_a$ at aphelion, then the eccentricity is defined as $e = (r_a - r_p)/(r_a + r_p)$. Variations in the eccentricity of the Earth's orbit follow cycles of 100 Ka and 400 Ka, giving a change in annual mean insolation on the order of $0.2\%$, or less. This change in insolation is believed to be too small to produce any significant effect on climate.

A more significant change in insolation is caused by variations in the seasonal and latitudinal distribution of insolation due to obliquity. Obliquity ($\varepsilon$) is the angle between Earth's axis of rotation and the normal to the Earth's plane around the sun (figure 2-1). This angle is $23.5°$ today, but varies between values of $22.1°$ and $24.5°$ with a period of 41 Ka. A decrease in obliquity decreases the seasonal insolation contrast, with the largest impact at high latitudes. At the same time, annual mean insolation at high latitudes is decreased compared to low latitudes. An example of the effect

of obliquity variations on seasonal insolation is shown in figure 2-2. During times when obliquity is small, high latitude summertime insolation decreases, whereas mid latitude wintertime insolation increases. The magnitude of the change in high latitude summer insolation due to obliquity variations can be as large as $10\%$.

The third and last variable affecting insolation is the longitude of perihelion ($\omega$). This parameter is defined as the angle between the line to the Earth from the sun at spring equinox and the line to the Earth at perihelion (figure 2-1). It determines the direction of Earth's rotational axis relative to the orientation of Earth's orbit around the sun, thereby giving the position of the seasons on the orbit relative to perihelion. Changes in the longitude of perihelion result in the Earth being closest to the sun at different times of the year. Today, the Earth is closest to the sun on the 4th of January, or very near winter solstice in the Northern Hemisphere. All other things being equal, this will result in relatively warm winter and cool summer seasons in the Northern Hemisphere, whereas the opposite is the case in the Southern Hemisphere. At the time of the last deglaciation, 11 Ka BP, the Earth was closest to the sun at summer solstice, resulting in extra warm summers and cool winters in the Northern Hemisphere.

If the Earth's orbit was a circle, the distance to the sun would remain constant at all times of the year and it would not make any difference where on the orbit the seasons were positioned. Therefore, the impact of variations in the longitude of perihelion depends on the eccentricity of the Earth's orbit and is described by the precession parameter ($esin\omega$). The combined effect of eccentricity and longitude of perihelion can give changes in high latitude summer insolation on the order of $15\%$ and varies with periods of 19 Ka, and 23 Ka, but is modulated by the longer period variations of eccentricity. Figure 2-3 shows the variations in obliquity ($\varepsilon$), longitude of perihelion ($\omega$), eccentricity ($e$), and the precession parameter ($esin\omega$) for $1800 - 1200$ Ka BP as computed by *Laskar et al.* (1993). Note that the two main periods of variability of precession are not present in the oscillation of longitude of perihelion ($\omega$), but rather are produced by the splitting of the basic precession period of about $22$ Ka, due to its modulation by eccentricity.

The main features of variations in insolation on orbital time scales are summarized as follows:

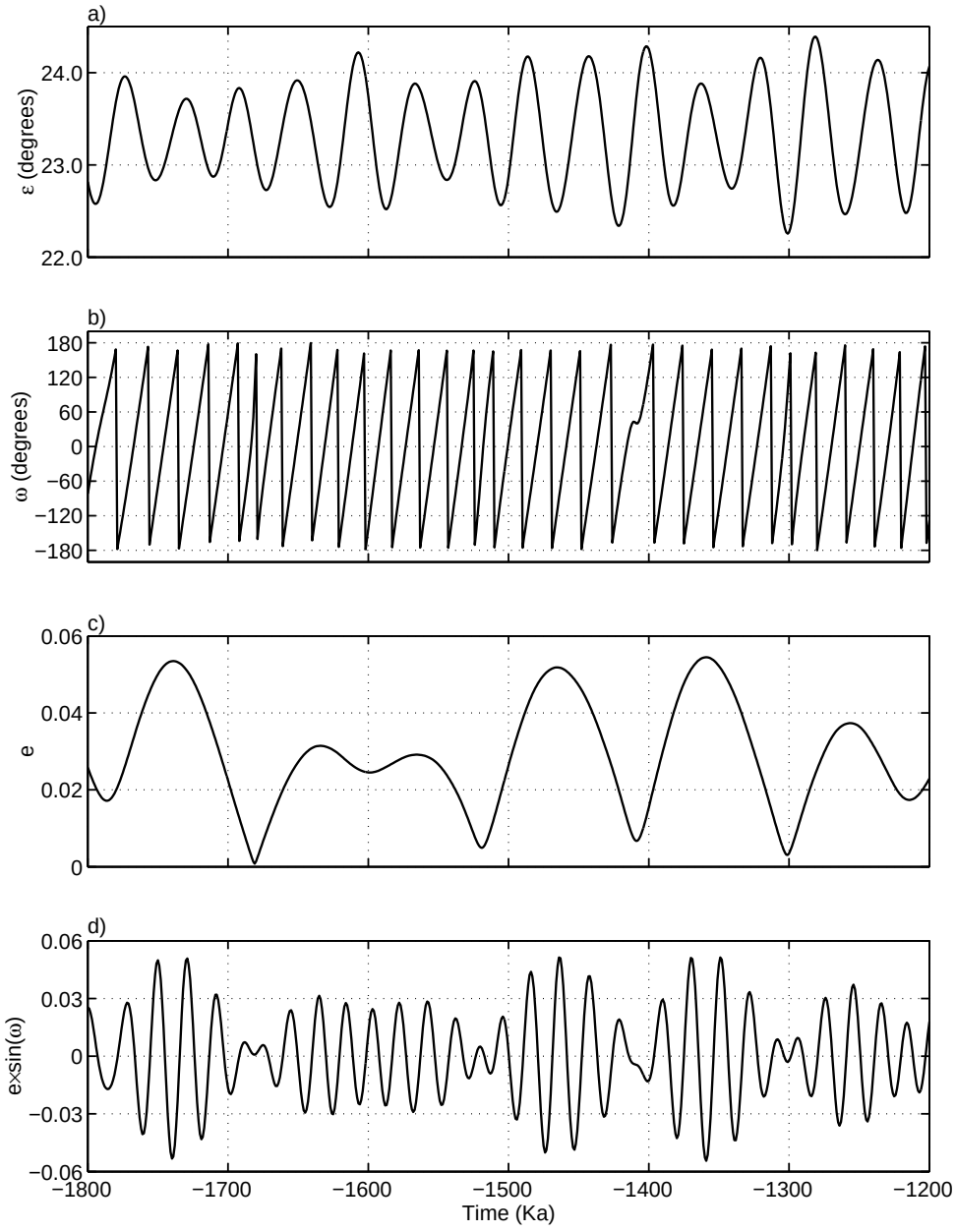


Figure 2-3: Variations in a) obliquity of the Earth's axis ($\varepsilon$), b) longitude of perihelion relative to the spring equinox ($\omega$), c) Earth's orbital eccentricity ($e$), and d) precession parameter ($esin\omega$) for $1800 - 1200$ Ka BP (***Laskar et al.***, 1993).

1. Annual mean insolation averaged over the globe, or over one hemisphere varies only as a result of eccentricity ($e$). The observed eccentricity range ($e < 0.06$), produces a change in insolation of less than $\sim 0.2\%$.

2. Annual mean insolation at a specific latitude is controlled by obliquity ($\varepsilon$) and eccentricity ($e$), and is independent of the longitude of perihelion ($\omega$). The observed range of obliquity ($22.0^\circ - 24.5^\circ$) can produce $\sim 10\%$ variations in insolation at high latitudes.

3. Seasonal mean insolation at a specific latitude varies with obliquity ($\varepsilon$) as well as the precession parameter ($esin\omega$) due to the influence of the latter on the length of the season. The combined effects of these parameters can cause variations in seasonal insolation as large as $\sim 30\%$ at high latitudes.

4. Daily mean insolation at a specific latitude depends on all the orbital parameters ($e, \omega, \varepsilon$).

## 2.2 Ice Volume and Oxygen Isotopes

Some of the longest continuous records of past climate come from deep sea sediment cores. Ocean sediments are laid down over time, and by drilling into the sea floor, layered sediment cores can be extracted containing valuable information about the conditions at the time when the layers where formed. The time resolution of the core depends on the sedimentation rate at the drill site, as well as the degree to which the top layer of sediments have been disturbed by bottom dwelling organisms (bioturbation).

By studying the relative abundance of oxygen isotopes in shells of tiny marine organisms (foraminifera) found in the sediments, it is possible to estimate the amount of water tied up in continental ice sheets and glaciers. This is because water molecules containing the lighter isotope of oxygen ($^{16}O$) are more readily evaporated and transported from the oceans to be deposited as ice on land (*Dansgaard*, 1954, 1964). Therefore, during glacial periods ocean water is enriched with the heavy oxygen isotope ($^{18}O$). Deviations of the oxygen isotope ratio relative to a standard is

defined as

$$\delta^{18}O = \frac{(^{18}O/^{16}O)_{sample} - (^{18}O/^{16}O)_{SMOW}}{(^{18}O/^{16}O)_{SMOW}} \times 10^3$$

where $SMOW$ signifies Standard Mean Ocean Water. The $\delta^{18}O$ value of surrounding sea water is recorded by foraminifera who build their shells from calcium carbonate ($CaCO_3$). However, the fractionation of the oxygen isotopes when forming $CaCO_3$ depends on water temperature (*Urey*, 1947; *Emiliani*, 1955): low water temperatures give high $\delta^{18}O$ values. To further add to the complexity, the $\delta^{18}O$ value of sea water is not uniform throughout the ocean due to the pattern of evaporation and precipitation. This problem can be partly avoided by studying benthic foraminifera living on the sea floor, rather than surface dwelling planktonic foraminifera. At depth, the water is far more homogeneous than on the surface. At the same time, water at the ocean floor is very cold, and would not have been much colder during glacial periods, thereby reducing the contribution of temperature variations to the $\delta^{18}O$ value.

The first continuous long benthic $\delta^{18}O$ ice volume records were extracted by *Shackleton and Opdyke* (1973) and *Hays et al.* (1976). These cores extend back to the Brunhes-Matuyama magnetic reversal event ($780$ Ka BP) making it possible to construct a time scale by assuming linear accumulation rates (e.g. *Shackleton and Opdyke*, 1973). Analysis of the data show cycles in ice volume with periods of about $20$ Ka, $40$ Ka and $100$ Ka; in agreement with the predictions of Milankovitch. Further studies with cores extending past the Brunhes-Matuyama reversal by *Pisias and Moore* (1981) and *Ruddiman et al.* (1986) show that the late Pliocene ($3.6 - 1.8$ Ma BP) and early Pleistocene records ($1.8 - 0.8$ Ma BP) are dominated by smaller amplitude cycles with a period of $41$Ka, rather than the large $100$ Ka cycles of the late Pleistocene.

Many records generated since this time have confirmed these early observations, namely:

1. the main period of ice volume change from 3.0 to 0.8 Ma, is $41$ Ka, which is the dominant period of orbital obliquity.

2. after $\sim 0.8$ Ma, ice sheets vary predominantly with a period of $100$ Ka and the amplitude of oscillations in $\delta^{18}O$ increases, implying growth of larger ice sheets.

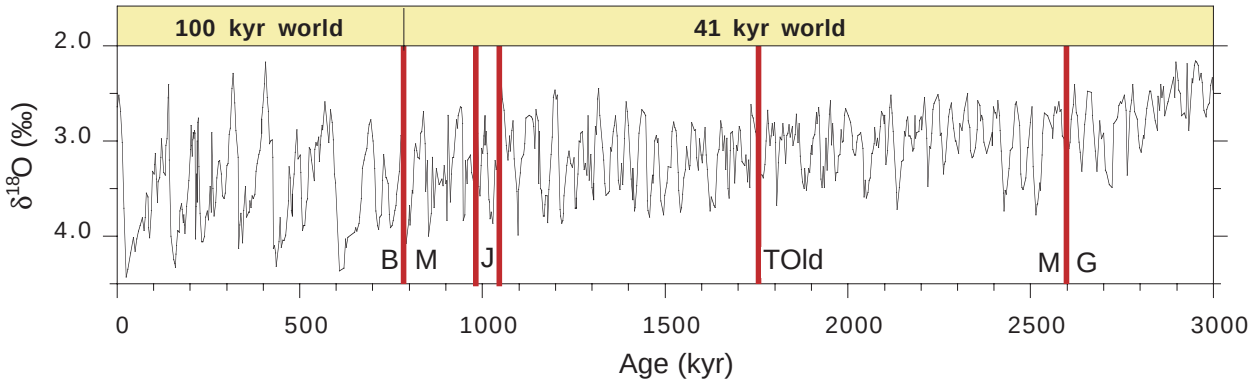


Figure 2-4: Benthic $\delta^{18}O$ record from DSDP site 607 (*Ruddiman et al.*, 1989; *Raymo et al.*, 1989) in the North Atlantic (solid line) plotted to a paleomagnetic time scale. The magnetic field reversals are marked, as well as the transition from a dominant 41 Ka to a 100 Ka periodicity in ice volume. B (Brunhes), M (Matuyama), J (Jaramillo), TOld (top of Olduvai), and G (Gauss).

| Depth (mcd) | Age (Ka) | Magnetic Event |
|---|---|---|
| 0.0 | 0 | top of core |
| 31.84 | 780 | Brunhes/Matuyama |
| 40.345 | 984 | Jaramillo top |
| 43.965 | 1049 | Jaramillo bottom |
| 73.655 | 1757 | Olduvai top |
| 111.58 | 2600 | Matuyama/Gauss |
| 129.50 | 3054 | Kaena top |

Table 2.1: Age control points used for paleomagnetic time scale at DSDP site 607.

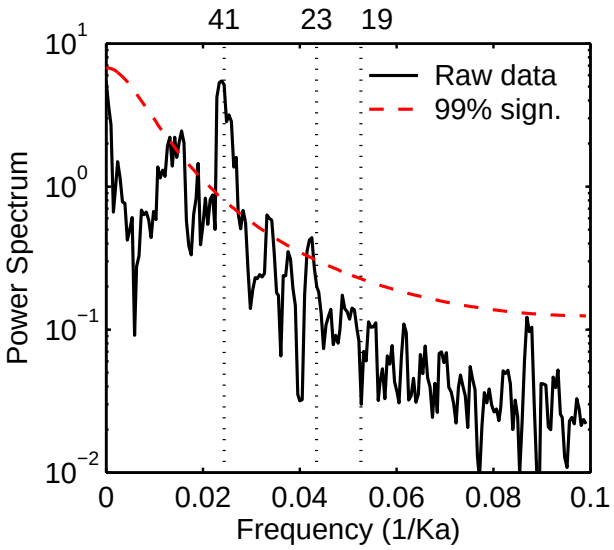


Figure 2-5: Power spectrum of benthic $\delta^{18}O$ from site 607 for the time period $2.75 - 0.8$ Ma BP using the same paleomagnetic time scale as in figure 2-4. The spectrum was calculated using the Multi Taper Method (MTM) (*Thomson*, 1982; *Percival and Walden*, 1993; *Ghil et al.*, 2002). The red dashed line represents the 99% significance level of the data relative to estimated background noise.

The benthic $\delta^{18}O$ record from DSDP 607 illustrates both these points (figure 2-4). Note that the isotope record is plotted with a paleomagnetic time scale (table 2.1) determined by the depth of magnetic field reversals recorded by ferromagnetic grains in the sediment core (*Clement and Kent*, 1987). Constant sedimentation rates are assumed between these magnetic reversal events which are dated by interpolating sea floor magnetic anomalies between fixed calibration points (*Cande and Kent*, 1992, 1995). The two calibration points used (B/M and M/G) are independently derived by both radiometric and astronomic tuning techniques *(Berggren et al., 1995).*

Using this simple time scale, which is not biased by orbital tuning, one can clearly observe the 41 Ka periodicity of the late Pliocene and Early Pleistocene ($3.0 - 0.8$ Ma). The obliquity periodicity is confirmed by plotting the power spectrum of the record (figure 2-5). Note the near complete lack of variance at the 19 Ka and 23 Ka precession, and 100 Ka eccentricity periods. The gradual increase in the strength of the $100$ Ka cycle can be seen when filtering the $\delta^{18}O$ record at the main orbital frequencies (figure 2-6). In this case the tuned time scale of *Shackleton et al.* (1990) is used. Note that the variance at the $41$ Ka period remains relatively unchanged, whereas

the influence of the precession periods increases toward the younger part of the record.

Because site 607 is located in the subpolar North Atlantic ($41°N$, $23°W$), it also contains a record of ice-rafted detritus (IRD) delivered to the open ocean over the Plio-Pleistocene (figure 2-7). Over the entire length of the record, the input of IRD co-varies with the $\delta^{18}O$ record (*Raymo et al.*, 1989; *Ruddiman et al.*, 1989). The sediment core data thus proves that the variability observed in benthic $\delta^{18}O$ must derive in part from the growth and decay of ice sheets bounding the North Atlantic.

## 2.3 Milankovitch Theory

Based mainly on climate proxy records covering the last 0.5 Ma a general scientific consensus has emerged that variations in summer insolation at high northern latitudes are the dominant influence on climate over tens of thousands of years. This theory is associated with *Milankovitch* (1936, 1941) and *Köppen and Wegener* (1924), who based their work on earlier studies by *Croll* (1875) and others. The basic idea is that at times of reduced summer insolation, snow and ice can persist at high latitudes through the summer melt season. At the same time, the cool summer seasons are proposed to be accompanied by mild winter seasons which could lead to enhanced winter accumulation of snow. When combined, reduced melting and a slight increase in accumulation, enhanced by a positive snow albedo feedback, could eventually lead to full glacial conditions. In relation to the orbital parameters, a minimum in summer insolation at high latitudes is achieved when obliquity is small, eccentricity is large, and northern summer solstice occurs when the earth is farthest from the sun (aphelion).

### 2.3.1 Daily Insolation

In the past, countless research papers have plotted, or even tuned, climate records to June or July $65°N$ insolation, following on Milankovitch's original idea. Using many of these records, *Imbrie et al.* (1992) shows that climate variance at precession and obliquity frequencies appears to be

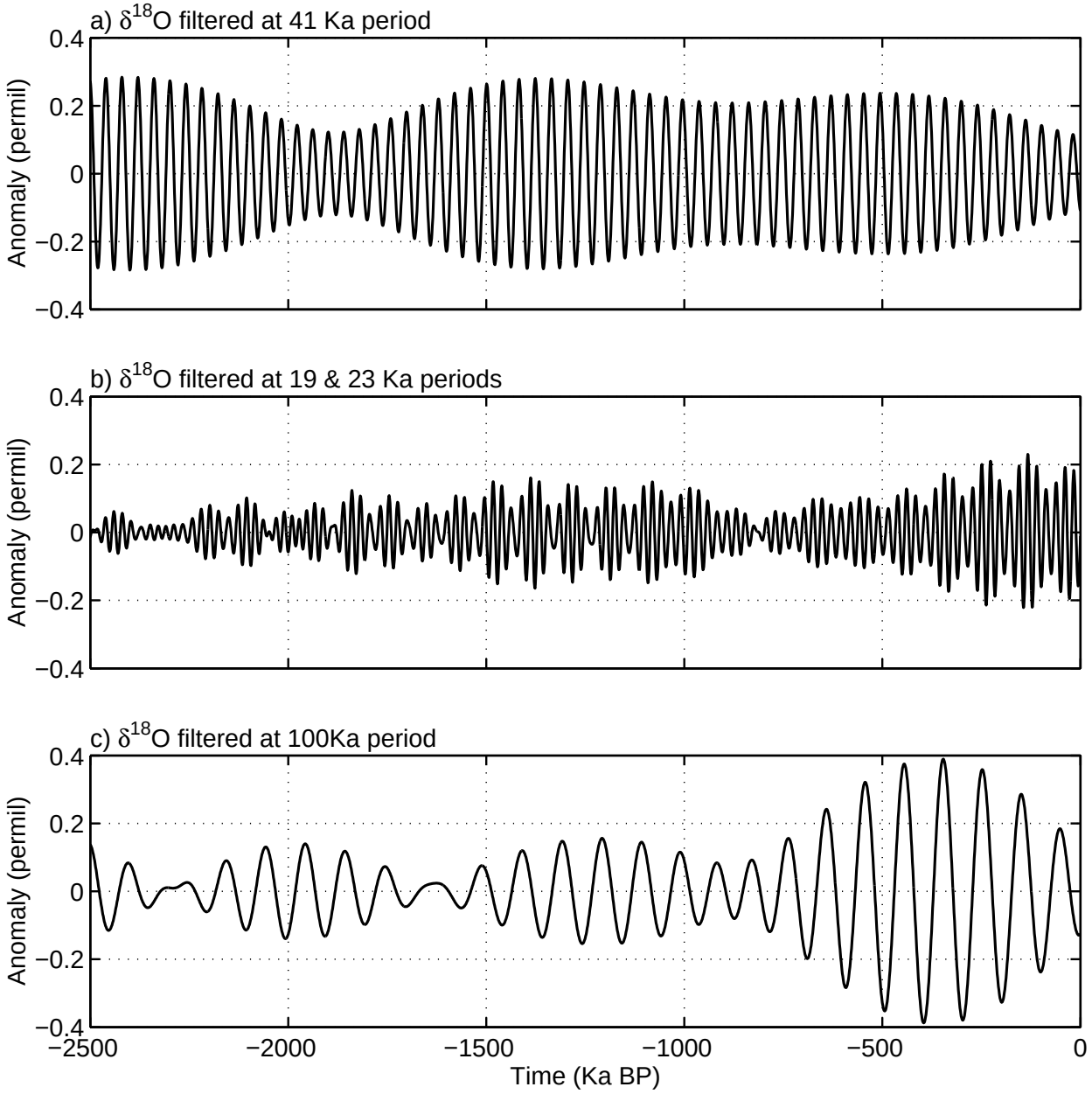


Figure 2-6: Benthic $\delta^{18}O$ record from site DSDP 607 filtered at the main orbital periods a) 41 Ka, b) 19 & 23 Ka, and c) 100 Ka. The data is plotted using the tuned time scale of *Shackleton et al.* (1990).

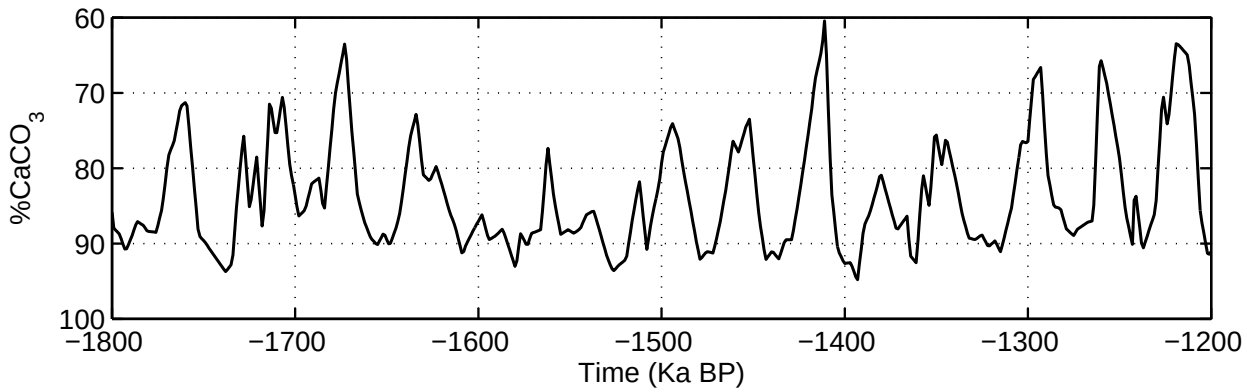


Figure 2-7: $\%CaCO_3$ at site 607 plotted to the same time scale as the $\delta^{18}O$ data in figure 2-4 (*Raymo et al.*, 1989; *Ruddiman et al.*, 1989). Decreases in $\%CaCO_3$ are caused by increases in lithic fragments (ice rafted detritus) within the sediment.

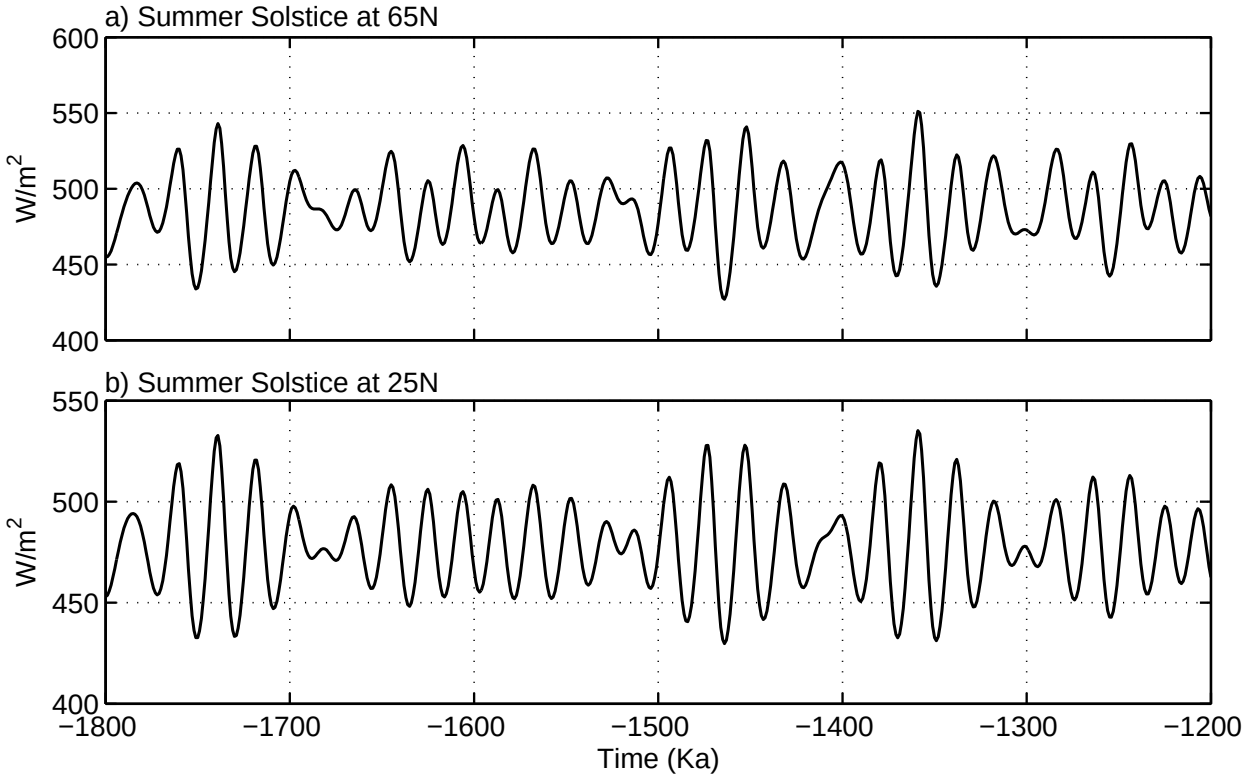


Figure 2-8: Summer solstice insolation ($\omega = 90°$) from 1.8 to 1.2 Ma BP at a) $65°N$, and b) $25°N$ (*Laskar et al.*, 1993). Today summer solstice occurs on June $21^{st}$.

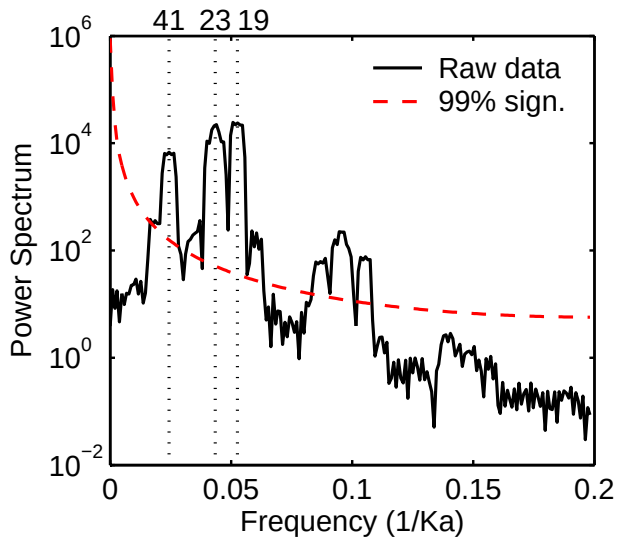


Figure 2-9: Power spectrum of summer solstice insolation at $65°N$ covering the time period from 1.8 to 1.2 Ma BP. The spectrum was calculated using the Multi Taper Method (MTM) (*Thomson*, 1982; *Percival and Walden*, 1993; *Ghil et al.*, 2002). The red dashed line represents the 99% significance level of the data relative to estimated background noise. Vertical dotted lines mark the main periods of obliquity ($41$ Ka), and precession ($19$ Ka, $23$ Ka).

linearly forced by and is coherent with northern summer insolation. Only the 100 Ka cycle is left unexplained by this model and is typically ascribed to non-linear variability arising internally within the climate system.

In the late Pliocene and early Pleistocene, no significant variance at the 100 Ka period is observed in benthic $\delta^{18}O$ or IRD records (figures 2-4 and 2-7). Therefore, it may be expected that global ice volume should vary linearly and coherently with northern high latitude summer insolation, as implied by the standard Milankovitch model. A comparison of the $\delta^{18}O$ ice volume record with the standard insolation record (figures 2-8 & 2-9) shows that although the ice volume proxies have a strong 41 Ka periodicity, summer insolation is dominated by the 19 Ka and 23 Ka periods of precession. As insolation time series at a given time of the year (e.g. June or July) are in phase across all latitudes of the same hemisphere (*Berger et al.*, 1993) the proxy records could be compared equally well with insolation from other latitudes than the typical choice of $65°N$.

Any direct response of climate at high latitudes to summer insolation would require a strong presence of precession in the geologic record. However, this frequency is barely discernible in

the late Pliocene and early Pleistocene ice volume record. It is therefore questionable whether summer insolation at high northern latitudes exerts a dominant influence on climate over most of the Northern Hemisphere ice ages.

### 2.3.2 Seasonal Insolation

An alternative to June or July insolation as the driver of high latitude climate, is seasonal, or annual mean insolation. It turns out that the influence of obliquity increases when averaging over parts of the annual cycle; e.g. for the case of annual mean insolation the effects of precession cancel, leaving only variations due to obliquity. The astronomical summer season, or summer half year, is defined as the section of the Earth's orbit between spring and fall equinox ($0^\circ < \lambda < 180^\circ$, see figure 2-1). Similarly the astronomical winter season is defined as $180^\circ < \lambda < 360^\circ$, where $\lambda$ is the position of the Earth in its orbit relative to spring equinox. Note that the summer season includes spring, and winter season includes fall.

As was observed by *Milankovitch* (1936, p. A40), the total insolation received during the astronomical seasons is independent of precession and varies at all latitudes with obliquity. There is also a phase reversal of the response at about $44^\circ N$ for annual insolation and $11^\circ N$ for seasonal insolation. The influence of precession is only included when taking into account the duration of the seasons. Variations in the duration of the seasons can amount to as much as 33 days (*Milankovitch*, 1936; *Berger*, 1978a). Therefore, when calculating the time mean insolation for the astronomical seasons, the result depends on both obliquity and precession (figure 2-10).

Because the relative duration of the astronomical seasons changes with time, *Milankovitch* (1923, 1941) argued for using a different measure of seasonal insolation. Instead of using the astronomical half years he imposed two restrictions when determining seasonal insolation: 1) the year should be divided into two time periods of equal duration, and 2) each day of the summer season should receive more insolation than any day of the winter season. The seasons following these requirements were defined as the caloric summer and caloric winter half years. Although the calculation is slightly more time consuming, the half years are of equal duration and the year to

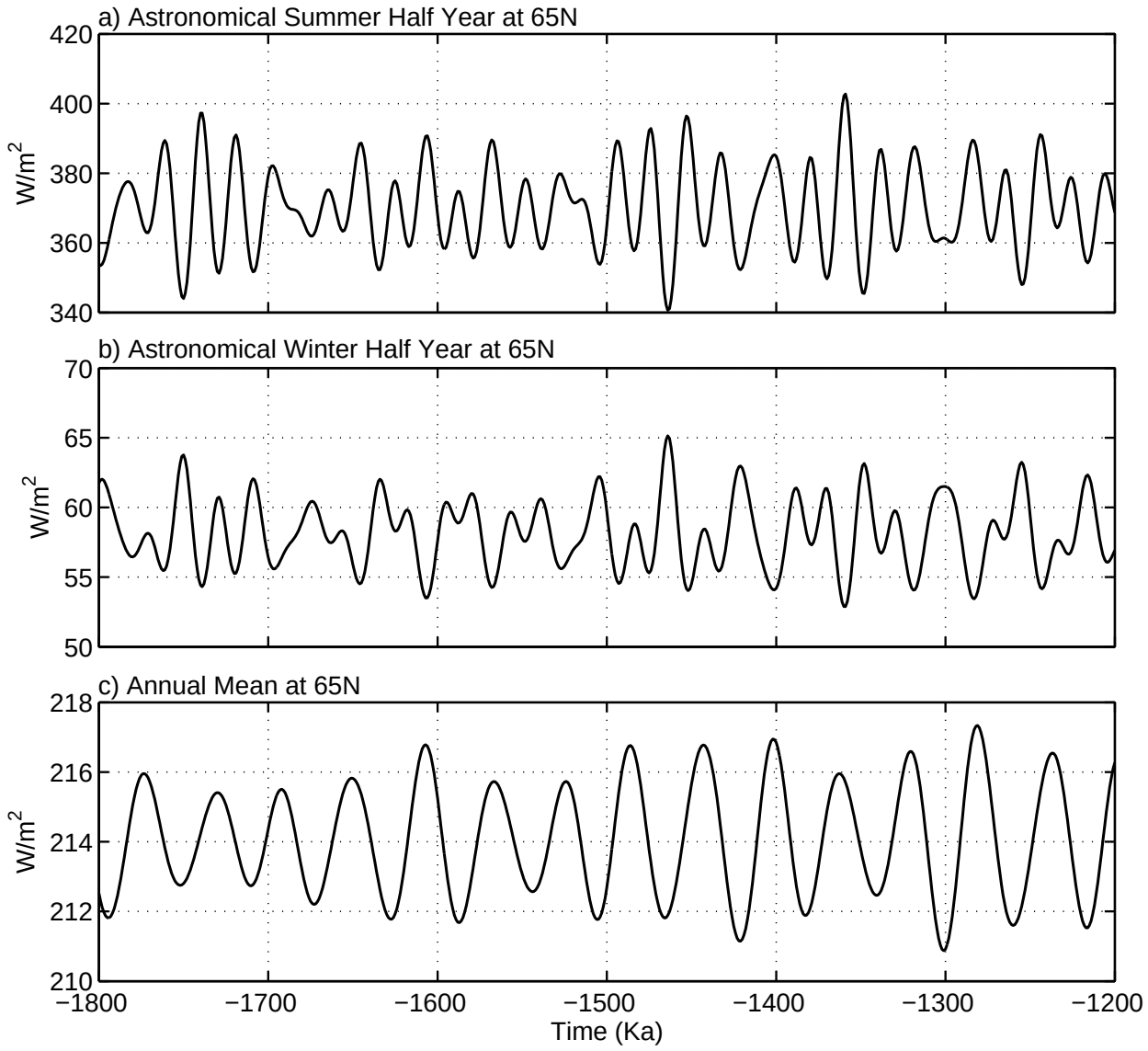


Figure 2-10: a) Astronomical summer half year ($0° < \lambda < 180°$), b) winter half year ($180° < \lambda < 360°$), and c) annual time mean insolation ($J/(m^2 s) = W/m^2$) at $65°N$ from 1.8 to 1200 Ka BP (*Laskar et al.*, 1993).

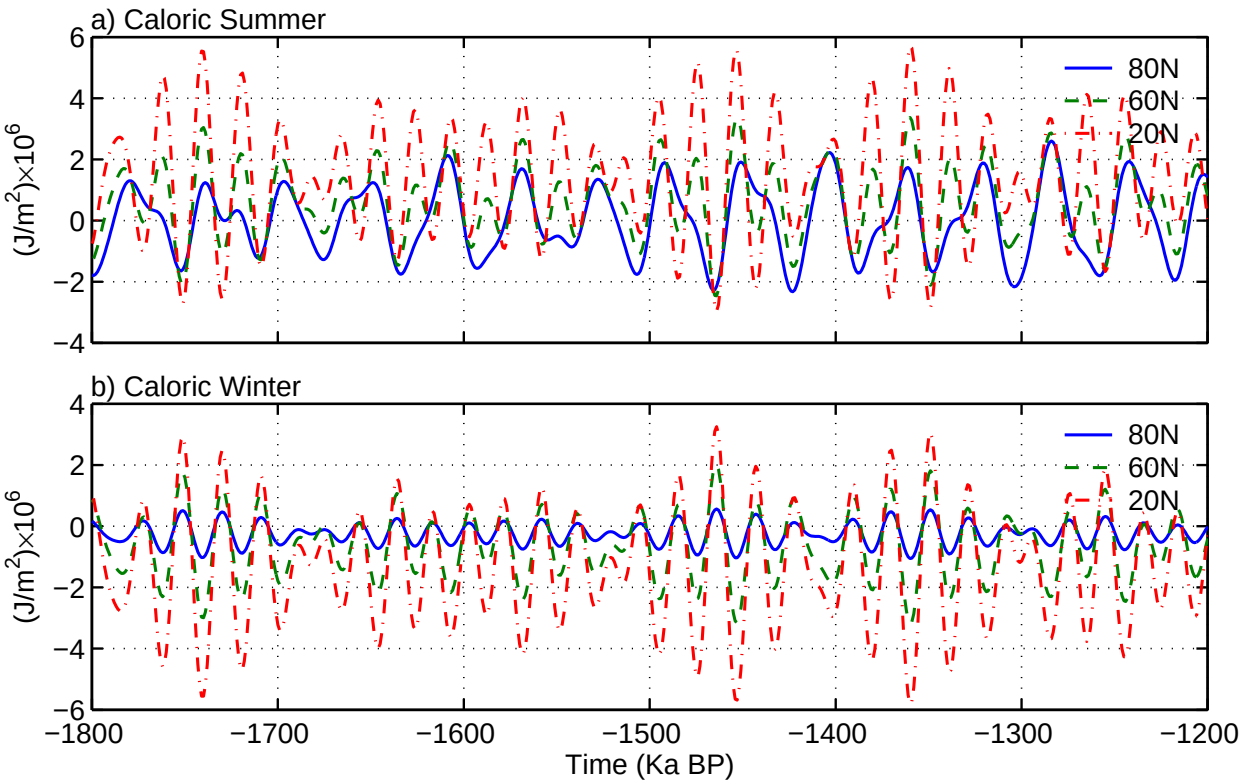


Figure 2-11: Caloric summer and winter half year insolation calculated using the orbital solution due to *Berger* (1978b), see also *Vernekar* (1972) Caloric half years are periods of equal duration where each day of the summer half year receives more insolation than any day of the winter half year (*Milankovitch*, 1923, 1941, p. 286).

year changes in caloric insolation can be compared.

Figure 2-11 shows cumulative caloric summer and winter half year insolation for the period 1.8 to 1.2 Ma BP at three different latitudes. For the caloric summer half year obliquity dominates at high latitudes ($> 65°N$), whereas climatic precession ($esin\omega$) dominates at low latitudes ($< 55°N$), as was pointed out by *Milankovitch* (1936, p. A157). In the mid latitudes ($\sim 55 - 65°N$) the contribution by obliquity and climatic precession are of similar magnitude. The figure only shows the insolation in the Northern Hemisphere. In the Southern Hemisphere, variations in caloric half year insolation due to obliquity are in phase with the Northern Hemisphere and could potentially amplify the global signal, whereas the variations due to climatic precession are out of phase.

Based mainly on geologic data from the last $0.5$ Ma BP, and without knowledge of the $41$ Ka cycles of the early Pliocene and late Pleistocene, *Berger* (1976, 1978a,b) reasoned that climatic

precession plays the leading role in past climates. Therefore, it was assumed that the seasonal contrast and the equinoctial, or monthly insolation are the most important parameters to be considered when modeling glacial-interglacial fluctuations. Following this lead most researchers replaced the caloric half year insolation as a driver of climate by mid-month, or monthly mean insolation for e.g. June or July at $65^{\circ}N$ (figure 2-8).

As was discussed earlier; mid-month, or monthly mean insolation is not a good candidate for explaining early Pliocene and late Pleistocene glacial cycles which were dominated by 41 Ka periods. The original caloric summer half year insolation of Milankovitch has a stronger obliquity signal and therefore would be a better candidate for explaining the 41 Ka cycles. Several components of the climate system, such as the oceans and ice sheets, have a long response time and integrate any external forcing, such as insolation, over time. However, it should be emphasized that choosing a preferred time period, or latitude for insolation when forcing a climate model will bias the results and should be avoided. Eventually, experiments with physical models should make it possible to understand which part of the insolation cycle is most important in driving the 41 Ka cycles in ice volume.

In the next section an alternative hypothesis is presented to explain the 41 Ka glacial cycles which does not involve choosing a preferred time period, or latitude for the insolation forcing.

## 2.4 The 41 Ka Glacial Cycles

While numerous studies have attempted to model the 100 Ka cycles of the late Pleistocene, few have focused on understanding the 41 Ka cycles. A notable exception is Andre Berger and colleagues who used the Louvain-la-Neuve intermediate complexity two dimensional climate model (LLN-2D) to simulate growth and decay of ice sheets over the past 3 Ma (*Berger et al.*, 1999). While the obliquity period is present in the modeled ice volume, the precession periods are also strongly present, and dominate at times. In other words, although the study successfully reproduced the lack of 100 Ka cycles in ice volume during the early part of the record, it was not able to model an ice

sheet that varies only at the obliquity period. This appears to be because the model is very sensitive to northern high latitude summer insolation, and variations in precession.

It is important to note that the majority of intermediate complexity climate models used for paleoclimate experiments, such as the LLN model, do not include an adequate representation of the hydrological cycle. Instead it is common to perturb a modern observed precipitation field according to changes in temperature. As a result; changes in atmospheric moisture flux have no direct impact on high latitude precipitation and the accumulation of ice sheets. In the present study it is hypothesized that atmospheric moisture flux is important in controlling growth and decay of ice sheets through its influence on accumulation, and will be explicitly included in the model configuration.

There have been very few alternative theories to explain the 41 Ka cycles in ice volume. *Kukla* (1968, in a reply to *Emiliani*, 1968) proposed that northern latitude winter insolation may drive late Pliocene/early Pleistocene climate cycles. However, the total insolation received in January is a factor of 20 less than summer insolation at the same latitude. At the same time, latitudes north of the Arctic circle are in darkness for several months in the winter. Therefore, high latitude winter insolation is thought to be of less importance in controlling ice volume.

## 2.5 Insolation Gradients

Given that local daily, and monthly mean summer insolation has too much precession and winter insolation appears too weak to explain the 41 Ka cycles in ice volume, an alternative explanation has to be found. Following *Raymo and Nisancioglu* (2003, appendix A) it is hypothesized that the gradient in insolation between high and low latitudes may play an important role in controlling climate from $\sim 3.0$ to $0.8$ Ma years ago, through its influence on the poleward flux of moisture.

Figure 2-12 shows the gradient in astronomical summer half-year insolation between $25°N$ and $65°N$, defined as the time mean insolation received between the spring ($\lambda = 0°$) and fall ($\lambda = 180°$) equinoxes. When calculating the spectra of the insolation gradient it can be seen that it is dominated

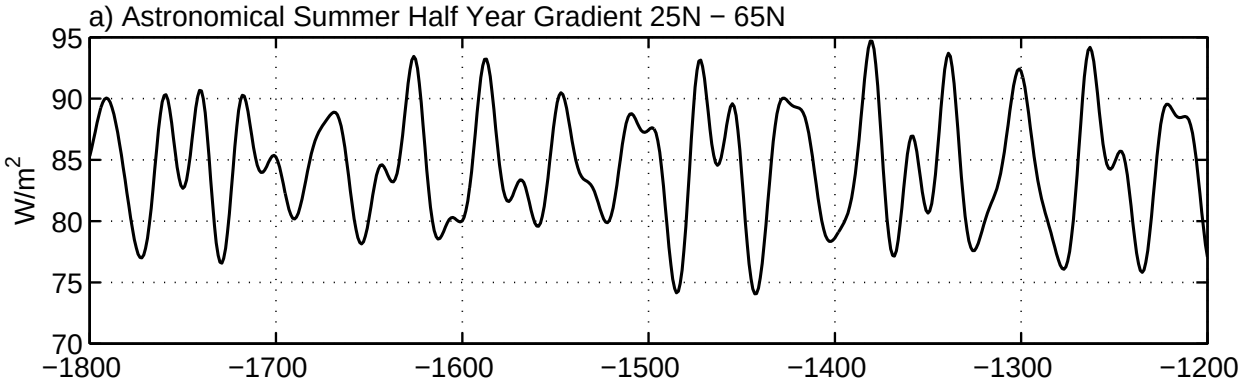


Figure 2-12: Gradient in astronomical summer half year insolation between $25°N$ and $65°N$ (*Laskar et al.*, 1993).

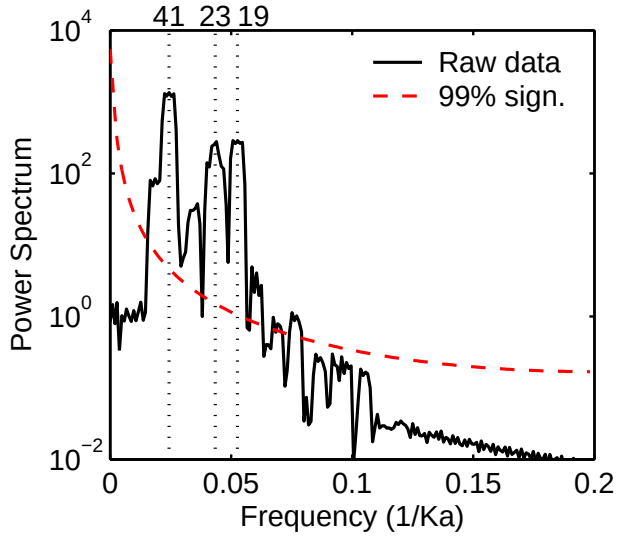


Figure 2-13: Power spectrum of the gradient in astronomical summer half year insolation between $25°N$ and $65°N$. The spectrum was calculated using the Multi Taper Method (MTM) (*Thomson*, 1982; *Percival and Walden*, 1993; *Ghil et al.*, 2002). The red dashed line represents the 99% significance level of the data relative to estimated background noise. Vertical dotted lines mark the main periods of obliquity ($41$ Ka), and precession ($19$ Ka, $23$ Ka).

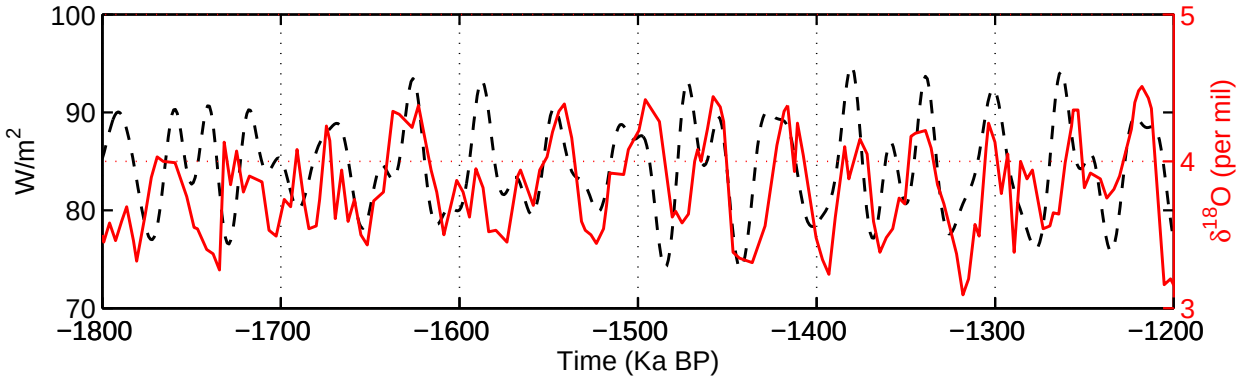


Figure 2-14: Benthic $\delta^{18}O$ record from site 607 (red solid line) plotted together with astronomical summer half year insolation gradient between $25°N$ and $65°N$ (black dashed line). The $\delta^{18}O$ data is plotted to the same paleomagnetic time scale as in figure 2-4.

by obliquity (figure 2-13). It is this insolation gradient that drives the poleward fluxes of heat and moisture in the atmosphere. The correlation between the insolation gradient and $\delta^{18}O$ ice volume record (figure 2-14) suggests that increased gradients promote ice sheet growth. Note that the $\delta^{18}O$ record in figure 2-14 appears to lag the insolation gradient by approximately $3$ Ka, which is slightly shorter than the response to obliquity observed in records from the late Pleistocene (e.g. *Imbrie et al.*, 1992). The true lag of response after forcing would be almost impossible to determine in sediments of this age.

Although no one has invoked the influence of insolation gradients as an explanation for the 41 Ka glacial cycles before *Raymo and Nisancioglu* (2003, appendix A), the notion that insolation gradients could influence climate on orbital time scales has been proposed in the past: *Kutzbach et al.* (1968) argued that the magnitude of orbitally driven changes in insolation gradient is great enough to have a significant impact on climate; and *Young and Bradley* (1984) suggested that hemispheric insolation gradients may have contributed to the growth and decay of continental ice sheets in the past $150$ Ka through their modulating influence on the poleward transport of moisture. They, and previously *Berger* (1976), suggest that times of rapid ice growth and decay correspond to especially pronounced deviations in latitudinal insolation gradients. *Johnson* (1991) similarly invokes a decrease in insolation gradient, rather than a change in direct summer insolation at high latitudes, as the immediate cause of deglaciation at Termination 2 ($127$ Ka BP), offering this mechanism as

the explanation for paleoclimate data which suggest that deglaciation occurred prior to the increase in summer insolation. This mismatch in timing between the deglaciation at Termination 2 and the timing predicted by Milankovitch theory has also been discussed by *Winograd et al.* (1992) and more recently by *Henderson and Slowey* (2000); *Gallup et al.* (2002), although their findings are contested by the early warming observed in the SSTs records of *Herbert et al.* (2001).

It is possible that in the effort to correlate proxy records to high latitude summer insolation, the influence of meridional fluxes of sensible and latent heat, driven by hemispheric temperature gradients, has been underestimated. The mass balance of an ice sheet is not governed by the rate of ablation alone, but by the relative rates of accumulation and ablation. At the same time, the rate of ablation is not only controlled by local incoming solar radiation, but also by local atmospheric temperature which is partially set by the strength of atmospheric and oceanic heat fluxes. The rate of accumulation is controlled by the amount of moisture supplied to the ice sheet and the local temperature. As atmospheric meridional heat and moisture fluxes strongly influence temperature and precipitation at high latitudes, it is expected that they will exert a strong influence on ice sheet mass balance.

It is plausible that long term variations in meridional heat and moisture fluxes, driven by orbital obliquity variations, dominate over the effect of local insolation, driven largely by precession, and thus imprint the 41 Ka signal on the climate record. The powerful ice-albedo feedback would enhance the effect of the insolation gradient on the meridional fluxes. As the atmospheric temperature cools at the onset of a glacial period, snow and ice expands into regions previously covered by surfaces such as forests with relatively low albedo. This increased snow and ice cover raises high latitude surface albedo significantly, reflecting incoming radiation, and causing a further decrease in temperature. In effect, ice-albedo is a very strong positive feedback mechanism, which strengthens the meridional temperature gradient, further enhancing the poleward flux of moisture which feeds the ice sheet.

The link between the insolation gradient and meridional atmospheric moisture flux is illustrated in a coupled atmosphere-ocean GCM study by *Khodri et al.* (2001). In this case, a simulation of

climate at the last glacial inception (115 Ka BP) is compared with a modern control experiment. At glacial inception, obliquity was about $1^\circ$ lower than today, and the model shows warming at low latitudes together with cooling at high latitudes, in agreement with estimates of sea surface temperatures from sediment core data (*Cortijo et al.*, 1999). This increased equator to pole temperature gradient is amplified by the response of the ocean, and causes a significant increase in mean annual poleward atmospheric heat transport, including a $6\%$ increase in latent heat transport. The model does not include a representation of ice sheets. However, the combination of relatively cold high latitudes and enhanced moisture transport could be beneficial for the growth of ice sheets, supporting the hypothesis presented here.

## 2.6 Summary

According to the benthic oxygen isotope record, oscillations in ice volume $3.0 - 0.8$ Ma BP are dominated by a period of $41$ Ka, which is the main period of orbital obliquity. Following this period, the influence of precession increases and there is a switch to a dominance of periods close to $100$ Ka. At the same time, the amplitude of ice volume oscillations increases by as much as 50%. Following the work of *Milankovitch* (1941), the present understanding of glacial cycles assumes that at times of reduced summer insolation, snow and ice can persist at high latitudes through the summer melt season. Combined with mild winter seasons and enhanced accumulation of snow, this could lead to growth of ice on land surfaces in the Northern Hemisphere. Based mainly on data from the last $0.8$ Ma, *Berger* (1976, 1978a,b) concluded that climatic precession plays the leading role in past climates. Following this lead most researchers plot, or even tune, climate records to June or July $65^\circ N$ insolation. However, summer insolation at high latitudes is governed by precession, and is not a good candidate to explain the $41$ Ka period cycles dominating the ice volume record $3.0 - 0.8$ Ma BP. Instead, an alternative proposal is discussed, where the obliquity dominated variations in meridional gradient in insolation influences the poleward flux of moisture and plays an important role in controlling high latitude ice volume (*Raymo and Nisancioglu*, 2003,

appendix A). Comparing an untuned $\delta^{18}O$ record with changes in the insolation gradient, suggests that increased gradients promote ice sheet growth. In the following chapter a simple model is developed in order to test this hypothesis.

# Chapter 3

# Coupled Atmosphere and Ice Process Model

At present, comprehensive earth system models require too much computing power to simulate climate on orbital time scales. However, even if the models were capable of simulations on these time scales, the large number of model parameters involved would significantly increase the number of possible parameter errors. As a result, the more sophisticated models become less determined even though the apparent fit of the model results to data is better (*Hasselmann*, 1981).

The model developed in this chapter is therefore kept as simple as possible to ensure that the physical processes and feedbacks involved can be tested and understood. Instead of a fully fledged coupled GCM, the model consists of an atmospheric box model with parameterized heat and moisture fluxes, coupled to a mixed layer ocean and a plastic ice sheet.

## 3.1 Atmosphere

The model developed here is similar to the atmospheric models of *Nakamura et al.* (1994), *Rivin and Tziperman* (1997), and *Gildor and Tziperman* (2001). It consists of one hemisphere with low, mid, and high latitude boxes, each covering $30^\circ$ of latitude (figure 3-1). Since the thermal adjustment time of the climate system is of order 1 Ka, and the focus is on forcing on orbital time scales ($> 10$ Ka), it is assumed that the climate system is in thermal equilibrium with the forcing. Thus the temperature of each box is calculated by balancing the inputs and outputs of

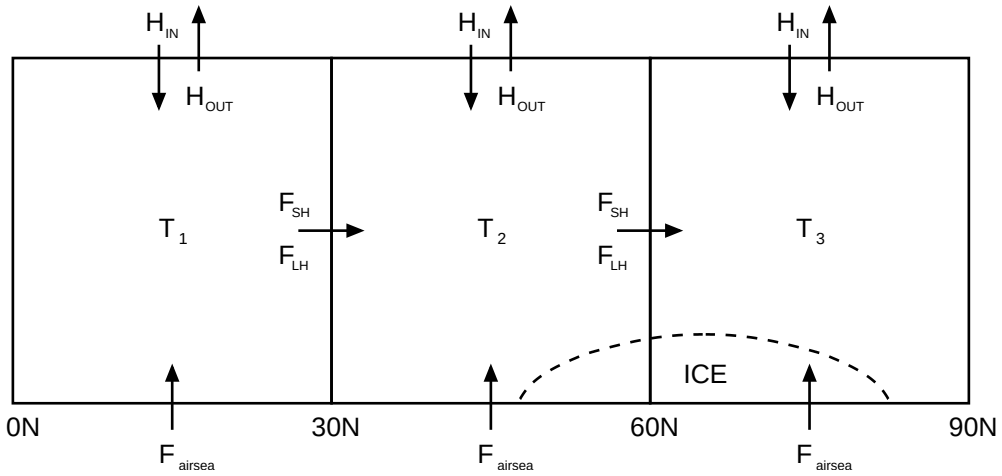


Figure 3-1: Sketch of the atmospheric box model. The ice sheet is coupled to the atmospheric model and extends south from the latitude of the Arctic ocean ($75^{\circ}N$). The balance of incoming and outgoing fluxes of heat ($H_{in}$, $H_{out}$, $F_{SH}$, $F_{LH}$) determines the mean temperature of each box ($T_1$, $T_2$, $T_3$).

energy. The important exchanges of energy are: ($H_{in}$) incoming short wave solar radiation at the top of the atmosphere; ($H_{out}$) outgoing long wave thermal radiation; and ($F_{SH},\ F_{LH}$) meridional atmospheric transports of sensible and latent heat (at the latitudes in question the flux of potential energy is negligible). Integrating over the volume of the individual atmospheric boxes gives the following expression for atmospheric surface temperature ($T_{atm}$):

$$C_{atm}\frac{\partial T_{atm}}{\partial t} = H_{in} - H_{out} + F_{SH} + F_{LH} + F_{airsea} \tag{3.1}$$

where $C_{atm} = \rho_w c_p \Delta z_{atm} A_{atm}$ is the effective heat capacity of each atmospheric box taken to be equivalent to a column of water 2 m deep, $A_{atm}$ is the surface area of the atmospheric box, and $F_{airsea}$ represents the exchange of heat between the atmosphere and a mixed layer ocean (described in section 3.2).

Incoming solar and outgoing thermal radiation in each box is parameterized following *Wang and Stone* (1980)

$$H_{in} \;=\; R_E^2 \int_0^{2\pi}\int_{\phi_1}^{\phi_2} Q(1-\alpha)cos\phi d\phi d\lambda \tag{3.2}$$

| Parameter | Value | Units | Description |
|---|---|---|---|
| $\Delta t_{atm}$ | $10$ | $days$ | Atmospheric time step |
| $\rho_w$ | $1000$ | $kg/m^3$ | Density of water |
| $c_p$ | $4180$ | $J/(kgK)$ | Specific heat of water at constant pressure |
| $\Delta z_{atm}$ | $2$ | $m$ | Equivalent water depth of atmospheric column |
| $R_E$ | $6.37 \times 10^6$ | $m$ | Earth's mean radius |
| $S$ | $1350$ | $W/m^2$ | Solar constant |
| $A_{out}$ | $211$ | $W/m^2$ | Outgoing radiation constant |
| $B_{out}$ | $1.7$ | $W/(m^2K)$ | Outgoing radiation constant |
| $K_{SH}$ | $1.0 \times 10^{26}$ | | Sensible heat flux constant |
| $K_{LH}$ | $6.0 \times 10^{38}$ | | Latent heat flux constant |
| $n$ | $2.0$ | | Eddy heat flux exponent |
| $B_{cc}$ | $5.42 \times 10^3$ | $K$ | Clausius Clayperon parameter |

Table 3.1: Atmospheric model parameters.

$$H_{out} = A_{out} + B_{out} T_{atm} \tag{3.3}$$

where $R_E$ is the radius of the Earth, $Q(\phi)$ is the flux of solar radiation incident at the top of the atmosphere, $\alpha(\phi)$ is the effective albedo of the box, $\phi$ is the latitude, $\lambda$ is the longitude, $T_{atm}$ is the area weighted mean surface temperature of each box in degrees Celsius, and ($A_{out}$, $B_{out}$) are constants. The albedo is calculated by accounting for the relative areas covered by snow, ice and bare land.

### 3.1.1 Insolation

Because the model will be run for time periods of several $100$ Ka, the seasonal insolation is only calculated at $1$ Ka intervals and interpolated to find the seasonal cycle for the current model year. In order to accurately represent the seasonal cycle and to compare the seasonal output from year to year, it is important to choose an appropriate yearly calendar (*Joussaume and Braconnot*, 1997).

In most studies of paleoclimate the conventional 365 day calendar with months and days will not be appropriate: it is specific to the current orbital configuration with March 21st at the spring equinox. As was discussed in section 2.1; the position of a conventional calendar date with respect to the equinox changes with time (figure 2-1). This is alleviated by fixing the spring equinox to

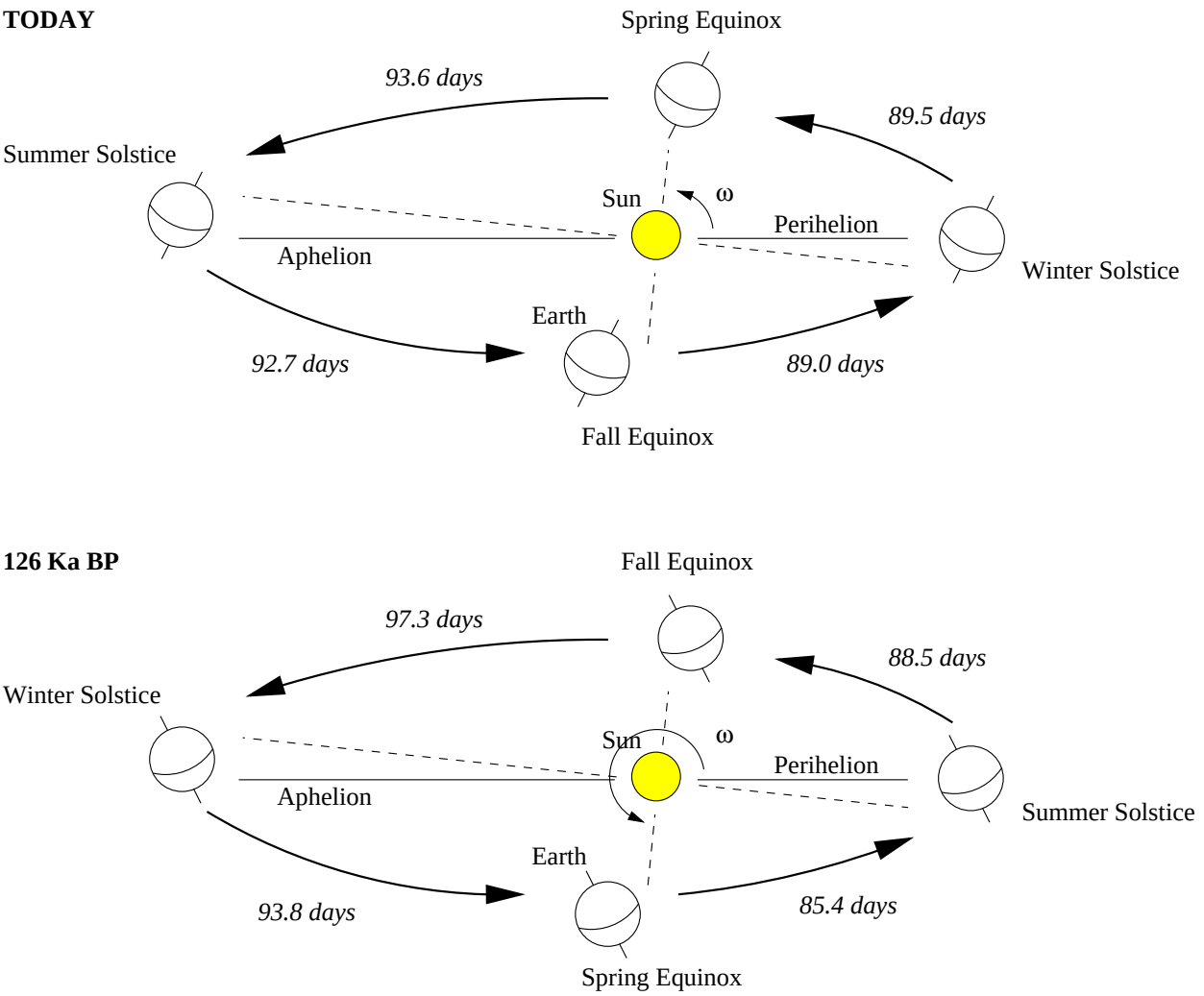


Figure 3-2: Sketch of Earth's orbit around the Sun today (0 Ka BP: $\varepsilon = 23.4°$, $\omega = -78.7°$, $e = 0.017$), and at Termination 2 (126 Ka BP: $\varepsilon = 24.0°$, $\omega = -111.2°$, $e = 0.041$), with the length of each season indicated in number of days as given by *Joussaume and Braconnot (1997)*. The duration of the seasons is proportional to the area covered between the astronomical positions, and can vary significantly with time.

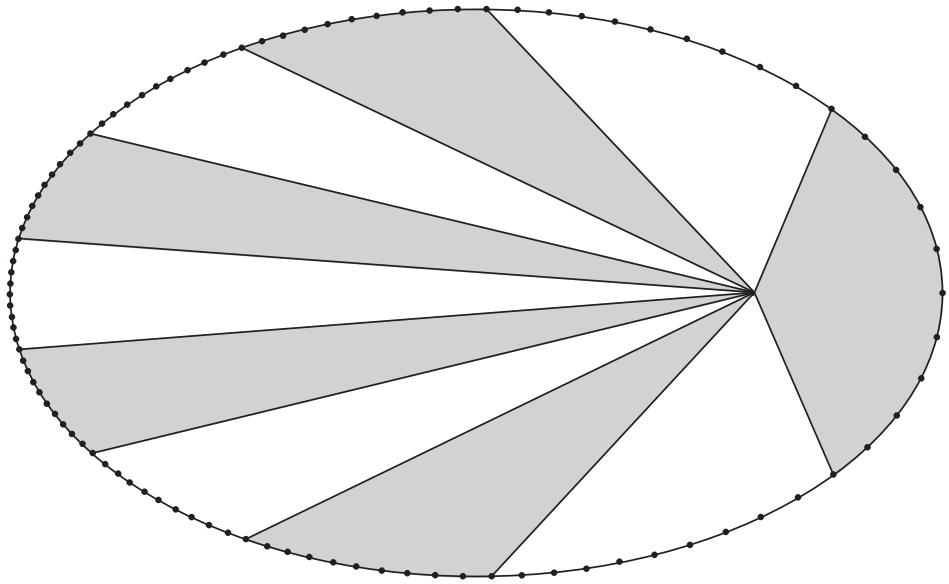

Figure 3-3: Sketch of the Earth's orbit around the Sun. The dots represent the position of the planet after equal intervals of time, and the shaded regions all have equal areas.

March 21st. However, because the number of days in each season varies with time, the solstices and fall equinox will occur on different dates (figure 3-2). For example, the time between equinoxes and solstices has varied from $82.5$ to $100$ days in the last $1$ Ma (*Berger and Loutre*, 1994). Therefore, it is misleading to use conventional calendar days to express an orbital position in the past.

Due to the problems with the modern calendar it is better to specify the Earth's position on its orbit in degrees relative to the spring equinox. In this case there are two options: 1) to use the *true longitude* of the Earth in its orbit, or 2) the *mean longitude* of the Earth with respect to spring equinox. Here mean longitude (option 2) is defined as the fictive angle described by the Earth if it were traveling around the sun at a constant velocity (*Laskar et al.*, 1993). In this case, mean longitude is proportional to time, and each "degree" on the orbit is equal to one day out of a 360 day year.

Figure 3-3 shows the path of a planet, such as the Earth, in its orbit around the sun. The line from the Sun to the planet sweeps out equal areas in equal times, following Kepler's second law. When using the mean longitude calendar (option 2) to specify the position of the planet on this orbit, the time interval between each point on the orbit is equal.

The true longitude calendar (option 1) is appropriate for plotting an insolation time series for a fixed angle on the orbit, such as the solstices or equinoxes. However, if this option is chosen when defining a calendar in a climate model, the model time step would be varying during the course of a year. Therefore, the mean longitude calendar (option 2), which has a constant time step, will be used in this study.

### 3.1.2 Albedo

Snow and ice albedo are important feedbacks in the climate system: when temperatures cool, snow and ice expand into regions previously covered by surfaces such as forests that have a relatively low albedo. This increased snow and ice cover raises the surface albedo dramatically, reflecting incoming radiation, and causing a further decrease in local temperature. In most of the calculations presented here the potential effects of sea ice are neglected; only variations in snow and ice cover over land contribute to changes in albedo.

The effective albedo at the top of the atmosphere for ice- and snow-free surfaces is calculated using the parameterization of *Wang and Stone* (1980);

$$\alpha_{land} = \alpha_0 + \frac{\alpha_2}{2}(3sin^2\phi - 1) \tag{3.4}$$

where the constants $\alpha_0 = 0.136$, and $\alpha_2 = 0.146$ are found using the annual mean zonal albedo and incident solar radiation distribution given by *Ellis and Vonder Haar* (1976). This parameterization takes into account the zenith angle effect which results in an increase in albedo at high latitudes where the solar zenith angle is large.

The extent of the snow line is controlled by the position of the zero degree isotherm: land areas with a surface temperature below freezing are assumed to be snow covered and have an albedo of $\alpha_{snow} = \alpha_{land} + \delta\alpha_{snow}$. In most cases, part of the area with temperatures below freezing is already covered by the ice sheet and will therefore have an albedo of $\alpha_{ice} = \alpha_{land} + \delta\alpha_{ice}$. When calculating the effective albedo the relative areas covered by bare land, snow ($f_{snow}$), and ice ($f_{ice}$)

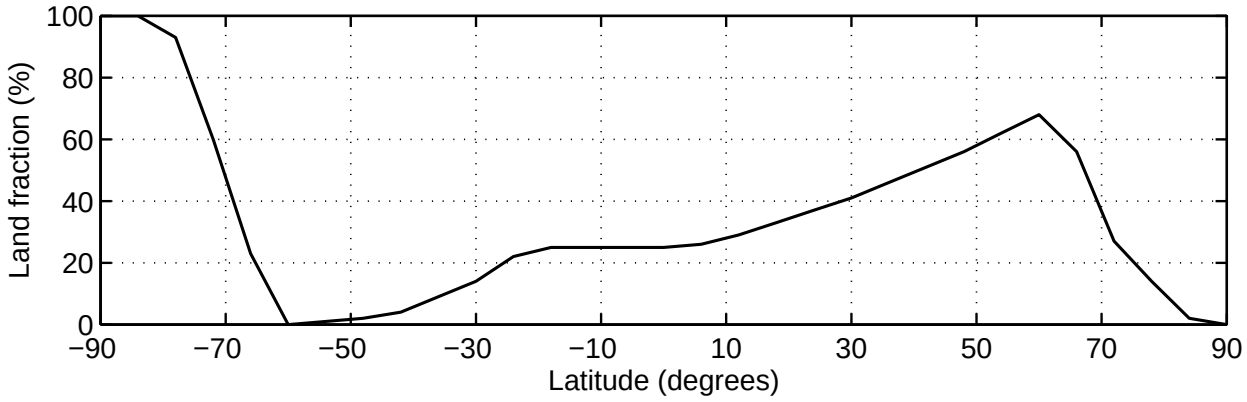


Figure 3-4: Latitudinal distribution of land masses (*Birchfield et al.*, 1982). The mean land fraction in the Northern Hemisphere is approximately $40\%$. However, at high northern latitudes south of the Arctic ocean the land fraction is closer to $60\%$.

are taken into account;

$$\alpha_{effective} = \alpha_{land} + f_{snow}\delta\alpha_{snow} + f_{ice}\delta\alpha_{ice} \tag{3.5}$$

For simplicity, the albedo of bare land and ocean surfaces are taken to be equal ($\alpha_{land}$). However, only $40\%$ of each latitude band can be covered by snow and ice ($(f_{snow} + f_{ice}) < 0.40$), which is roughly equal to the average land fraction in the Northern Hemisphere (figure 3-4). At latitudes north of $75°N$, in the Arctic ocean, the surface is assumed to be permanently covered by sea ice with an albedo fixed at $\alpha_{snow}$.

The strength of the snow and ice albedo feedback is strongly dependent on the values chosen for $\delta\alpha_{snow}$ and $\delta\alpha_{ice}$. Using results from a 1-D radiative convective model *Wang and Stone* (1980) estimated that the change in zonal earth-atmosphere albedo from ice-free to ice covered conditions is approximately $\delta\alpha_{ice} = 0.186$. A similar value for $\delta\alpha_{ice}$ is obtained when using the empirical relations of *Cess* (1976) and *Coakley* (1979) to convert surface albedo into effective top of the atmosphere albedo taking into account the effect of clouds and solar zenith angle (*Lian and Cess*, 1977). Figure 3-5 shows latitudinal profiles of zonal and annual mean top of the atmosphere albedo over land surfaces with ice-free conditions with an albedo of $0.25$, versus completely ice covered conditions with an albedo of $0.65$. Note that the value of $\delta\alpha_{ice}$ increases slightly at lower latitudes,

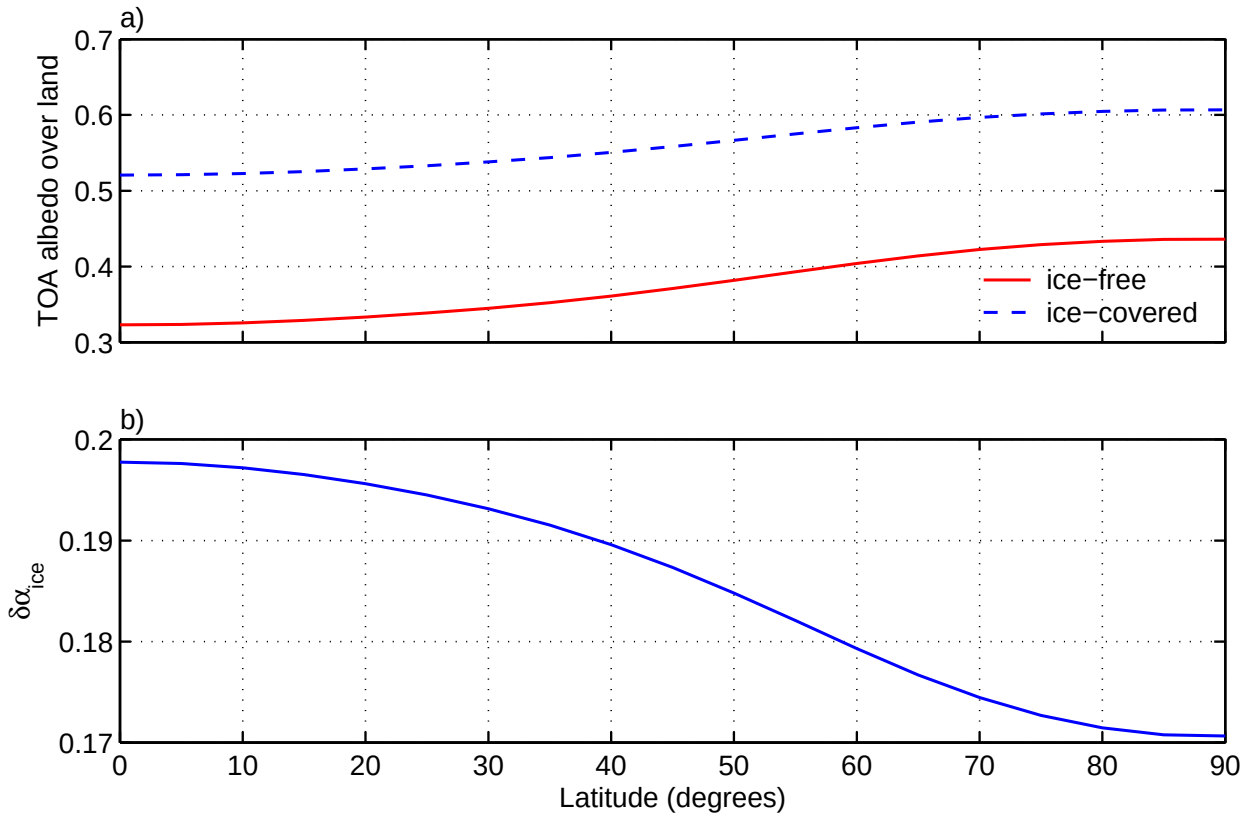


Figure 3-5: a) Zonal and annual mean top of the atmosphere (TOA) albedo over land surfaces where the ice-free surface albedo is $0.25$ and ice-covered surface albedo is $0.65$ estimated using the empirical relations described in *Coakley* (1979). b) Difference in TOA albedo for ice-free and ice-covered conditions. The cloud cover fraction is assumed to be constant at $50\%$ at all latitudes: the observed zonal annual mean cloud cover in the Northern Hemisphere varies from about $40\%$ to $65\%$ (*Cess*, 1976).

suggesting that the strength of the ice-albedo feedback increases as snow and ice moves toward the equator. However, this effect is quite small, and $\delta\alpha_{snow}$ and $\delta\alpha_{ice}$ are both kept fixed at a value of $0.186$ in the model.

When calculating global mean planetary albedo, local albedo is weighted by insolation;

$$\alpha_p = \frac{\int_{-\pi/2}^{\pi/2} Q(\phi)\alpha_{effective}(\phi)d\phi}{\int_{-\pi/2}^{\pi/2} Q(\phi)d\phi} \tag{3.6}$$

where $Q(\phi)$ is the mean annual distribution of radiation reaching the top of the atmosphere, and $\alpha_{effective}(\phi)$ is mean top of the atmosphere albedo at latitude $\phi$. The latitudinal profile of the

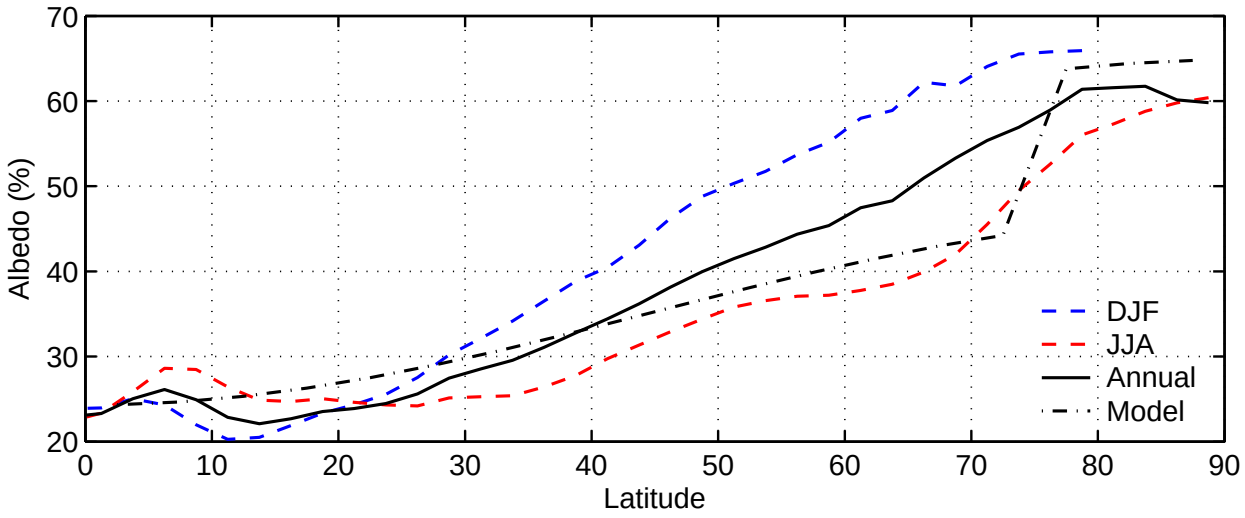


Figure 3-6: Observed top of the atmosphere albedo in percent from the Earth Radiation Budget Experiment (ERBE) averaged over the period from November 1984 to February 1990, for mean summer (June, July, August: JJA), winter (December, January, February; DJF), and annual conditions (*Li and Leighton*, 1993). The dash-dotted line is the albedo profile estimated by the model, assuming all latitudes above $75°N$ are permanently covered by sea ice.

Earth's albedo for summer, winter, and annual mean conditions from the Earth Radiation Budget Experiment (ERBE) is plotted in figure 3-6. Observed annual mean planetary albedo from ERBE is $0.297$ (*Li and Leighton*, 1993). Albedo estimated from equation 3.4, with latitudes above $75°N$ assumed to be permanently covered by sea ice, is plotted in the same figure. In this case the planetary albedo is $\alpha_p = 0.30$, which agrees well with the ERBE data.

Absorbed incoming radiation in each box of the atmospheric model is calculated by approximating the latitudinal insolation distribution with a polynomial expansion;

$$Q(\phi) = Q_0 + \frac{Q_2}{2}(3\sin^2\phi - 1) + \frac{Q_4}{8}(35\sin^4\phi - 30\sin^2\phi + 3) \tag{3.7}$$

where the polynomial coefficients ($Q_0$, $Q_2$, $Q_4$) are found by fitting the insolation profile ($Q(\phi)$) to insolation calculated at the mid-points of the three atmospheric boxes as described in the previous section.

### 3.1.3 Atmospheric Eddy Heat Flux Parameterization

In the model it is assumed that meridional atmospheric transport is dominated by baroclinic transient eddy transport. This is a good approximation at latitudes at and above about $30°N$, where the contribution to atmospheric transport by stationary components is relatively small (*Trenberth and Stepaniak*, 2003). From the theory of baroclinic eddies, meridional atmospheric eddy sensible heat flux ($F_{SH}$) can be parameterized as (*Green*, 1970; *Stone*, 1972)

$$F_{SH}(\phi) = K_{SH}\left(\frac{\partial T_{atm}(\phi)}{\partial \phi}\right)^{n} \tag{3.8}$$

where $T_{atm}(\phi)$ is the zonal mean surface temperature at latitude $\phi$, and $K_{SH}$ is chosen such that the heat fluxes between the atmospheric boxes are close to the modern observed values. The exponent is kept constant at all latitudes at a value of $n = 2.0$, which is at the lower range of the theoretical and empirical estimates: *Held* (1978) found that the heat flux should depend on the meridional temperature gradient to a power between $2.0$ and $5.0$, with the higher powers being favored at low latitudes where the $\beta$ effect is strong. By using seasonal data *Stone and Miller* (1980) estimated that the power varies from $1.6 \pm 0.5$ at $60°N$ to $3.4 \pm 0.8$ at $30°N$, which is consistent with the results of *Held (1978)*. The equation for the heat flux can also be derived from more sophisticated parameterizations, which have been tested against GCM simulations (*Stone and Yao*, 1990). However, it should be noted that the parameterization has not been tested for climates significantly different from the modern, such as during the glacial periods.

In addition to sensible heat flux, a parameterization for meridional atmospheric moisture flux ($F_w$) is required. The moisture flux is particularly important because of its effect on accumulation of snow on the ice sheets. A common procedure is to relate the meridional eddy flux of latent heat to the flux of sensible heat as follows (*Leovy*, 1973; *Stone and Yao*, 1990)

$$F_{LH}(\phi) = \frac{L_v}{c_p} q_r \frac{\partial q_s(T_{atm}(\phi))}{\partial T} F_{SH} \tag{3.9}$$

where $L_v$ is the latent heat of vaporization, and $q_r$ is the relative humidity. The saturation specific

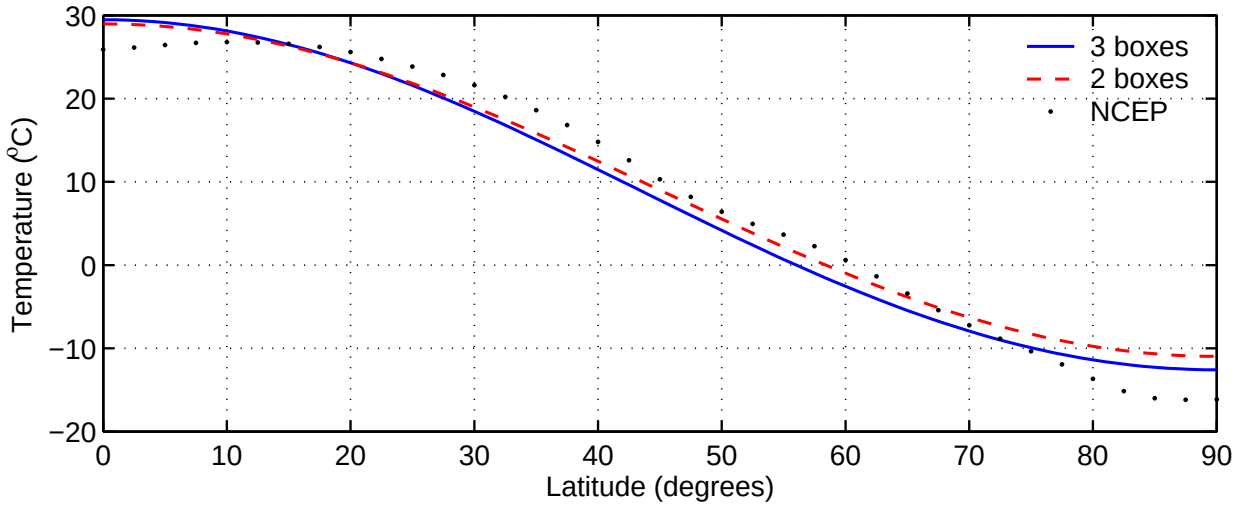


Figure 3-7: Approximate annual and zonal mean temperature profiles calculated using even order Legendre Polynomials compared with NCEP 1000 mb temperatures (*Kalnay et al.*, 1996). The first two and three even order polynomial coefficients are retained in a two and three box version of the model, respectively.

humidity $q_s(T_{atm})$ depends on the local atmospheric temperature at latitude $\phi$, as described by the Clausius-Clapeyron relation;

$$q_s(T_{atm}) = \frac{A_{cc}}{P_s} e^{-B_{cc}/T_{atm}} \tag{3.10}$$

where $P_s$ is the surface pressure, and $(A_{cc}, B_{cc})$ are constants. Substituting into equation 3.9 gives

$$F_{LH}(\phi) = K_{LH} \frac{e^{-B/T_{atm}}}{T_{atm}^2} \left( \frac{\partial T_{atm}(\phi)}{\partial \phi} \right)^n \tag{3.11}$$

where the relative humidity ($q_r$) is assumed constant, and incorporated into $K_{LH}$.

### 3.1.4 Approximate Meridional Temperature Profile

The fluxes of sensible and latent heat between the boxes depend on the meridional surface temperature gradient at the interfaces. At the same time, the flux of latent heat depends on local temperature through the Clausius-Clapeyron relationship. To estimate these quantities at specific latitudes, the meridional profile of zonal mean sea level temperature ($T_{atm}(\phi)$) is approximated using even order

Legendre Polynomials as follows;

$$T_{atm}(\phi) = P_0 + \frac{P_2}{2}(3\sin^2\phi - 1) + \frac{P_4}{8}(35\sin^4\phi - 30\sin^2\phi + 3) \tag{3.12}$$

where the coefficients ($P_0$, $P_2$, $P_4$) are determined by fitting the temperature profile ($T_{atm}(\phi)$) to the mean temperatures of the atmospheric boxes as given by the energy balance (equation 3.1). Thus, $P_0$, $P_2$, and $P_4$ become the primary dependent variables of the model, and are determined by the heat balance equations for each box. *North* (1975) tested the performance of the Legendre Polynomial approximation in an energy balance model and found a good fit to the observed meridional temperature profile when retaining the first two even polynomial coefficients ($P_0$ & $P_2$), as well as a small improvement when including three coefficients (equation 3.12). A plot of the two approximate modern temperature profiles as well as the zonal and annual mean 1000 mb temperatures from NCEP are shown in figure 3-7.

Similarly, the temperature gradient at specific latitudes is found by differentiating equation 3.12:

$$\frac{\partial T_{atm}(\phi)}{\partial \phi} = \frac{P_2}{2}(3\sin^2 2\phi) + \frac{P_4}{2}\cos\phi(35\sin^3\phi - 15\sin\phi) \tag{3.13}$$

The resulting meridional profile of atmospheric temperature gradient is used together with local temperature to estimate the fluxes of heat at the box interfaces, as well as the flux of latent heat at the edge of the ice sheet which controls the accumulation of new ice.

It should be noted that by only including even order terms in the polynomial expansions, it is implicitly assumed that the temperature gradient at the equator is zero. To account for seasonal fluxes across the equator in an inter hemispheric model, it is necessary to include the odd order terms in the expansion.

| Parameter | Value | Units | Description |
|---|---|---|---|
| $\Delta z_{mix}$ | $75$ | $m$ | Mixed layer depth |
| $f_{land}$ | $0.40$ | | Fraction of each latitude covered by land |
| $\tau_{airsea}$ | $2.5 \times 10^7$ | $s$ | Restoring time scale for air-sea flux |

Table 3.2: Mixed layer ocean parameters.

## 3.2 Mixed Layer Ocean

As the model does not include a representation of the ocean, it is necessary to couple the atmospheric boxes to a mixed layer ocean in order to correctly resolve the seasonal cycle (*North and Coakley*, 1979).

Here, the energy balance of the mixed layer is given by

$$C_{mix}\frac{\partial T_{mix}}{\partial t} = -F_{airsea} \tag{3.14}$$

where $C_{mix} = \rho_w c_p \Delta z_{mix} A_{atm}(1 - f_{land})$ is the effective heat capacity equivalent to a layer of water $\Delta z_{mix} = 75\,m$ deep, and $T_{mix}$ is the mean temperature of the mixed layer. The flux of heat between the mixed layer boxes and atmospheric boxes ($F_{airsea}$) is defined as a restoring flux following the work of *Haney* (1971)

$$F_{airsea} = \frac{C_{mix}}{\tau_{airsea}}(T_{mix} - T_{atm}) \tag{3.15}$$

where $\tau_{airsea}$ is a restoring time scale, and $T_{atm}$ is the temperature of the overlying atmospheric box. $f_{land}$ is the fraction of each latitude belt covered by land. Although this factor depends on latitude it will be kept constant at $40\%$ in the following experiments. The time scale for the interaction between the atmosphere and mixed layer ($\tau_{airsea}$) is adjusted in order to give the correct amplitude and phase of the modern observed seasonal cycle for the specified mixed layer depth.

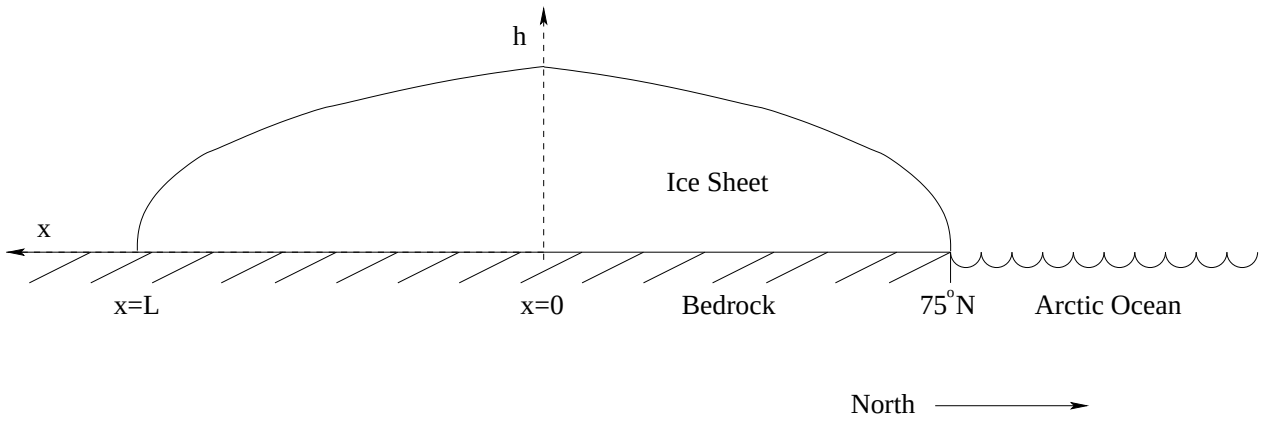


Figure 3-8: Sketch of the ice sheet configuration. The ice sheet extends south from the Arctic ocean at $75^{\circ}N$ with a total meridional extent of $2L$.

## 3.3 Ice Sheet

A common procedure when investigating the sensitivity of Earth's climate to changes in size of the polar ice sheets is to fix the ice extent to the latitude of the zero degree isotherm (e.g. *Budyko* (1969); *Sellers* (1969); *North* (1975); *Schneider and Thompson* (1979); *North and Coakley* (1979)). Although this is a valuable exercise, it assumes that the glacial growth and retreat of the major ice sheets is controlled exclusively by local surface temperature. Here, a different approach is taken where the extent of the ice sheet is calculated with a simplified ice sheet model, taking into account the balance of snowfall and melt (figure 3-8).

The ice in the model is treated as a perfectly plastic material (*Orowan and Perutz*, 1949; *Nye*, 1951; *Reeh*, 1982). In this case the deformation is negligible when the applied stress is below some critical value, defined as the yield stress ($\tau_0$). When the stress is larger than the yield stress, the material is assumed to deform instantly to relieve the applied stress. Although this may not be realistic, it gives a reasonable approximation for reconstructing the large ice sheets found during glacial periods (*Weertman*, 1976, 1964).

As the stress in the ice cannot exceed the yield stress, the drag at the base of the ice sheet (basal drag) must be equal to $\tau_0$, such that

$$-\rho_{ice} g h \frac{\partial h}{\partial x} = \tau_0 \tag{3.16}$$

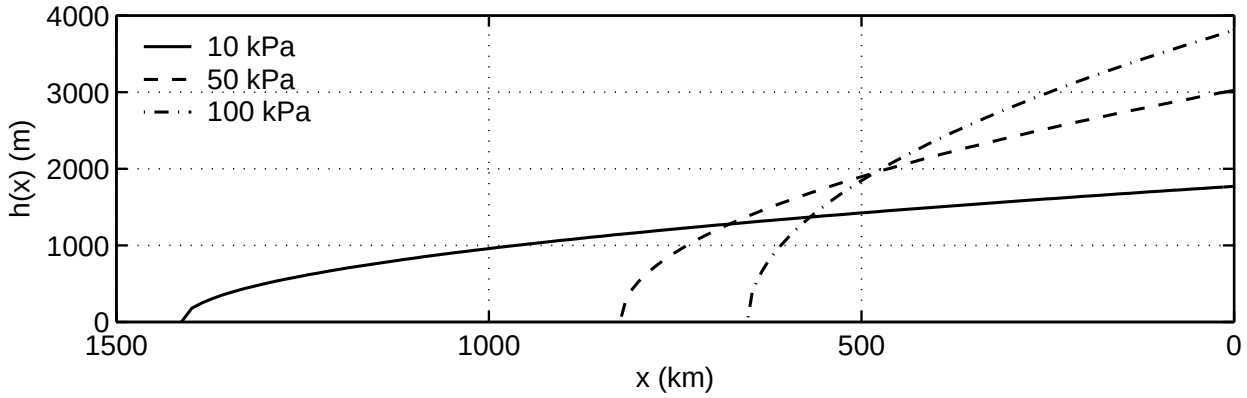


Figure 3-9: Height profiles of a plastic ice sheet with a constant volume per unit width of $3.0 \times 10^9 m^3$, but with varying values for the yield stress $\tau_0$. A small value of $\tau_0$ reduces the ice thickness.

where $\rho_{ice}$ is the density of ice, $g$ is the acceleration due to gravity, $x$ is the distance from the center of the ice sheet, and $h$ is the elevation of the ice surface. Assuming that the ice sheet is resting on a flat bed, this equation can be integrated to give

$$h^2(x) - h^2(0) = \frac{2\tau_0}{\rho_{ice} g}(x - x_0) \tag{3.17}$$

By applying the condition that the ice thickness has to be zero at the edges, and prescribing the half length of the ice sheet by $L$ it follows that the profile is parabolic;

$$h^2(x) = \frac{2\tau_0}{\rho_{ice} g}(L - x) \tag{3.18}$$

The value of the plastic yield stress determines the height to length ratio of the ice sheet: a large value of $\tau_0$ corresponds to a thick ice sheet; whereas a small value of $\tau_0$ reduces the ice thickness, which could result from larger ice velocities (figure 3-9). The thickness at the center of the ice sheet ($x = 0$) is $H = (2\tau_0 L/\rho g)^{1/2}$.

Based mostly on measurements from Alpine valley glaciers, the yield stress is estimated to vary in the range $\tau_0 = 50 - 150kPa$ ($1kPa = 10^3 Pa$) (*Patterson*, 1994, p. 240). Using a value of $\tau_0 = 100kPa$, together with the observed size of the ice sheet in central West Greenland ($L = 500km$) gives a maximum ice thickness of $3200m$, which compares well with the observed

| Parameter | Value | Units | Description |
|---|---|---|---|
| $\phi_{arctic}$ | $75N$ | $degrees$ | Latitude of edge of Arctic ocean |
| $\rho_{ice}$ | $920$ | $kg/m^3$ | Density of ice |
| $\tau_0$ | $5 \times 10^4$ | $Pa$ | Yield stress of ice |
| $\alpha_{abl}$ | $0$ | $m/s$ | Ablation constant |
| $\beta_{abl}$ | $3.0 \times 10^{-8}$ | $m/(s \times K)$ | Ablation constant for temperature |
| $\beta_{atm}$ | $7.0 \times 10^{-3}$ | $K/m$ | Atmospheric lapse rate |
| $L_v$ | $2.5 \times 10^6$ | $J/(kg \times K)$ | Latent heat of vaporization |
| $\delta\alpha_{snow}$, $\delta\alpha_{ice}$ | $0.186$ | | Albedo anomaly for snow and ice |

Table 3.3: Ice sheet model parameters.

value of $3150m$. However, in most cases $\tau_0 = 100kPa$ is too high a value for present observed ice sheets, where the yield stress is observed to vary from 0 to $100kPa$ with a mean of $\sim 50kPa$ (*Patterson*, 1994, p. 242).

The Laurentide ice sheet is believed to have been considerably flatter than modern ice sheets due to an underlying bed of deformable sediment with a low yield stress (*Clark et al.*, 1999). This deformable sediment layer is suggested to have been underlying the entire Laurentide ice sheet prior to the middle Pleistocene (*Clark and Pollard*, 1998). As a result, the ice sheet is thought to have been as extensive as in the late Pleistocene, while only containing about one third to one half as much ice (figure 2-4). For this to be possible the basal yield stress would have been lower than what is observed in Greenland and Antarctica today, resulting in a relatively thin ice sheet. Based on these assumptions a yield stress of $\tau_0 = 10kPa$ is chosen: In this case, an ice sheet with about half the estimated LGM volume of the Laurentide will have the same meridional extent as observed for the LGM.

### 3.3.1 Ice Sheet Mass Balance

When using the plastic ice sheet model described in the previous section to calculate fluctuations in size of the ice sheet it has to be coupled to the surface mass balance. Assuming that the ice sheet is symmetric and integrating the parabolic height profile (equation 3.18) over the southern half ($x = 0$

to $x = L$), the volume per unit width of half the ice sheet is

$$V = \int_0^L h(x)dx = \frac{2}{3}\left(\frac{2\tau_0}{\rho_{ice}g}\right)^{1/2} L^{2/3} \tag{3.19}$$

Change in ice volume over time is governed by the relative rates of snowfall and melting;

$$\frac{\partial V}{\partial t} = \int_0^L (acc - abl)dx \tag{3.20}$$

where $acc$ is accumulation (snowfall) and $abl$ is ablation (melting). Using this equation, together with the parabolic height profile, the volume and area covered by the ice sheet can be calculated, giving a value for the albedo. Note that it is implicitly assumed that any changes in the mass balance of the northern half of the ice sheet is balanced by calving into the Arctic ocean (*Weertman*, 1964).

### 3.3.2 Ablation

There are several options for estimating melting of ice and snow on the ice sheet. The first two are based on the model surface temperature as the only input, whereas the third involves calculating the energy balance at the surface of the ice.

(1) The simplest option is based on a linear relation between temperature at the ice surface and ablation. From observations in Greenland, *Ohmura et al.* (1996) found that the total annual ablation can be expressed as a linear function of mean summer temperature:

$$abl = 0.930 + 0.514 \times T_{JJA} \quad \text{when} \quad T_{JJA} > -1.8^{\circ}C \tag{3.21}$$

where ablation ($abl$) is given in units of $(m$ water equivalent$)/yr$ and $T_{JJA}$ is the mean surface temperature (in $^{\circ}C$) during the three summer months (June, July, & August). Because this relationship is based on the observed annual loss of ice mass it takes into account the effects due to re-freezing of melt water at the surface of the ice sheet.

*Pollard* (1980) suggests including a similar dependency of ablation on net radiation. However,

melting already depends to a large degree on incoming long wave radiation, which is strongly influenced by the air temperature above the ice (*Ohmura*, 2001). At the same time, observations show that incoming short wave solar radiation is poorly correlated with ablation (*Braithwaite and Olesen*, 1989). Therefore, including a term relating insolation to ablation does not improve the ablation parameterization.

(2) A more common procedure used to calculate ablation is based on the Positive Degree Day (PDD) method. It was first used to estimate ablation on glaciers in the Alps, and was later tested for conditions on Greenland (*Braithwaite and Olesen*, 1989; *Reeh*, 1989; *Huybrechts et al.*, 1991; *Braithwaite*, 1995). In this case, daily ablation rate ($m/day$) at any location on the ice sheet is related to local air temperature when the temperature is above the melting point;

$$abl(m/day) = \alpha_{abl} + \beta_{abl} T_s \tag{3.22}$$

where $\alpha_{abl}$ and $\beta_{abl}$ are empirical constants. However, the observed correlation between ablation and temperature is found to be higher when averaged over periods of months, rather than days (*Braithwaite and Olesen*, 1989). Therefore, ablation is often given as the total annual ablation ($m/yr$), and related to the number of days with temperatures above the melting point ($N$) as well as a positive degree day sum ($PDD$)

$$abl(m/yr) = \alpha_{abl} N + \beta_{abl} PDD \tag{3.23}$$

where the positive degree day sum is defined as the yearly sum of daily temperatures above the melting point:

$$PDD = \int_0^{year} T_s dt \quad \text{where} \quad T_s > 0°C \tag{3.24}$$

Physically $\alpha_{abl}$ represents the rate of melting when the air temperature is at $0°C$, while $\beta_{abl}$, often called the degree-day factor, describes the increase of melt rate with temperature. The relation between ablation and temperature has been tested on several glaciers in Greenland and their cor-

relation has been found to be fairly strong: for the glacier Qamanârssûp sermia in West Greenland the correlation between monthly temperature and ablation is $r = 0.93$ with a degree-day factor $\beta_{abl} = 0.08m/(day°C)$ (*Braithwaite and Olesen*, 1989). However, the value for $\alpha_{abl}$ (rate of melting when $T_s = 0°C$) is not found to be significantly different from zero. The data also indicates that the degree-day factor is reasonably constant throughout the year, with no marked differences between summer and winter.

It should be noted that the degree-day factor quoted above has been found for ice surfaces with little or no snow cover throughout the year, and observations suggest that the positive-degree day factor for snow is on the order of $\beta_{abl} = 0.03m/(day°C)$, i.e. less than half that for ice (*Braithwaite*, 1995; *Braithwaite and Zhang*, 2000). This indicates that the rate of ablation could decrease significantly during times of net accumulation, resulting in different ablation rates for growing and shrinking glaciers and ice sheets.

(3) The third and perhaps most sophisticated method to estimate ablation involves calculating the energy balance at the ice sheet surface. In this case the latent heat of melt is found as a residual, after accounting for all the processes involved in supplying and removing heat to the layer of ice and snow at the surface of the ice sheet. The variables necessary to perform this calculation are difficult to measure, and in a model the different processes involved in the surface energy balance are not well understood. Therefore, the two previous options have been the ones most frequently used in the literature.

In the model presented here, the two first ablation parameterizations are tested. At the same time, the difference between using daily, or seasonal mean temperatures when calculating ablation with the degree day method is investigated. The temperature at the surface of the ice sheet is found using the Legendre Polynomial expansion (equation 3.12). Whereas accumulation occurs over the whole area of the ice sheet, melting only takes place in a relatively narrow zone on the steep margins of the ice sheet. Therefore, it is necessary to take into account the atmospheric lapse rate when calculating the local temperature for ablation. Here a constant lapse rate of $\beta_{atm} = 6.0 \times 10^{-3} K/m$ is chosen.

### 3.3.3 Accumulation

Partly because Milankovitch theory is based on the assumption that ablation controls the growth and decay of ice sheets on orbital time scales, the treatment of accumulation in conceptual models has been very crude. In the simplest models the snow line is fixed to the latitude of the zero degree isotherm, thereby completely ignoring any contribution by the advection of moisture (e.g. *Budyko* (1969); *Sellers* (1969); *Schneider and Thompson* (1979); *North et al.* (1983)). *Suarez and Held* (1979) improve this simple representation by specifying a fixed rate of accumulation with latitude whenever temperatures fall below freezing, and find that the sensitivity of the model is sharply reduced. Similarly, in a model including a physical representation of ice sheets, *Pollard et al.* (1980) estimate accumulation by simply applying a modern observed precipitation pattern wherever the model compute temperatures below freezing. Even in more sophisticated GCMs a similar approach is often used (e.g. *Huybrechts* (1990); *Gallee et al.* (1991); *Deblonde et al.* (1992); *Tarasov and Peltier* (1997); *Huybrechts and de Wolde* (1999)), where a precipitation field is taken from present day climatology, but perturbed by taking into account the deviation of the simulated temperature field from present values. This means that only the rate of accumulation can change, but not its pattern. At the same time the change in the rate is only a function of local temperature with no influence by atmospheric transport.

As opposed to these previous model studies, the effect of atmospheric transport is explicitly included in the calculation of accumulation in the present model. In this case, net precipitation (precipitation - evaporation) on the ice sheet is set by the meridional moisture flux at the southern edge of the ice ($\phi_{icedge}$)

$$acc = F_{LH}(\phi_{icedge})/(L_v \rho_{ice}) \tag{3.25}$$

where $F_{LH}(\phi_{icedge})$ is the latent heat flux at the ice edge from equation 3.11 on page 45, $L_v$ is the latent heat of vaporization, and $\rho_{ice}$ is the density of ice. All the precipitation is assumed to fall as snow, contributing to accumulation of additional ice. This is not considered a serious constraint, since only a small fraction of yearly precipitation on an ice sheet falls as rain, and a large part of

this rainfall is expected to re-freeze into superimposed ice (*Huybrechts et al.*, 1991).

## 3.4 Summary

An atmosphere-ice process model is developed which is efficient enough to perform multiple experiments covering long time periods ($> 1$ Ma). At the same time, the model is kept simple, in order to be able to understand the underlying physics. There are a few important difference between the new model and existing similar models. An explicit parameterization is included for calculating atmospheric moisture flux and accumulation on the ice sheet, instead of assuming that accumulation is only related to local temperature. At the same time, the ice-albedo feedback is improved compared to the early one dimensional energy balance models, and found to agree well with empirical data on the change in albedo from ice free to ice covered surfaces. These two factors will be important in the following chapters when investigating the impact of insolation changes on changes in the mass balance and albedo of high latitude ice sheets.

# Chapter 4

# Model Validation and Climate Sensitivity

Climate sensitivity is most often measured as the response of global mean surface temperature to changes in insolation or atmospheric $CO_2$. In the following chapter the sensitivity of the model climate is evaluated and compared with previous model studies. Sensitivity studies with energy balance models often use a simplified parameterization of the ice-albedo feedback (e.g. *Budyko* (1969); *Sellers* (1969); *North* (1975); *North and Coakley* (1979); *Schneider and Thompson* (1979)). In this case, ice, or snow extent is fixed to the zero degree isotherm. In reality, the extent of an ice sheet is set by the relative rates of accumulation and ablation. The strength of the ice-albedo feedback and the sensitivity of climate when using these two different approaches in modeling ice extent will be discussed.

Before investigating climate sensitivity it is important to ensure that the model control climate yields surface temperatures close to the observed climate. This increases the likelihood that the important feedbacks in the system that depend on temperature will have strengths which are comparable to the current climate. Therefore, in the following section the control experiment is described, and the simulated modern climate is compared to observations.

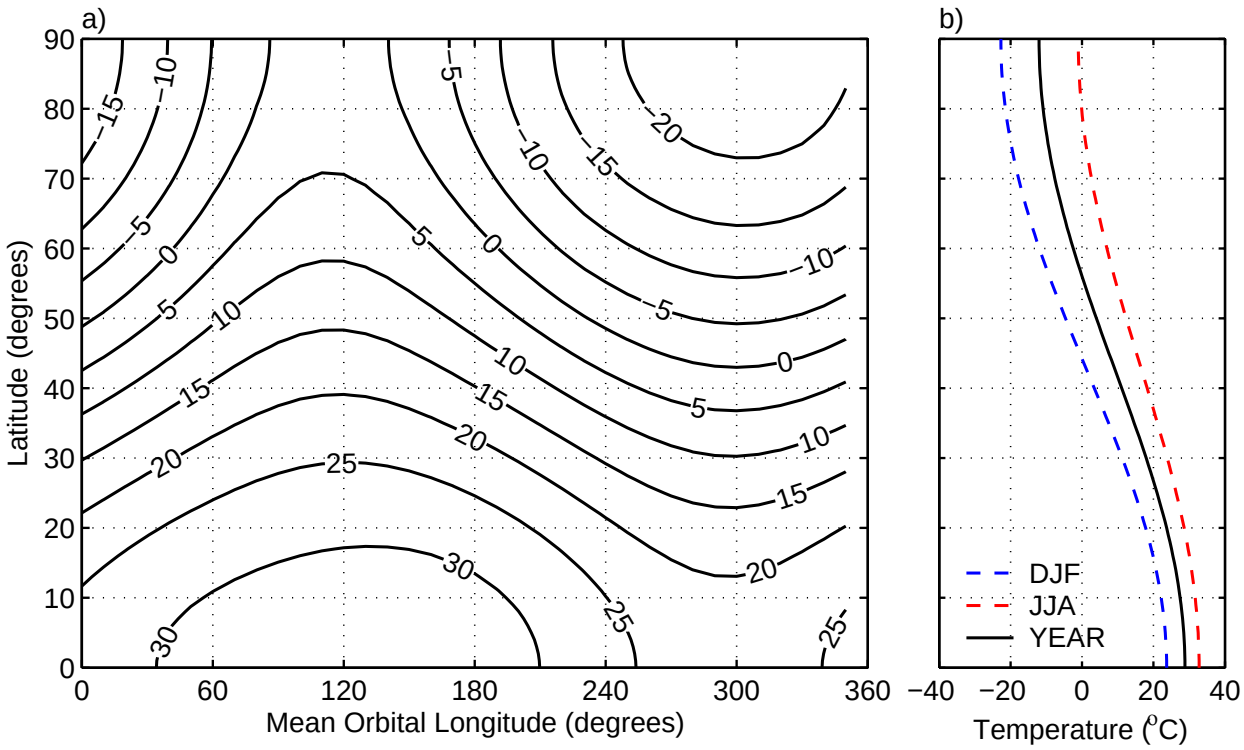


Figure 4-1: Modern atmospheric meridional temperature as calculated by the model ($^{\circ}C$): a) daily mean values as a function of latitude; b) winter (DJF), summer (JJA) and annual (YEAR) mean as a function of latitude. The start of the year is fixed at spring equinox and the year is divided into $360$ degrees, where $90^{\circ}$ is summer solstice (see section 3.1.1 on page 37).

## 4.1 Control Experiment with Modern Insolation

The control experiments described here are all forced with modern seasonal insolation and the standard parameters given in table 3.1. An equilibrium solution with a stable seasonal cycle is attained by integrating the equations in section 3.1 forward using a leapfrog scheme with a time-step of 10 days. This process takes about 100 years.

### 4.1.1 Atmospheric Meridional Temperature Profile

The equilibrium surface temperature structure is plotted in figure 4-1a as a function of time of year and latitude. Figure 4-1b shows summer (June, July, & August), winter (December, January, February), and annual mean temperature as a function of latitude.

The model temperatures agree reasonably well with observed 1000 mb atmospheric temperature

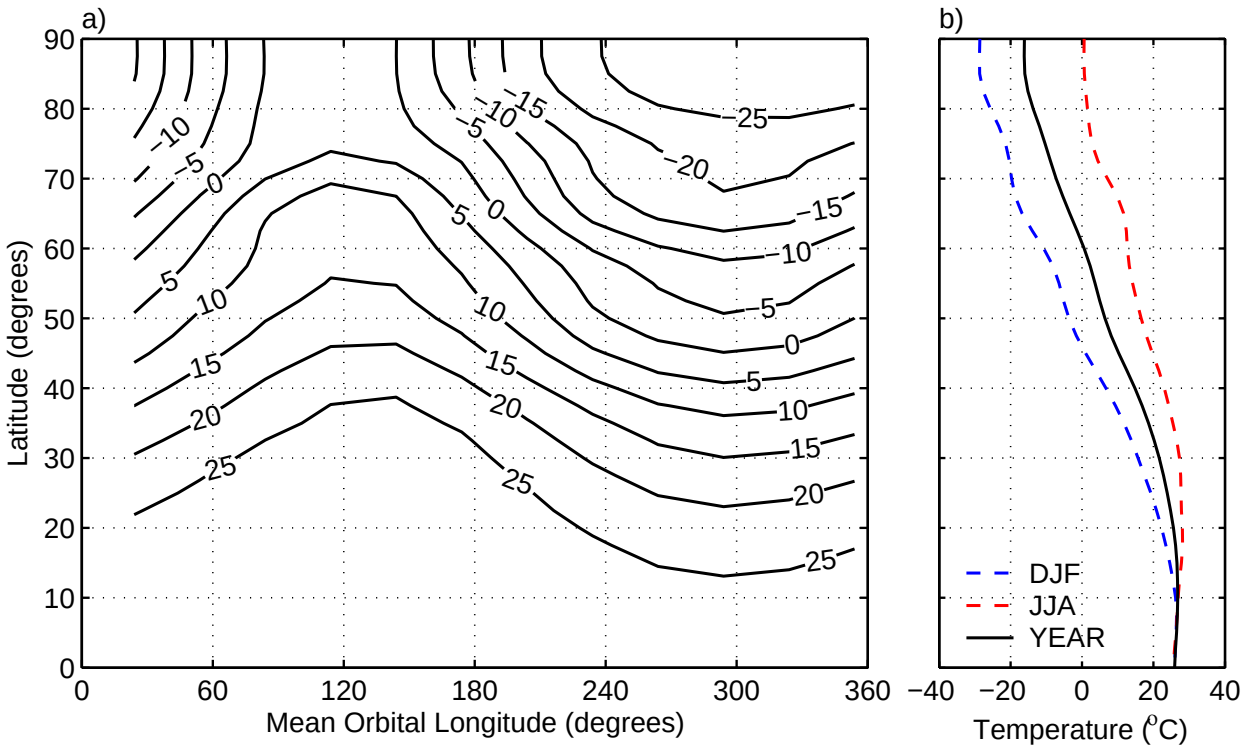


Figure 4-2: Modern atmospheric meridional temperature climatology at the 1000 mb level from NCEP data covering the period 1979-2001: a) Daily values as a function of latitude; b) winter (DJF), summer (JJA) and annual (YEAR) mean as a function of latitude.

climatology from NCEP reanalysis data covering the period 1979-2001 shown in figure 4-2. The phase of the model seasonal cycle is comparable to observations, but the increase in amplitude of the seasonal cycle with latitude is smaller. Disagreement between the model and observations is mainly found at low latitudes. This is due to the inability of the heat flux parameterization to capture the meridional heat flux due to the Hadley cell, as well as the neglect of cross-equatorial heat transports.

The fit of the amplitude of the seasonal cycle is accomplished by adjusting the relaxation time of the atmospheric and mixed layer temperatures ($\Delta t_{airsea}$ in equation 3.15): increasing $\Delta t_{airsea}$ increases the amplitude of the seasonal cycle. Similarly, the meridional temperature structure is fit to observations by adjusting the strength of the meridional heat fluxes (equations 3.8 & 3.11): increasing the constants $K_{SH}$ and $K_{LH}$ decreases the meridional temperature gradient.

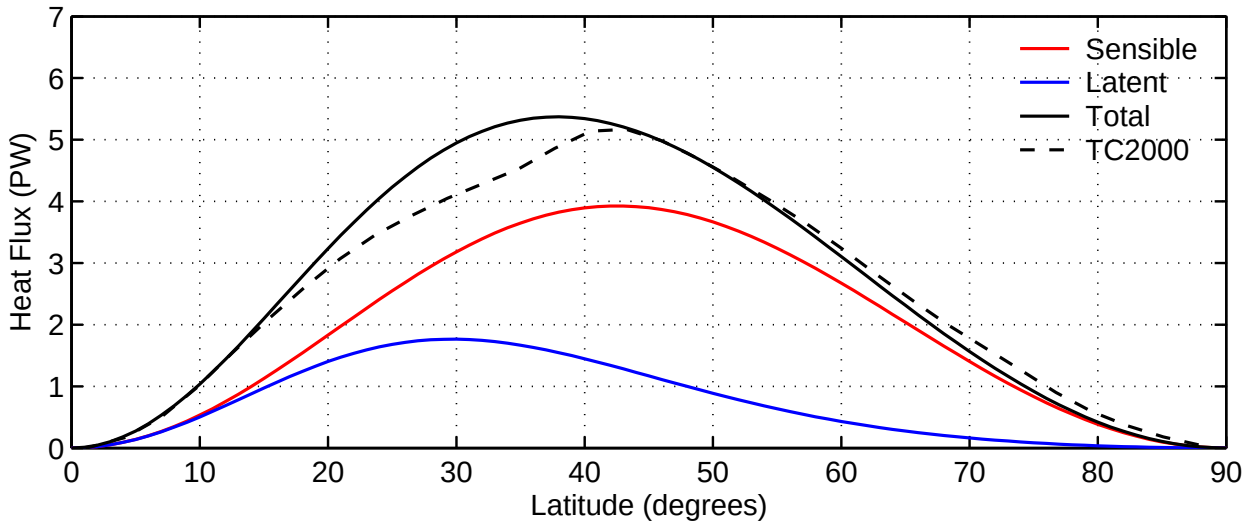


Figure 4-3: Modern meridional profiles of annual and zonal mean atmospheric sensible, latent, and total heat fluxes as calculated by the model ($1\ PW = 10^{15}\ W$). Also shown is estimated total atmospheric heat flux from NCEP (*Trenberth and Caron*, 2001).

### 4.1.2 Atmospheric Eddy Heat Flux

The model profiles of annual mean atmospheric meridional sensible and latent heat fluxes are shown in figure 4-3 together with observed total atmospheric heat flux estimated from NCEP data by *Trenberth and Caron* (2001). The total heat flux calculated by the model is slightly larger than the observed value. However, any contribution by ocean heat fluxes is not included in the model. Therefore, the atmospheric heat flux is forced to compensate in order to obtain a reasonable meridional temperature structure, in particular at low latitudes. The relative contribution by sensible and latent heat fluxes is comparable to observations, where the maximum latent heat flux has a magnitude about half that of the sensible heat flux. The components of the observed meridional heat flux are shown in figure 4-4: at latitudes poleward of $30^\circ$ sensible and latent heat fluxes dominate, whereas at lower latitudes the influence by the flux of potential energy becomes important. As this study is mostly concerned with high latitude processes related to the growth and decay of ice sheets, the inadequate representation of low latitude heat fluxes is not thought to be a problem.

At equilibrium, the atmospheric heat flux calculated by the model agrees reasonably well with observations. However, a more important question is whether the sensitivity of the flux to changes

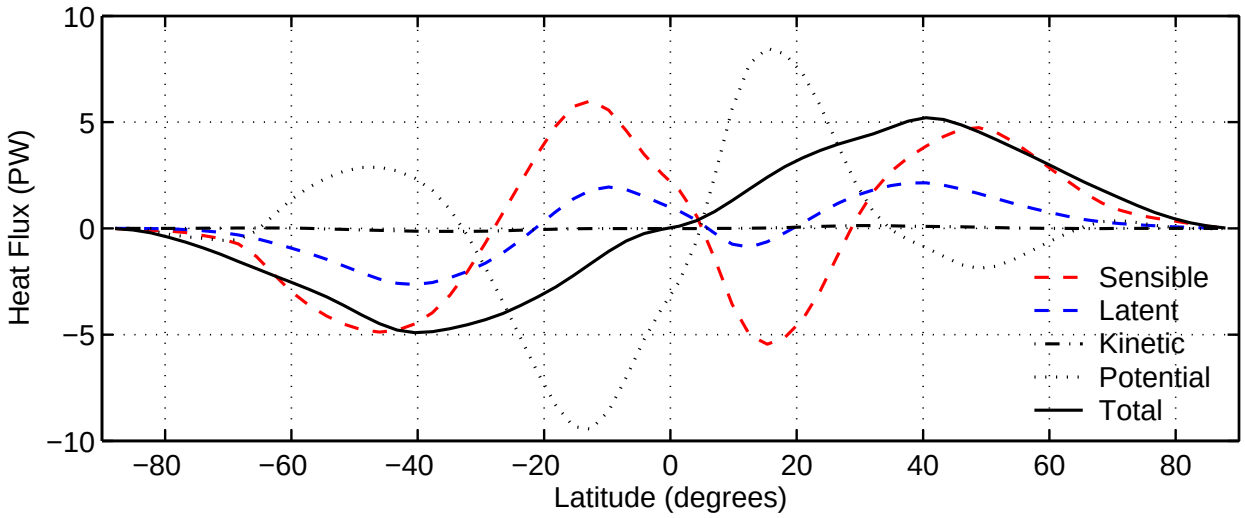


Figure 4-4: Modern meridional profiles of annual and zonal mean atmospheric sensible, latent, kinetic, and geopotential heat fluxes from NCEP climatology based on data covering the period 1979-2001 (PW) (*Trenberth and Stepaniak*, 2003).

in meridional temperature structure implied by the parameterizations discussed in section 3.1.3 is realistic. An empirical study by *Stone and Miller* (1980) based on mean seasonal data finds a high correlation ($90\%$) between total meridional atmospheric sensible heat flux and the 1000 mb meridional temperature gradient. When comparing the temperature gradient to fluxes due to only transient and stationary eddies, the correlation is increased to $97\%$. Similar high correlations are found when comparing the observed flux of latent heat by transient eddies with those calculated using the observed meridional temperature structure and equation 3.11 on page 45 (*Scott*, 1995).

Figure 4-5 taken from *Scott* (1995) shows the log-log correlation between latent heat flux as estimated by the parameterization in equation 3.11 on page 45 with the observed meridional flux of latent heat in the atmosphere by all eddies, transient eddies alone, and stationary eddies alone. The data used are 10 years of zonally averaged monthly data for the period $1963 - 1973$ from *Oort* (1983). The temperature data is vertically averaged, and the gradient is computed as the temperature difference between two latitude belts, separated by a distance of $30°$. This distance is large enough to ensure that primarily planetary scale forced variations are diagnosed (*Lorenz*, 1979; *Stone and Miller*, 1980). The dashed line in the figure represents the $99.9\%$ confidence level according to the Student's t-test, as discussed in *Stone and Miller* (1980).

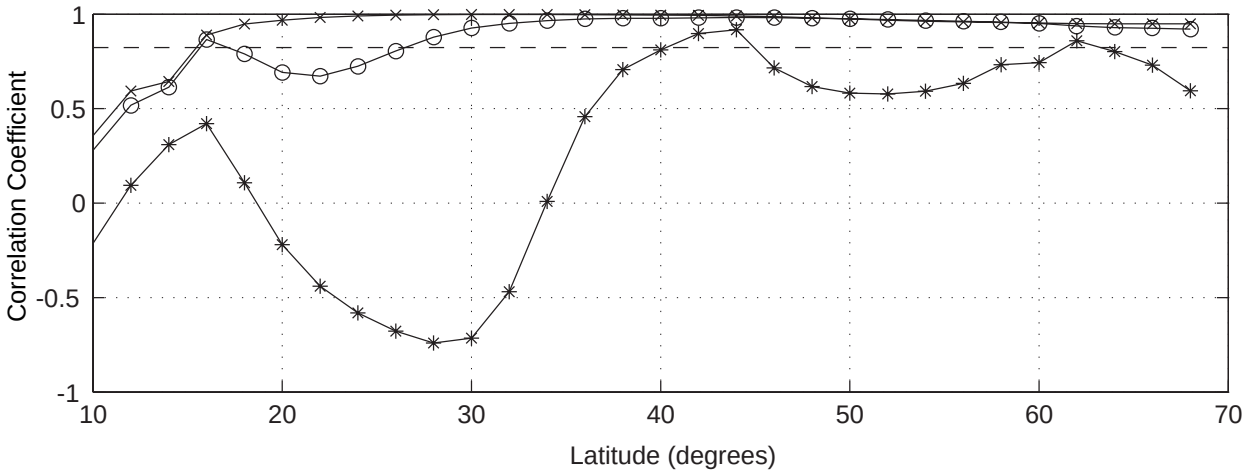


Figure 4-5: Log-log correlation of eddy latent heat flux estimated using the parameterization in equation 3.11 on page 45 with the observed meridional flux of latent heat in the atmosphere by all eddies ($\circ$), transient eddies alone ($\times$), and stationary eddies alone ($*$) as a function of latitude (*Scott*, 1995). The dashed line represents the $99.9\%$ confidence level.

Figure 4-5 shows a very high correlation for both total and transient eddy fluxes of latent heat, comparable to the results of *Stone and Miller* (1980). It makes very little difference whether the correlation with the mean flux is calculated using vertically averaged temperature (figure 4-5), or surface temperature (not shown). The correlation for the stationary eddy flux is relatively low, and there is a negative correlation near $30^{\circ}N$ due to the summer Indian monsoon (*Scott*, 1995). However, the contribution by stationary eddy fluxes to the total eddy heat flux is relatively small, in particular at mid and high latitudes.

The same study also investigated the values of the exponent $n$ in equation 3.11 on page 45 which gives the best power law fits to the eddy flux of latent heat in the atmosphere. Figure 4-6 shows that the best power law fits for latitudes north of $30^{\circ}N$ have exponents in the range $n = 1-2$, with the highest values found for the total latent eddy heat flux.

During glacial times the meridional temperature structure would have been significantly different from today. At the same time, the presence of large ice sheets at high latitudes of the Northern Hemisphere could have influenced atmospheric circulation. Experiments with an atmospheric GCM by *Kageyama et al.* (1999) with specified modern sea surface temperatures and insolation

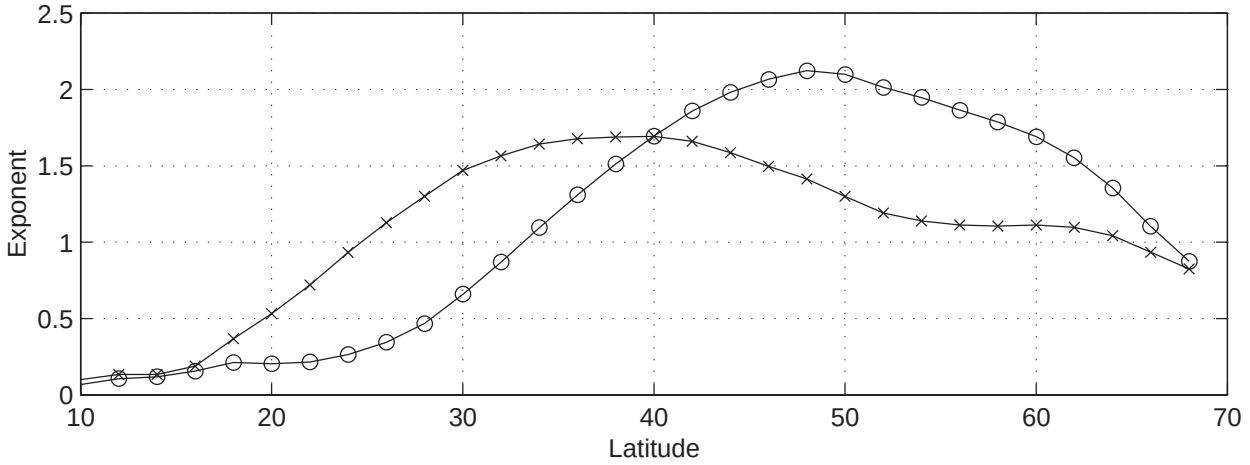


Figure 4-6: Exponent $n$ in equation 3.11 on page 45 giving the best fit for the zonal mean atmospheric flux of latent heat by all eddies ($\circ$), and transient eddies only ($\times$) as a function of latitude (*Scott*, 1995).

fixed to values appropriate for the last glacial inception ($\sim$ 115 Ka BP) indicate an increase in storm activity and precipitation at high latitudes. These changes are a direct result of an increase in the meridional temperature gradient forced by the change in insolation. In similar experiments with last glacial maximum (LGM) boundary conditions, the change in weather patterns is more severe. There is a significant increase in storm activity, however this is only partially translated into precipitation changes due to much colder temperatures at high latitudes.

Similar results for the last glacial inception are found by *Khodri et al.* (2001) in experiments with a coupled atmosphere-ocean GCM: poleward moisture flux is strengthened in response to a stronger meridional temperature gradient. The strong response of the atmosphere is partly a result of a weakened meridional overturning circulation and heat transport by the ocean. These model studies suggest that in the past, there is a strong connection between atmospheric heat fluxes and the temperature gradient, similar to what is observed today (*Stone and Miller*, 1980).

| | no snow /no ice | active snow /no ice | no snow /active ice |
|---|---|---|---|
| Sensitivity parameter $\beta$ (°) | 138 | 166 | 219 |
| $\Delta T$ when $S + 2\%$ (°$C$) | $+2.8$ | $+3.2$ | $+3.4$ |
| $\Delta T$ when $S - 2\%$ (°$C$) | $-2.8$ | $-3.4$ | $-4.1$ |

Table 4.1: Sensitivity ($\beta$) of different model configurations with and without active snow and ice covers. In all three experiments the land fraction is set to $40\%$.

## 4.2 Climate Sensitivity

When comparing different climate models it is useful to measure their sensitivities. Climate sensitivity ($\beta$) is defined as the change in global mean sea level temperature ($T_{mean}$) in response to a small change in solar constant ($S$)

$$\beta = S\frac{\partial T_{mean}}{\partial S} \tag{4.1}$$

Another common measure for sensitivity is the equilibrium response of global surface temperature to a doubling of atmospheric $CO_2$. This is approximately equal to a $2\%$ increase in solar constant. According to the Intergovernmental Panel on Climate Change (IPCC) sensitivity of climate to a doubling of $CO_2$ is likely to be in the range $1.5 - 4.5°C$ (*Cubasch and Meehl*, 2001, p. 527). These estimates are given by experiments with coupled ocean atmosphere GCMs.

The response of the simple process model to changes in solar constant can be compared with sensitivity estimates from the IPCC as well as other climate models. The sensitivity parameter ($\beta$) and the change in temperature due to a $2\%$ change in solar constant in model experiments with and without interactive snow and ice components are given in table 4.1.

The sensitivity of the most basic version of the model without an active snow- or ice-albedo feedback is $\beta = 138°$, which implies a $1.38°C$ global mean temperature decrease for a $1\%$ decrease in solar constant. This only accounts for the effect of the negative thermal radiation feedback, which regulates the amount of outgoing radiation. The strength of this feedback is set by the value chosen for the parameter $B$ in equation 3.3, and implicitly accounts for water vapor and cloud feedbacks.

When including an active snow-albedo feedback, where the snow line over land follows the

| Model | $\beta$ no snow | $\beta$ with snow |
|---|---|---|
| *Budyko* (1969) | $155°$ | $400°$ |
| *Sellers* (1969) | $150°$ | $326°$ |
| *North* (1975) | $140°$ | $400°$ |
| *Lian and Cess* (1977) | $147°$ | $184°$ |
| *Coakley* (1979) | $152°$ | $207°$ |
| *Wetherald and Manabe* (1975) | $146°$ | $185°$ |
| *Wang and Stone* (1980) | $135°$ | $188°$ |

Table 4.2: Climate sensitivity ($\beta$) found in model studies with and without an active snow-albedo feedback. In the studies where the value of $\beta$ is not given, it is evaluated using equation 4.1 with the appropriate change in $S$ as considered in the model experiments.

$0°C$ isotherm, the sensitivity is increased to $\beta = 166°$. This is lower than the values found in the energy balance model studies of *Budyko* (1969); *Sellers* (1969); *North* (1975), mostly due to different albedo parameterizations: in these early model studies the change in albedo as the surface changes from ice-free to ice-covered ($\delta\alpha_{snow}$) is significantly larger than the value used in this study. On the other hand, the sensitivity found here is similar to that obtained with the improved albedo parameterizations used in the studies of *Lian and Cess* (1977) and *Coakley* (1979), as well as the GCM experiments of *Wetherald and Manabe* (1975) (table 4.2). The albedo parameterization introduced by *Lian and Cess* (1977) and *Coakley* (1979) takes into account the effect of clouds and solar zenith angle (see section 3.1.2 on page 40).

Note that the strength of the albedo feedback is also influenced by the negative dynamical flux feedback: as snow cover increases, high latitudes cool, and the meridional temperature gradient increases. Thus, the flux of heat to high latitudes increases, hindering the advance of the snow line. The strength of the dynamical feedback depends on the exponent in the parameterization of atmospheric heat flux (equations 3.8 & 3.11). In most previous studies with energy balance models, heat transport is represented by linear diffusion ($n = 1$). As discussed in section 3.1.3, the empirical value is closer to $n = 2$. This increases the strength of the dynamical feedback, and reduces the sensitivity in models with an active snow-albedo feedback.

Replacing snow cover with an active ice sheet results in a sensitivity of $\beta = 219°$. This is significantly larger than the sensitivity found with the simplified snow-albedo feedback. In the case

of the ice sheet, growth is not limited as strongly by the zero degree isotherm. Instead, surface melt increases as the margin moves toward the equator and temperatures increase. The strength of this negative feedback is controlled by the melt factor ($\beta_{abl}$) in the ablation parameterization (equation 3.22). If the ice margin is to be constrained to follow the zero degree isotherm, the melt factor has to be increased significantly beyond its empirical value. At the same time as ablation increases with the advance of the ice margin, accumulation increases. This is because the meridional moisture flux is larger at mid latitudes as shown in figure 4-3, and results in a positive feedback which further enhances the sensitivity of the model. When both an active snow cover and ice sheet are included (not shown) the results are similar to the case with only an active ice sheet. This is because the surface area sufficiently cold for there to be snow in summer is covered by the ice sheet already, and the change in winter snow has a minor influence on the sensitivity.

Changes in global mean surface temperature due to a $2\%$ increase in solar constant (table 4.1), are within the range given by the IPCC ($1.5 - 4.5°C$). Note that a $2\%$ increase in solar constant is equivalent to a radiative forcing of $3.4W/m^2$, which is very close to the radiative forcing of $3.7W/m^2$ expected from a doubling of atmospheric $CO_2$ (*Myhre et al.*, 1998). In the experiment with an active ice sheet, all the ice melts in response to a $2\%$ increase in solar constant. Once the ice has completely melted, the sensitivity of the system is reduced. Because of this, there is a significant difference between the response of climate to an increase, versus a decrease in solar constant. In effect, modern climate is most sensitive to decreases in solar constant, or $CO_2$ if the perturbation is sufficiently large.

## 4.3 Ice Sheet Stability

Since the early model studies by *Budyko* (1969) and *Sellers* (1969), ice-albedo has been recognized as one of the most important feedback mechanisms determining the sensitivity of climate. At present, perennial ice with a high albedo exists at both poles. If the climate is cooled, these ice areas will grow, leading to a higher planetary albedo and a further cooling. This strong positive

feedback mechanism enhances climate sensitivity, and has the potential to cause multiple climate equilibria. According to *North et al.* (1981) these multiple equilibria are associated with two types of instabilities:

1. Small Ice Cap Instability (SICI); where if an ice cap decreases sufficiently in size it becomes unstable and rapidly melts.

2. Ice Covered Earth Instability (ICEI); in this case an instability arises when the ice cap grows too large, and the climate moves to a state where the entire globe is covered with ice.

In studies with simple one dimensional energy balance models where the ice-albedo feedback is parameterized by fixing the ice limit to the zero degree isotherm, it has been shown that there are three possible solutions for the present level of solar forcing: one with a small ice cap, one with a large ice cap, and one completely ice covered. This type of multiple equilibria, except for the small ice cap instability, has even been shown to exist in some GCM experiments (*Lee and North*, 1995).

The small ice cap instability has been proposed as a mechanism for the initiation and growth of the Greenland and Antarctic ice sheets and for the oscillations in size of the Laurentide ice sheet (*North and Crowley*, 1985). However, the small ice cap instability only exists in energy balance models where the meridional heat flux is represented by linear diffusion (*North*, 1984). In this case, the model has no stable ice cap smaller than a certain finite size. In the model presented here, meridional atmospheric heat flux is nonlinear, and the small ice cap instability is not expected to occur.

The ice covered earth instability is not only found in simple energy balance models, but also in radiative convective equilibrium models (*Wang and Stone*, 1980), as well as in an atmospheric GCM (*Lee and North*, 1995). In this case there are two possible solutions for the same solar forcing: one corresponding to an ice covered earth, and the other with a small ice cap. A small perturbation in insolation from the present value can cause the system to rapidly move to the ice covered state. However, once ice covered, the solar constant has to be increased to as much as $40\%$ above its present value before ice starts to melt (*Crowley and North*, 1991, p. 17). This observation is the

origin of the "faint young sun paradox": over the past several billion years the sun's luminosity has been steadily increasing, therefore the question is raised why the earth is not completely ice covered. One explanation often cited is that the concentration of $CO_2$ in the atmosphere was much greater in the past and therefore prevented the initial build up of ice (*Owen et al.*, 1979).

### 4.3.1 Temperature Dependent Albedo

To test the stability and possible existence of multiple equilibria in the atmosphere-ice process model, experiments are constructed where the solar constant is increased from $80\%$ to $120\%$ of today's value. The first set of experiments are carried out without an active ice sheet. Instead, the ice-albedo feedback is represented by a varying snow line over land which follows the latitude of the zero degree isotherm. Figure 4-7 shows the annual mean equilibrium latitude of the snow line as a function of normalized solar constant ($S/S_0$). For large values of the solar constant ($15\%$ above modern) there is no snow in the model. As $S$ decreases, snow gradually covers the surface until it is completely snow covered. For values of $S$ smaller than about $0.86S_0$, the earth is covered with snow and the global mean temperature is below $-20°C$. At the present value of $S$, annual mean snow cover reaches about $60°N$, with a global mean temperature of $14°C$, and a planetary albedo of about $0.30$.

Once in the completely snow covered state, increasing the solar constant (analogous to increasing atmospheric $CO_2$) starts melting snow when $S$ reaches a value of about $0.86S_0$. Thus, for the range of $S$ tested there is only one equilibrium solution, and there is no hysteresis loop as found in similar experiments with one dimensional energy balance models (*Budyko*, 1969; *Sellers*, 1969; *North*, 1975). There is no evidence of an ice covered earth (ICEI), or small ice cap instability (SICI), and a relatively small value of $S$ is required to escape from the completely ice covered situation.

The seasonal range in snow cover is also sensitive to changes in solar constant, as can be seen in figure 4-8. Here, winter and summer extremes of snow cover are shown as functions of normalized solar constant for the experiment where insolation is gradually reduced. For a solar constant larger

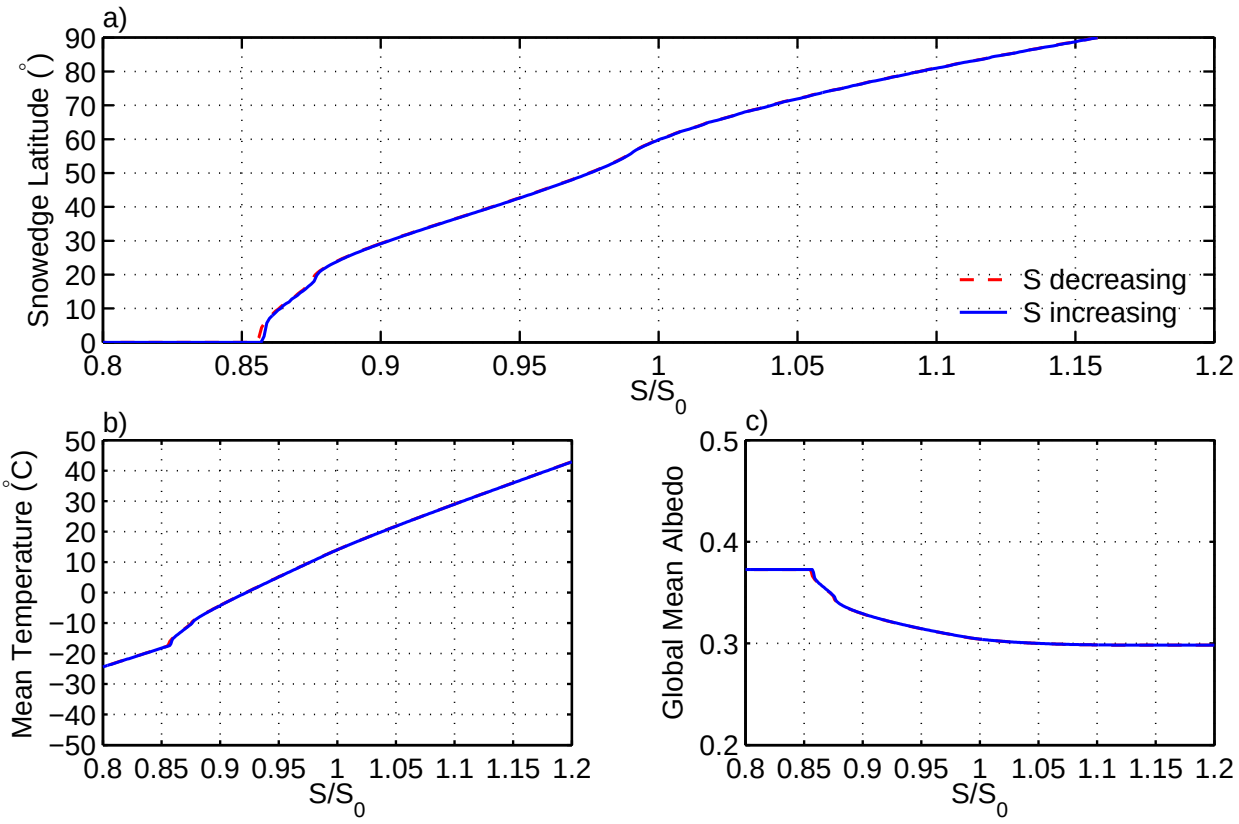


Figure 4-7: a) Annual mean snow edge latitude (degrees), b) global annual mean temperature ($^{\circ}C$), and c) global annual mean planetary albedo as a function of normalized solar constant ($S/S_0$) in an experiment without an active ice sheet and where $\delta\alpha_{snow} = 0.186$. Two experiments are plotted: one where $S/S_0$ is increasing, and one where $S/S_0$ is decreasing. However, the results from the two cases are indistinguishable.

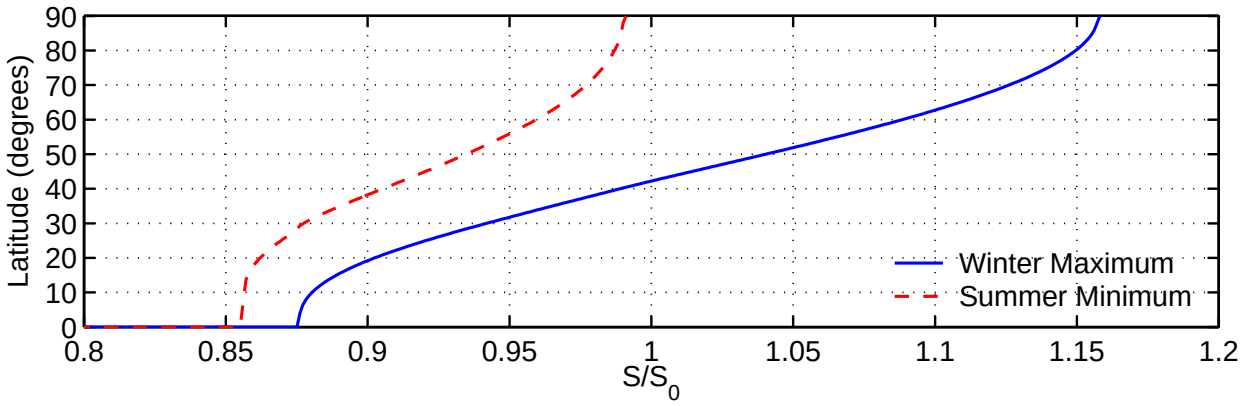


Figure 4-8: Seasonal snow cover limits as a function of normalized solar constant ($S/S_0$) in an experiment with a temperature dependent snow cover (SNOW).

than $0.99S_0$ there is no snow in the summer months, whereas insolation has to be increased to about $1.16S_0$ for all months of the year to be free from snow. At present, snow cover varies from about $90°N$ in summer to $40°N$ in winter. The latitude of permanent, or summer minimum snow cover, is more sensitive to changes in solar constant than the maximum winter snow cover. In summer, the meridional surface temperature gradient is weaker than in winter. Therefore, a change in global temperature can cause a large change in the meridional extent of summer snow cover, whereas the change in winter snow cover is relatively small. This agrees with the results of *Held and Suarez* (1974), who find that for an annual mean climate model, the sensitivity of the snow line is inversely proportional to the temperature gradient near the snow line.

In the one dimensional energy balance model of *North et al.* (1981) an ice covered earth instability (ICEI) occurs if the solar constant is lowered by just a few percent from its present value, and does not recover again until $S$ is increased to about $40\%$ above its current value. However, the change in albedo from snow-free to snow-covered conditions ($\delta\alpha_{snow} = 0.32$) is significantly larger than what is used here ($\delta\alpha_{snow} = 0.186$).

Figure 4-9 shows the result of increasing the strength of the snow-albedo feedback to a value of $\delta\alpha_{snow} = 0.40$. An ice covered earth instability sets in when $S$ is lowered to about $0.94S_0$. For smaller values of the solar constant, all land surfaces are covered with ice. Once in the snow covered state, increasing the solar constant does not result in melting of snow until $S$ reaches a value

of about $0.99S_0$. Thus, there are two equilibrium states when the solar constant is between $0.94S_0$ and $0.99S_0$: one with a relatively small snow cover, and one where the planet is completely snow covered. The resulting hysteresis loop is similar to that found in experiments with one dimensional energy balance models, however there is no small ice cap instability (SICI). At the same time, the snow cap is more stable to decreases in $S$ and does not require a very large increase in $S$ in order to escape from the completely ice covered state.

Figure 4-9b shows global mean sea level temperature versus normalized solar constant for the experiment with $\delta\alpha_{snow} = 0.40$. This illustrates that climate sensitivity is greater for the state with relatively small snow cover (upper branch) compared to the completely snow covered state (lower branch). The sensitivity $\beta$, is approximately $290^\circ$ for the state with partial snow cover, whereas it is only $110^\circ$ in the completely snow covered state. Sensitivity in the ice covered state is lower because the ice albedo feedback becomes insignificant when the area of ice remains unchanged.

### 4.3.2 Inclusion of an Active Ice Sheet

The simple albedo feedback mechanism adopted in the preceding section and in most previous studies with energy balance models is far from realistic: ice caps are treated as snow caps with instantaneous response to temperature, ignoring any effects of accumulation and ablation rates. In the following experiment the temperature dependent snow line is replaced by an active ice sheet which responds to changes in the balance of accumulation and ablation.

Figure 4-10 shows the response of the ice sheet to changes in solar constant. There is no ice present for values of $S$ above $1.01S_0$. As $S$ decreases, the ice sheet gradually expands, and for values of $S$ below $0.80S_0$ nearly all land areas are covered by ice. However, as ice approaches the equator, rates of accumulation and ablation are extremely small and the growth of the ice sheet is very slow. Once in the ice covered state, increasing the solar constant does not result in a retreat of the ice sheet until $S$ reaches a value of about $0.87S_0$. Thus, there are two equilibrium states when $S$ is sufficiently small. There is no rapid switch to a completely ice covered state as implied by the ice covered earth instability. However, it should be kept in mind that accumulation is given by the

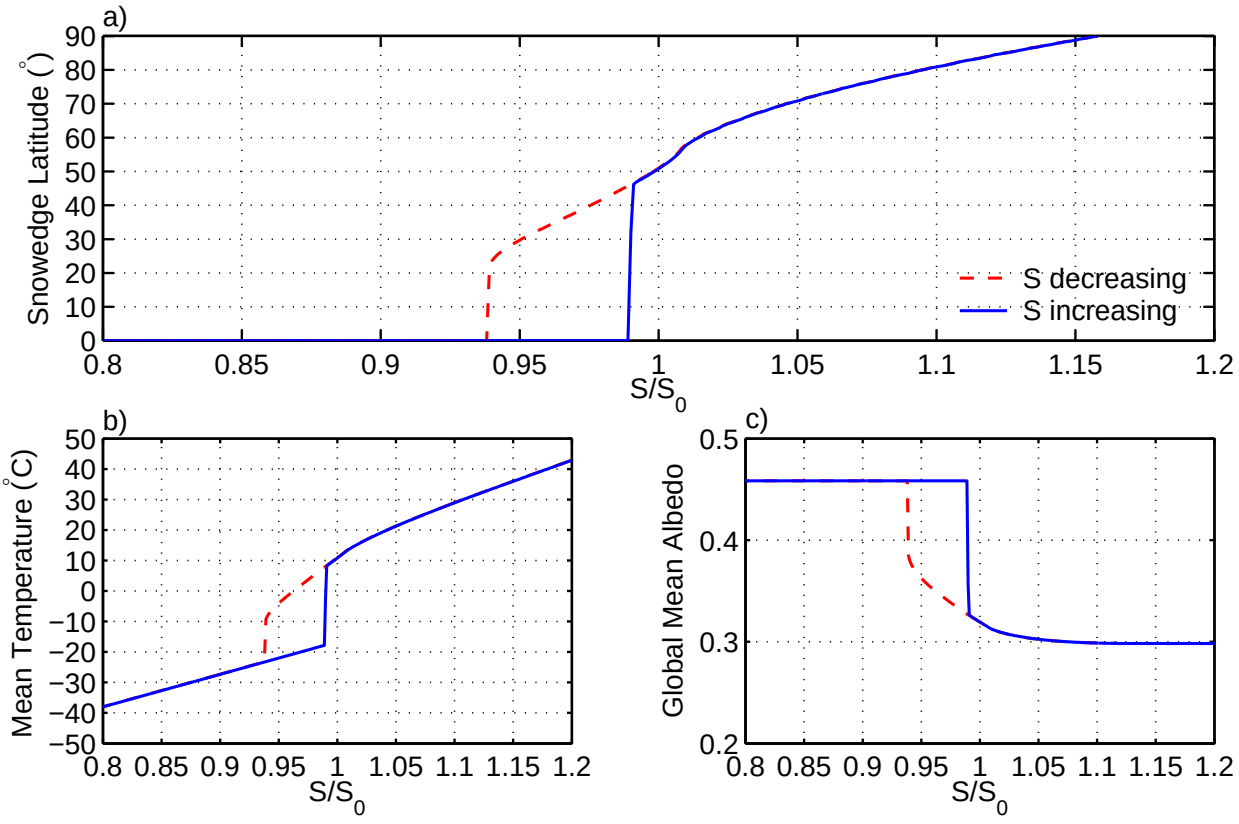


Figure 4-9: a) Annual mean snow edge latitude (degrees), b) global annual mean temperature ($^{\circ}C$), and c) global annual mean planetary albedo as a function of normalized solar constant ($S/S_0$) in an experiment without an active ice sheet and where $\delta\alpha_{snow} = 0.40$.

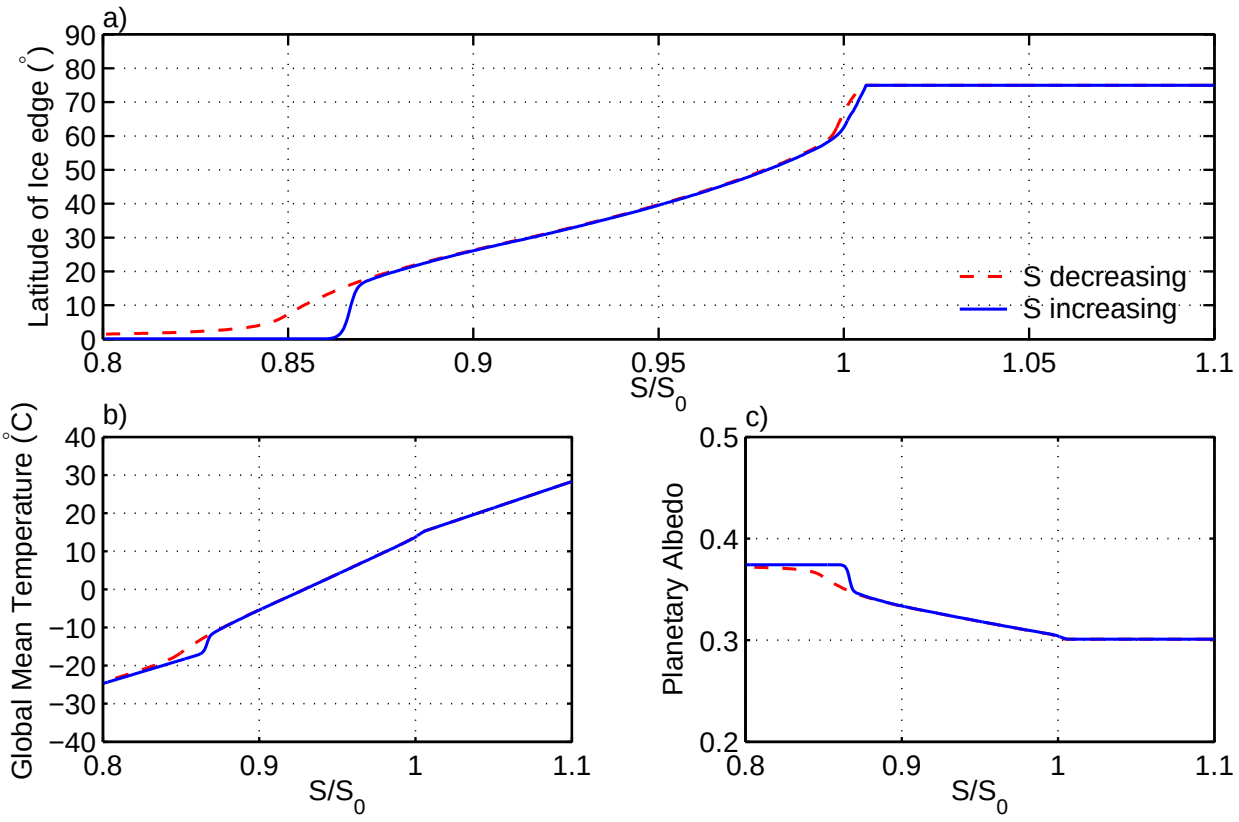


Figure 4-10: a) Annual mean ice edge latitude (degrees), b) global annual mean temperature ($^{\circ}C$), and c) global annual mean planetary albedo as a function of normalized solar constant ($S/S_0$) in an experiment with an active ice sheet.

parameterized moisture flux which is not accurate at low latitudes.

As the solar constant increases, the ice sheet retreats until it is completely melted for values of $S$ above $1.01S_0$. As in the experiments with a temperature dependent snow line, there is no evidence suggesting that a small ice sheet is unstable. There is a very small difference between the increasing and decreasing branches of the experiment when the ice sheet is small (figure 4-10a). However, this difference diminishes as the rate of change in solar constant is reduced, and is thought to be insignificant. In the experiment shown, the rate of change in $S$ is fixed at $1\%$ every $500$ Ka.

### 4.3.3 Parameterized Sea Ice

The experiments in the previous sections only take into account the effects of an ice sheet and temperature dependent snow cover over land surfaces. The effect of an interactive sea ice cover

| | no snow /no ice | active seaice /no ice | active seaice /active snow |
|---|---|---|---|
| Sensitivity parameter $\beta$ (°) | 138 | 187 | 282 |
| $\Delta T$ when $S + 2\%$ ($^\circ C$) | $+2.8$ | $+3.7$ | $+4.6$ |
| $\Delta T$ when $S - 2\%$ ($^\circ C$) | $-2.8$ | $-3.8$ | $-5.8$ |

Table 4.3: Sensitivity ($\beta$) of different model configurations with and without active snow, ice, and sea ice cover. In all four experiments the land fraction is set to $40\%$.

is not considered, as it requires an appropriate representation of the thermal mass and circulation in the ocean. Nevertheless, with these caveats in mind, an experiment with parameterized sea ice is briefly discussed here. In this simplified case, latitudes where the seasonal mixed layer temperatures are below freezing are considered to be covered by sea ice. The model does not account for any variations in the thickness of the sea ice, and as for snow and ice cover over land, the albedo of surfaces covered by sea ice is increased by $\delta\alpha_{seaice} = 0.186$.

Table 4.3 gives a summary of climate sensitivity for different model configurations when including an active sea ice cover. The experiment where both sea ice and snow cover is active is closest to previous studies with energy balance models without an interactive ice sheet (table 4.2). As expected, the sensitivity is increased when sea ice is included, as compared to the experiment with only an active snow cover in table 4.1. However, the sensitivity in the case with both an active sea ice and snow cover ($\beta = 282^\circ$) is comparable to the sensitivity found when increasing the snow albedo feedback to $\delta\alpha_{snow} = 0.40$ ($\beta = 290^\circ$; section 4.3.1).

To test the effect of including both a temperature dependent sea ice and snow cover on the stability of the model, the experiment in figure 4-7 on page 68 is rerun. Again, as can be seen in figure 4-11, the result is similar to that obtained when increasing the strength of the ice albedo feedback to $\delta\alpha_{snow} = 0.40$ (figure 4-9 on page 71), although the hysteresis loop is slightly wider.

Investigating the seasonal snow and sea ice cover as a function of normalized solar constant (figure 4-12), in the case when the solar constant is decreasing, shows that the seasonal cycle of sea ice is too small. At the same time, the sea ice cover extends to about $55^\circ N$ in summer for the current climate. This is partly due to the simple mixed layer ocean used in the model, and indicates

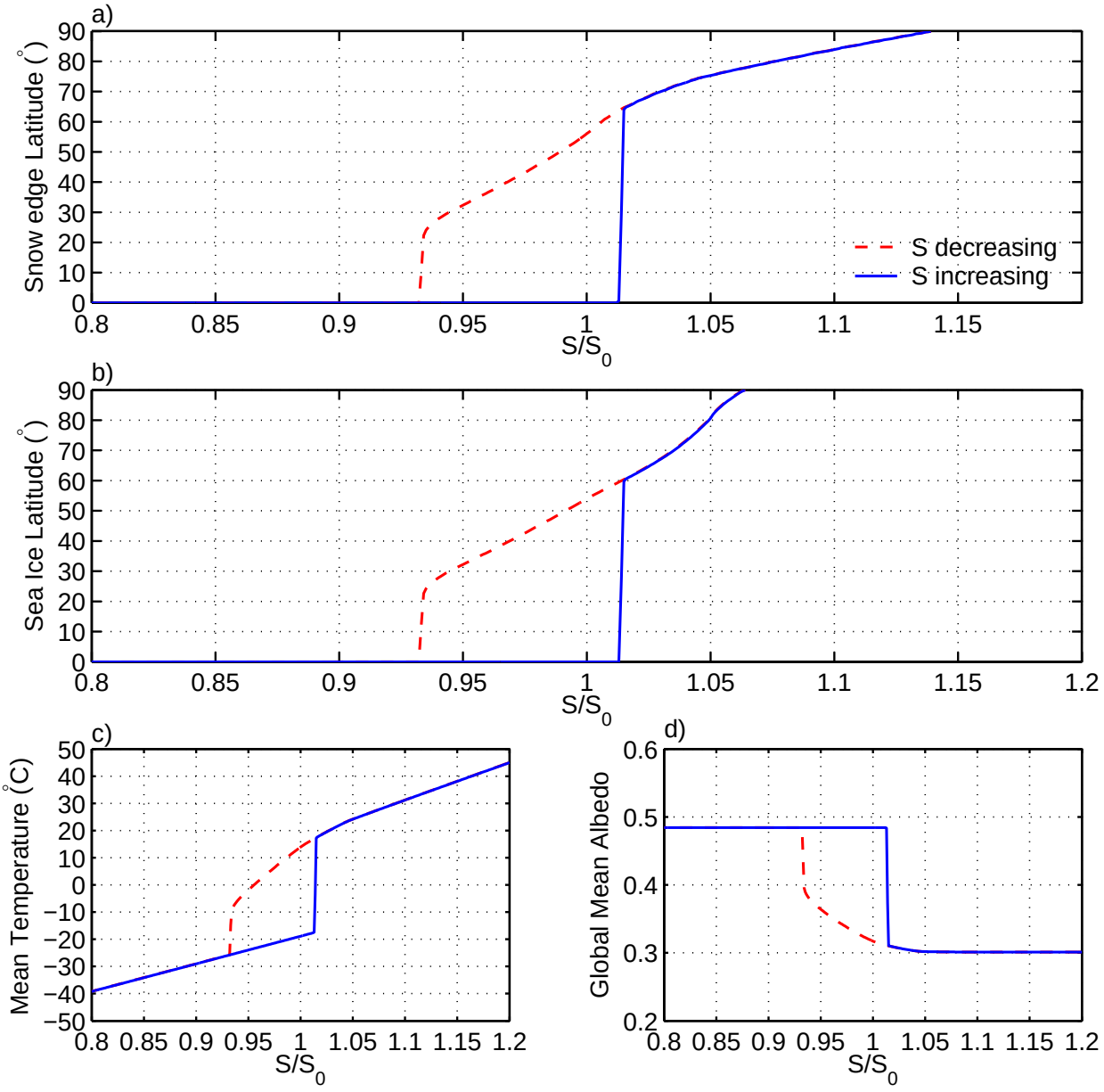


Figure 4-11: a) Annual mean snow edge latitude (degrees), b) annual mean sea ice latitude (degrees), c) global annual mean temperature ($^{\circ}C$), and d) global annual mean planetary albedo as a function of normalized solar constant ($S/S_0$). The experiment is run without an active ice sheet, but with snow cover over land and sea ice over ocean surfaces, both with $\delta\alpha_{snow} = \delta\alpha_{seaice} = 0.186$.

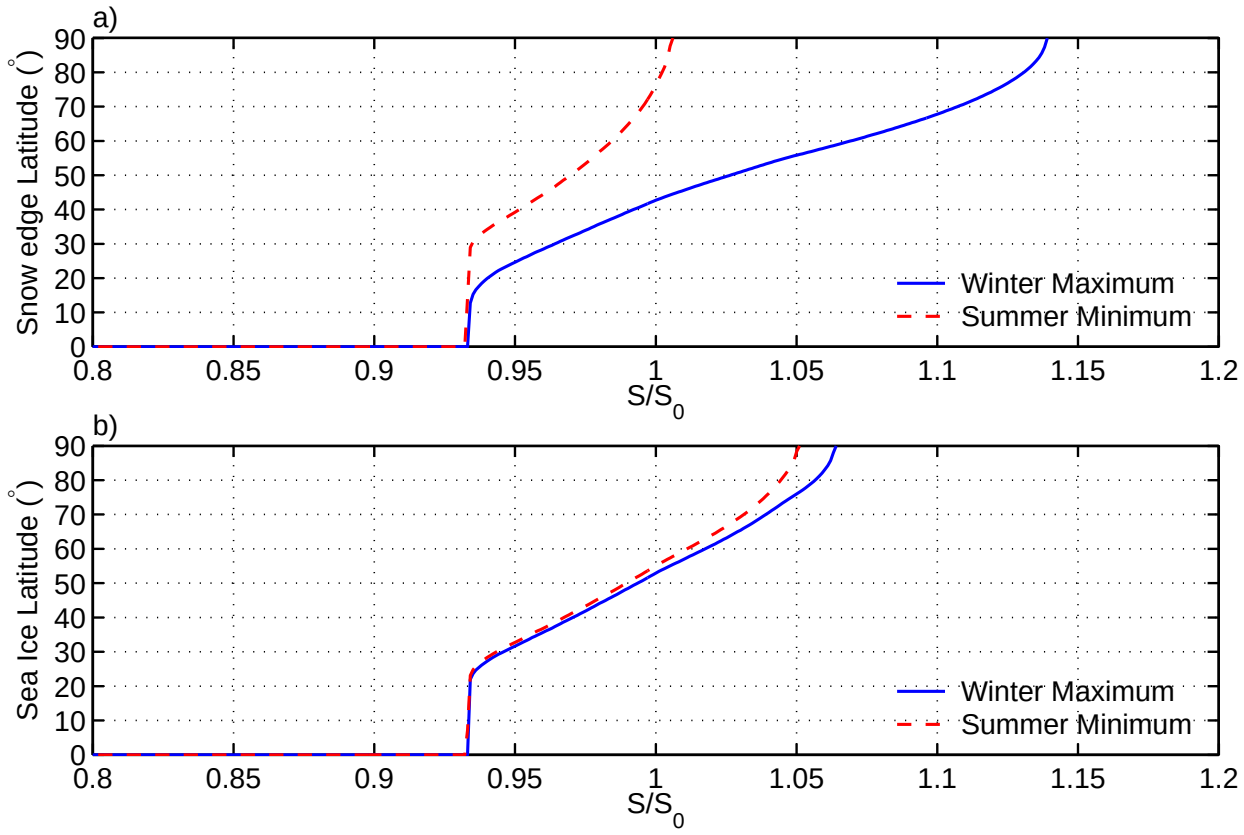


Figure 4-12: Seasonal a) snow, and b) sea ice cover limits as a function of normalized solar constant ($S/S_0$). The experiment is run without an active ice sheet, but with snow cover over land and sea ice over ocean surfaces, both with $\delta\alpha_{snow} = \delta\alpha_{seaice} = 0.186$.

that an appropriate representation of the deep ocean as well as an interactive ocean heat transport is required in order to accurately model sea ice.

## 4.4 Summary

A comparison of simulated and observed climate shows that the model does a reasonable job at estimating the present seasonal cycle and atmospheric fluxes of sensible and latent heat. However, a good apparent fit between simulated and observed climate is no guarantee that the response of the model to changes in external forcing, such as insolation, is realistic. Therefore, the sensitivity of the model to changes in solar constant is calculated and found to lie within the range $\beta = 138 - 219°$. The lowest sensitivity is found in an experiment without an active ice-albedo feedback, and the largest is found in an experiment with an active ice sheet. When parameterizing the ice-albedo feedback by fixing the snow line to the latitude of the $0°C$ isotherm, the sensitivity is $\beta = 166°$. This is significantly lower than values found in past studies with energy balance models, partly due to the improved albedo parameterization used in this study, and the increased strength of the negative dynamical flux feedback. When varying the solar constant within a range from 80% to 120% of today's value, the ice sheet is found to be relatively stable without any indications of the existence of multiple equilibria. However, when the strength of the snow-albedo feedback is increased, or when a simplified representation of sea ice is included, the sensitivity of the model is increased and multiple equilibria exist, in agreement with previous studies with energy balance models.

# Chapter 5

# Orbital Insolation and Ice Sheet Mass Balance

Changes in the solar constant result in a global change in insolation comparable at all latitudes and seasons. The only orbital parameter which gives a similar uniform change in insolation is eccentricity. However, the magnitude of the change in insolation due to variations in eccentricity is negligible. On the other hand, variations in obliquity and precession have a significant impact on the spatial and temporal distribution of insolation. Obliquity controls the relative amount of insolation received at low and high latitudes, and the main effect of precession is to redistribute insolation between summer and winter. As a result, the sensitivity of climate to changes in the orbital parameters is significantly different from changes in the solar constant and will be discussed in the following sections.

## 5.1 Obliquity

To test the sensitivity of the model climate to obliquity variations, the orbit is kept perfectly circular with eccentricity $e = 0$, thereby excluding the influence of variations in precession. Obliquity is varied within the range $21^\circ$ to $25^\circ$, where today's value is about $23.5^\circ$. The change in seasonal insolation due to a $4^\circ$ reduction in obliquity ($21^\circ - 25^\circ$) is shown in figure 2-2 on page 14: high

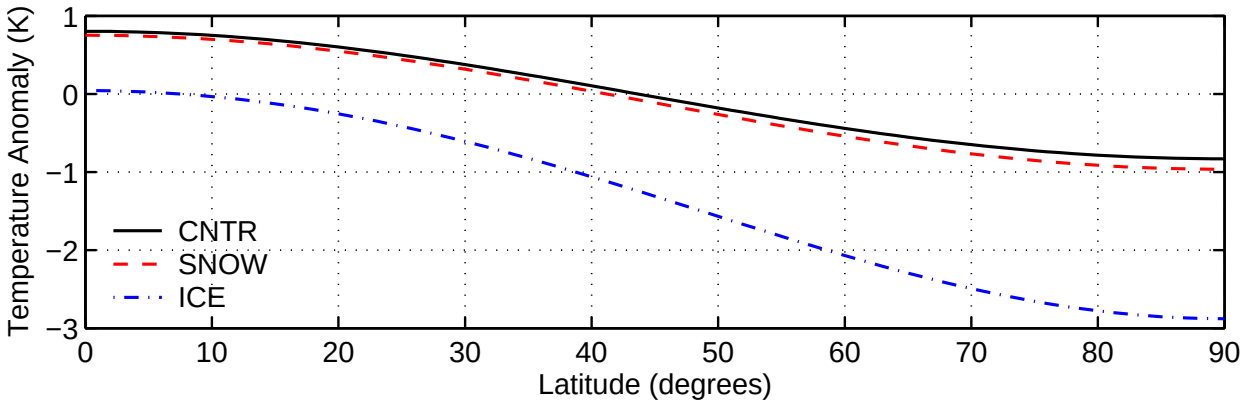


Figure 5-1: Change in annual mean meridional temperature structure of the model produced by a $4°$ decrease in obliquity ($21° - 25°$) for the case without snow or ice (CNTR), with a temperature dependent snow albedo (SNOW), and with an active ice sheet, but no snow (ICE).

latitude summertime insolation decreases, whereas mid latitude wintertime insolation increases.

To test the impact of changing obliquity on climate, three different model experiments are constructed as follows:

(CNTR) snow line is fixed at the latitude of the Arctic ocean ($75°N$), and there is no ice sheet;

(SNOW) seasonal snow cover over land follows the latitude of the $0°C$ isotherm;

(ICE) snow line is fixed at the latitude of the Arctic ocean, and an active ice sheet is included.

The difference in annual mean meridional temperature structure produced by a $4°$ decrease in obliquity from $25°$ to $21°$ is shown in figure 5-1 for the three different model experiments. Annual and zonal mean temperature is increased at low latitudes and reduced at high latitudes in the control experiment (CNTR) in response to the reduction in obliquity. This result does not change much when including an active snow cover (SNOW). However, in the experiment with an active ice sheet (ICE), the increase in meridional temperature gradient is amplified. In this case, tropical temperatures remain unchanged, whereas temperatures at high latitudes cool significantly when obliquity is reduced.

Figures 5-2a and 5-2b show the impact of obliquity variations on seasonal snow limits and ice cover over land in experiments SNOW and ICE, respectively. As found earlier when testing the

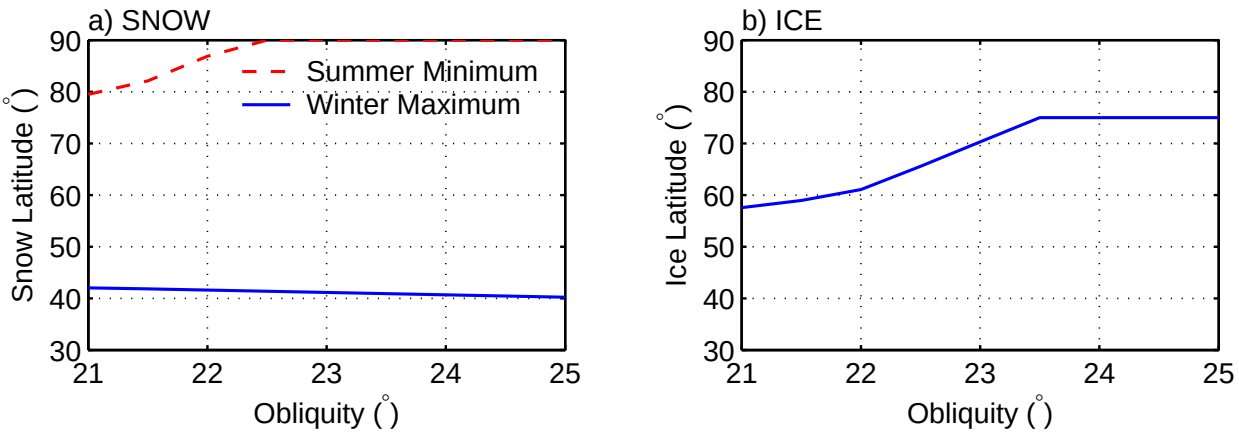


Figure 5-2: a) Seasonal snow cover limits as a function of obliquity in the experiment without an active ice sheet (SNOW). b) Latitude of the ice sheet margin as a function of obliquity for the experiment with an active ice sheet, but no snow (ICE).

response to changes in solar constant (section 4.3.1), the sensitivity of the minimum extent of snow in summer, is larger than the sensitivity of maximum snow extent in winter. Because minimum summer snow latitude represents the position of perennial, or permanent snow cover, it is often used as an indication of the position of the ice margin in climate models without an active ice sheet(e.g. *Budyko* (1969); *Sellers* (1969); *North* (1975); *Suarez and Held* (1979); *Schneider and Thompson* (1979)). In experiment SNOW, the permanent snow line retreats from $80°N$ to $90°N$ as obliquity is increased from $21°$ to $25°$. The maximum winter snow limit remains relatively unchanged close to $40°N$, with a slight retreat when obliquity is low.

The response of the ice sheet is larger than that observed for the snow line. In experiment ICE, the margin of the ice sheet retreats from $58°N$ to $75°N$, as obliquity is increased. This suggests that an active ice sheet with an explicit formulation of the surface mass balance is more sensitive to changes in obliquity than a temperature dependent snow line.

The response of climate to obliquity variations can be further understood by investigating the change in seasonal temperature structure. Figure 5-3 shows the change in zonal mean temperature over one seasonal cycle in response to a $4°$ decrease in obliquity. The results of experiments CNTR and SNOW are similar, with a decrease in high latitude summer temperatures and increase in low latitude winter temperatures. Maximum cooling ($\sim 3°C$) occurs about 20 days after sum-

mer solstice. When including an active ice sheet, the temperature change is increased significantly: summer temperatures at high latitudes are reduced by about $6°C$, whereas the change at low latitudes is less pronounced.

There are several feedbacks influencing the sensitivity of the system to obliquity changes. In experiment SNOW, a decrease in obliquity cools high latitude temperatures, resulting in the snow line moving toward the equator. This increases land surface albedo and enhances the initial cooling. However, a low obliquity also results in a steep meridional temperature gradient. This constrains the movement of the snow line and stabilizes the system. The experiments with and without a temperature dependent snow-albedo feedback (CNTR and SNOW) give similar results, suggesting that the sensitivity of the temperature dependent snow line to obliquity changes is small.

In the case with an active ice sheet, the increase in temperature gradient when obliquity is low enhances the transport of moisture to the ice sheet and therefore accumulation. At the same time, low obliquity cools high latitudes, reducing ablation. As a result, the ice sheet grows and cools high latitudes further. However, the expansion of the ice sheet is restricted by an increase in ablation as the margin of ice moves toward the equator. This constraint on ice growth is weaker than that imposed on the extent of the snow cover, and the ice sheet can expand beyond the zero degree isotherm. As a result, the change in high latitude temperature when including an active ice sheet is twice as large as when only including an active snow cover. This suggests that climate is more sensitive to changes in obliquity when including an explicit formulation of ice sheet mass balance.

## 5.2 Precession

The following set of experiments are designed to test the sensitivity of the model climate to changes in precession. Obliquity is kept constant at today's value of $\epsilon = 23.439°$. Eccentricity is fixed at a value of $e = 0.030$, which is about twice the current value, thereby increasing the amplitude of variations in precession. Figure 5-4 shows the change in annual mean meridional temperature due to a $180°$ change in longitude of perihelion ($\omega = -90°$ minus $\omega = +90°$) for the three different

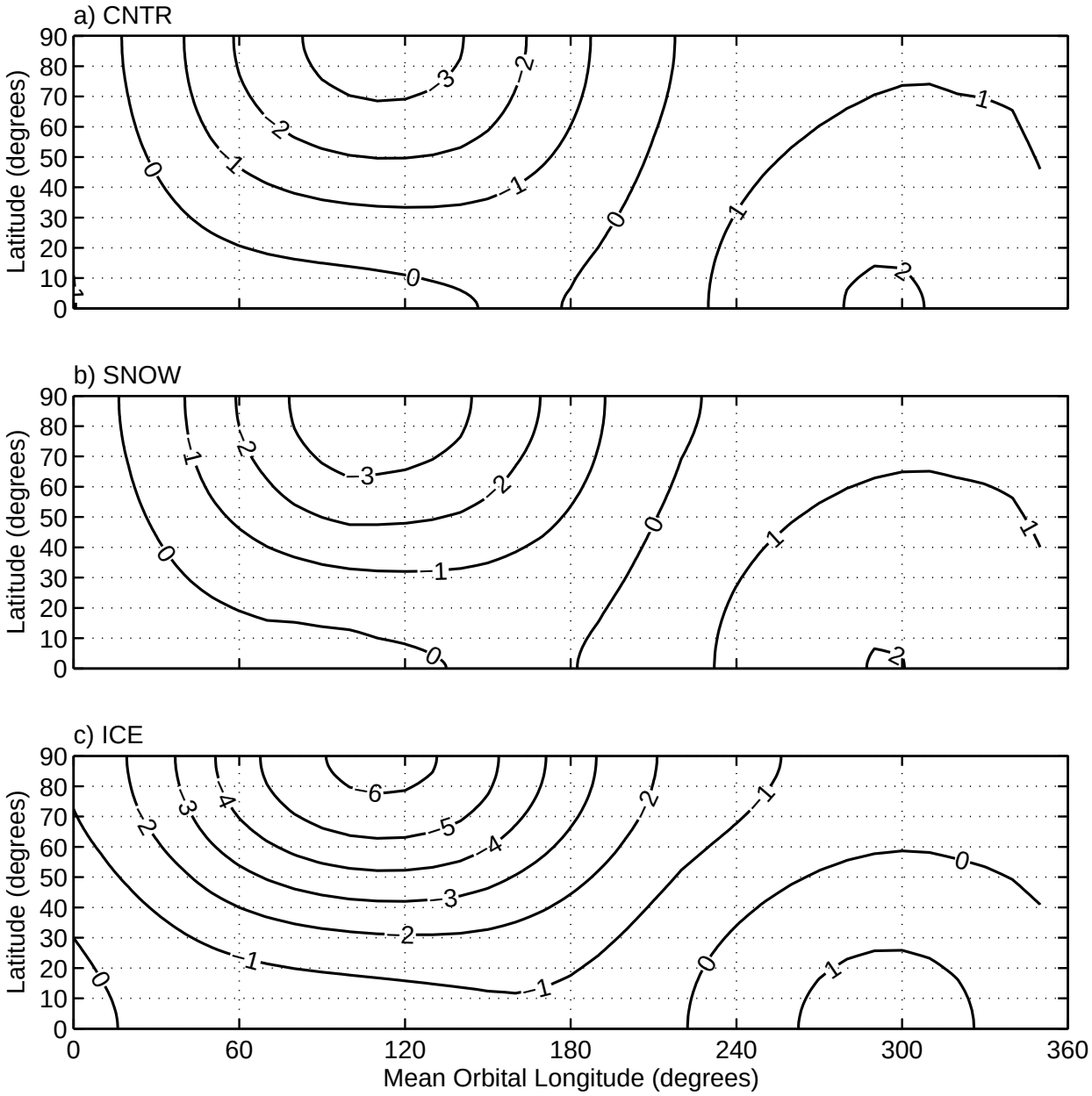


Figure 5-3: Change in zonal mean temperature of the model in response to a $4^\circ$ decrease in obliquity ($21^\circ - 25^\circ$) for experiments a) without varying snow or ice covers (CNTR), b) with temperature dependent snow albedo (SNOW), and c) with an active ice sheet, but no snow (ICE). The start of the year is fixed at spring equinox and the year is divided into $360$ degrees, where $90^\circ$ is summer solstice.

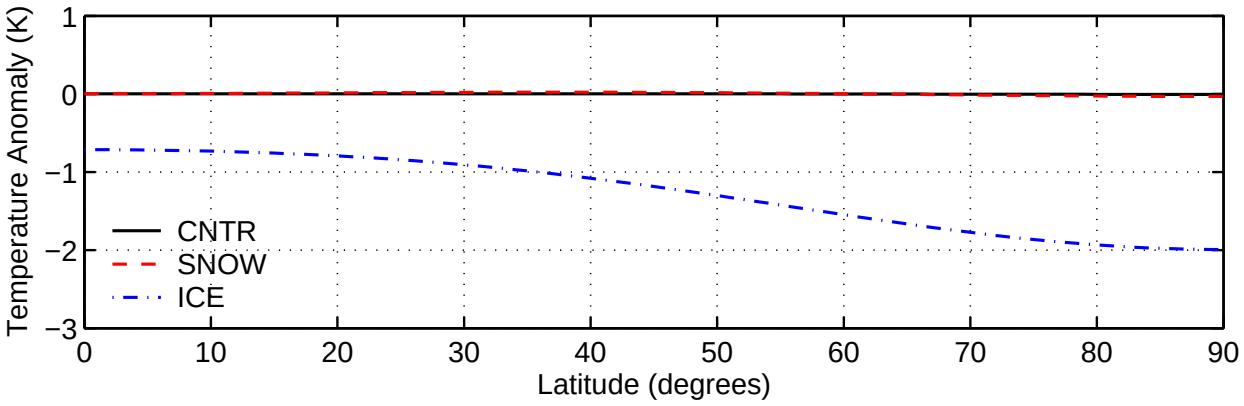


Figure 5-4: Change in annual mean meridional temperature structure of the model produced by a $180°$ change in the longitude of perihelion ($\omega = +90°$ minus $\omega = -90°$) for the case without snow or ice (CNTR), with a temperature dependent snow albedo (SNOW), and with an active ice sheet, but no snow (ICE).

model experiments described in the previous section (CNTR, SNOW, & ICE). At $\omega = -90°$, perihelion coincides with winter solstice, giving warm winter and cool summer seasons. Conversely, at $\omega = +90°$, perihelion coincides with summer solstice, giving cool winter and warm summer seasons (figure 2.1 on page 14).

Figures 5-5a and 5-5b show the impact of changes in longitude of perihelion on seasonal snow limits and ice cover over land in experiments SNOW and ICE, respectively. As opposed to the previous set of experiments (figure 5-4), which gives the response to a fixed change in longitude of perihelion, these two experiments give the equilibrium response of snow and ice cover at all possible longitudes of perihelion.

As can be seen in figure 5-4, annual and zonal mean temperature remains unchanged in experiment CNTR regardless of the change in longitude of perihelion. In this experiment there is no active snow- or ice-albedo feedback, and the effects of changes in longitude of perihelion on insolation cancel when averaged over an annual cycle. Therefore, the annual mean response is expected to be negligible. On the other hand, seasonal variations in snow, or ice cover can result in an annual mean temperature change. When including a temperature dependent albedo (SNOW) this response is very small: there is a slight warming of mid-latitudes due to a small retreat of the winter snow line and a slight cooling at high latitudes as the summer snow line advances (figure 5-5a).

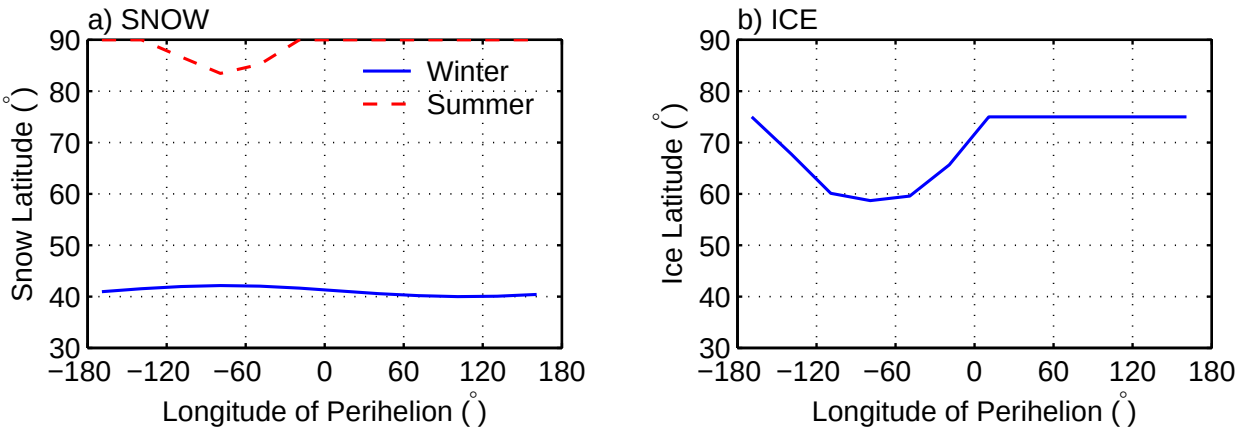


Figure 5-5: a) Seasonal snow cover limits as a function of longitude of perihelion ($\omega$) in the experiment without an active ice sheet (SNOW). b) Latitude of the ice sheet margin as a function of $\omega$ for the experiment with an active ice sheet, but no snow (ICE).

In the experiment with an active ice sheet (ICE) the response of annual mean temperature to a change in longitude of perihelion is significantly larger, and increases with latitude (figure 5-4). This is caused by an expansion of the ice sheet from $75°N$ to about $60°N$ when $\omega = -90°$, and perihelion coincides with winter solstice (figure 5-5b). On the other hand, when perihelion coincides with summer solstice ($\omega = +90°$), the ice sheet is completely melted.

Figure 5-6 gives the change in zonal mean meridional temperature over one seasonal cycle in response to a $180°$ change in longitude of perihelion, going from an orbital configuration where perihelion coincides with summer solstice ($\omega = +90°$) to a situation where it coincides with winter solstice ($\omega = -90°$). The results for experiments CNTR and SNOW are similar, with a decrease in summer temperatures at all latitudes, and a slight increase in temperatures during the rest of the year. When including an active ice sheet, cooling is enhanced at high latitudes during summer. The maximum cooling is about the same magnitude as obtained in the experiment with a $4°$ change in obliquity. However, here the expansion of the ice sheet is dominated by a reduction in melting, rather than an increase in accumulation as observed when reducing obliquity.

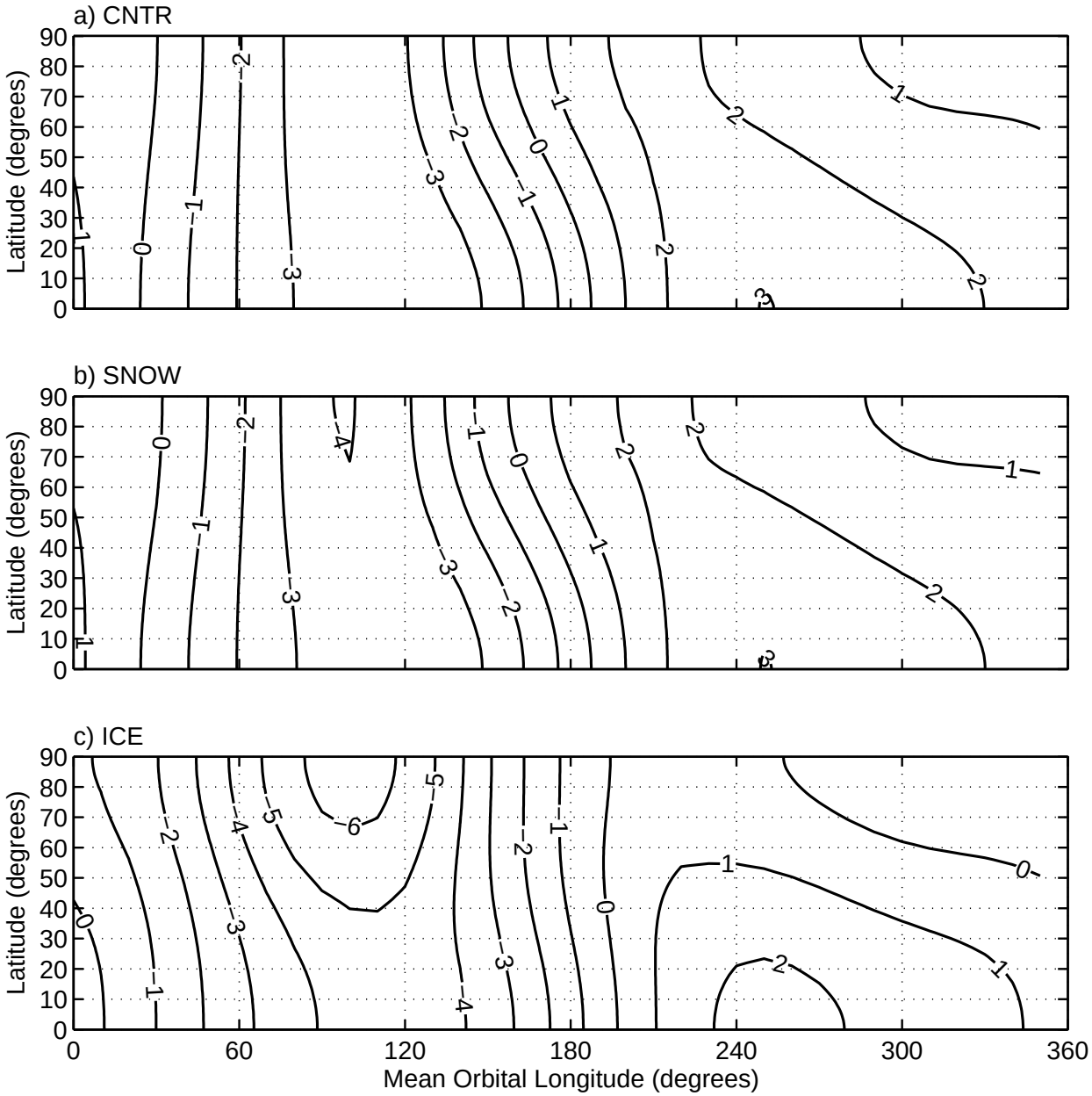


Figure 5-6: Change in zonal mean temperature of the model in response to a $180°$ change in longitude of perihelion ($\omega = -90°$ minus $\omega = +90°$) for experiments a) without varying snow or ice covers (CNTR), b) with temperature dependent snow albedo (SNOW), and c) with an active ice sheet, but no snow (ICE). The start of the year is fixed at spring equinox and the year is divided into $360°$, where $90°$ is the summer solstice.

| | Obliquity ($\varepsilon$) | Perihelion ($\omega$) | Eccentricity ($e$) |
|---|---|---|---|
| Glacial Inception | low | $-90^\circ$ | high |
| Deglaciation | high | $+90^\circ$ | high |

Table 5.1: Optimal orbital configurations for growth (glacial inception) or decay (deglaciation) of ice sheets in the Northern Hemisphere.

## 5.3 Last Interglacial and Glacial Inception

Combining the results of the previous two sections, it is possible to predict the orbital configuration which is most conducive to growth, or decay of ice sheets in the Northern Hemisphere. The optimal conditions are listed in table 5.1: a combination of low obliquity, perihelion at winter solstice, and high eccentricity is preferential for the growth of ice. Low obliquity enhances poleward transport of moisture during all seasons, and increases accumulation on the ice sheets. When perihelion coincides with winter solstice the Earth is closest to the Sun in winter, resulting in warm winter and cool summer seasons, with relatively low melting in summer. However, the impact of changes in longitude of perihelion is only significant if eccentricity is high.

Optimal conditions for deglaciation is a combination of high obliquity, perihelion at summer solstice, and high eccentricity. High obliquity reduces accumulation by weakening the meridional temperature gradient. Perihelion at summer solstice results in cool winter and warm summer seasons, with relatively high rates of summer melt. Note that in the case of obliquity and eccentricity, the same criteria for glacial growth or decay are valid in the Southern Hemisphere. However, the effect of longitude of perihelion is opposite in the Southern Hemisphere. This means that variations in ice sheet mass dominated by obliquity, or eccentricity would be synchronous in both hemispheres, whereas ice sheets dominated by precession would be of opposite phase in the two hemispheres.

Two time periods which are often discussed in the literature are the last interglacial at about $126$ Ka BP, and the last glacial inception at about $115$ Ka BP (*Gallimore et al.*, 1995; *Khodri et al.*, 2001). As shown in table 5.2 these two time periods have orbital configurations close to the optimal conditions for growth and decay of ice. Eccentricity is almost at its maximum, and perihelion is

| Time (Ka BP) | Obliquity ($\varepsilon$) | Perihelion ($\omega$) | Eccentricity ($e$) |
|---|---|---|---|
| $0$ | $23.44°$ | $-78.67°$ | $0.017$ |
| $115$ | $22.45°$ | $-68.99°$ | $0.044$ |
| $126$ | $23.99°$ | $111.24°$ | $0.041$ |

Table 5.2: Values of obliquity, longitude of perihelion, and eccentricity at the last glacial inception ($\sim 115$ Ka BP) and last interglacial ($\sim 126$ Ka BP), in addition to the modern values ($0$ Ka BP).

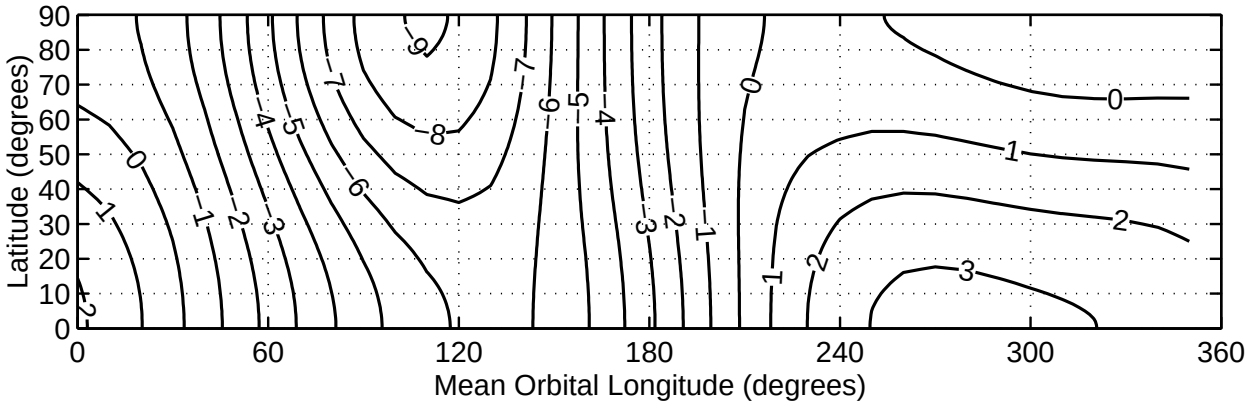


Figure 5-7: Difference in zonal mean temperature between the last interglacial ($126$ Ka BP) and glacial inception ($115$ Ka BP) as a function of mean orbital longitude in experiments with an active ice sheet, but no snow.

close to either winter or summer solstice. The difference in obliquity between the two time periods is not optimal, but it is relatively low at glacial inception and high during the interglacial.

When applying the two orbital configurations in experiments with an active ice sheet but no snow cover, the ice extends to $55°N$ at $115$ Ka BP, whereas it is completely melted at $126$ Ka BP. The difference in zonal mean temperature between $126$ and $115$ Ka BP as a function of time of the year is shown in figure 5-7. High latitude summer temperatures at $115$ Ka BP are $-9°C$ colder than at $126$ Ka BP, mostly in response to the difference in longitude of perihelion and the presence of a relatively large ice sheet. The magnitude of the response is significantly larger than the $-6°C$ cooling found in the previous two sections where obliquity and precession are varied individually (figures 5-3 & 5-6). However, it should be noted that the change in obliquity between the last glacial inception and last interglacial is only about $1.5°$. This is smaller than the possible range of obliquity variations, suggesting that the response of the climate system can be significantly larger.

The seasonal variation in accumulation and ablation during the two time periods is shown in

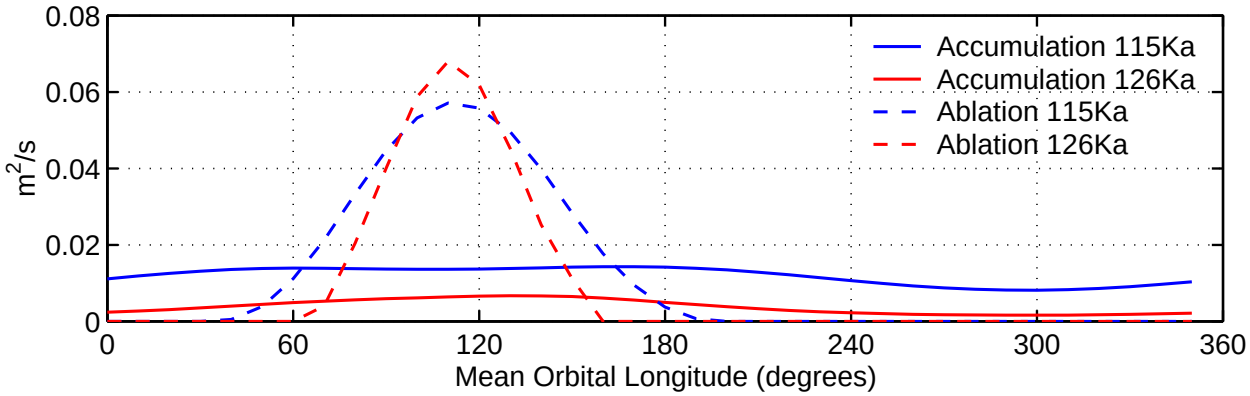


Figure 5-8: Seasonal variation in accumulation and ablation at the last interglacial ($\sim 126$ Ka BP) and glacial inception ($\sim 115$ Ka BP) as estimated by the model with an active ice sheet.

figure 5-8. At glacial inception ($115$ Ka BP) obliquity is low, and the meridional temperature gradient is enhanced, resulting in an increase in accumulation. In contrast to precession, a change in obliquity does not have a strong seasonal preference, and accumulation is increased at all times of the year. At the same time, the earth is furthest from the sun at summer solstice giving relatively cool summer and warm winter seasons. As a result, the maximum rate of ablation in summer is reduced, whereas the length of the melt season is slightly increased.

During the interglacial period ($126$ Ka BP), obliquity is large and the meridional temperature gradient is weak, thereby reducing accumulation. Perihelion is at a longitude of $111.2°$, meaning that the earth is close to the sun at summer solstice. In effect, the summer season is relatively warm and ablation is high, whereas the melt season is short.

## 5.4 Summary

At equilibrium, changes in obliquity and precession have a relatively large impact on ice cover and high latitude climate. However, the response of snow cover, as represented by the $0°C$ isotherm, is small when averaged over an annual cycle. The change in snow cover is only significant in summer when the temperature gradient is relatively weak.

In the case of the ice sheet, optimal conditions for ice growth are attained when: 1) obliquity is low; 2) eccentricity is high; and 3) perihelion coincides with winter solstice. Low obliquity

strengthens the meridional temperature gradient, which in turn increases the flux of moisture to high latitudes and the accumulation of ice. At the same time, low obliquity cools high latitudes, reducing surface melt in summer. When perihelion coincides with winter solstice, the Earth is closest to the Sun in winter, resulting in relatively warm winter and cool summer seasons. As a result, summer surface melt on the ice sheet is reduced. This effect is particularly strong when eccentricity is large.

It should be kept in mind that the experiments described here are all run to equilibrium. In this case, the response can be relatively large, and it is not certain that the response to a time varying forcing will be of similar magnitude. Although, the time scale for changes in orbital insolation is longer than the response time of the atmosphere-ocean system, it is comparable to the response time of large continental ice sheets and the underlying bedrock. However, the three criteria for ice growth summarized above are thought to be valid for the time varying problem, and will be used in the following chapter in at attempt to understand what physical mechanisms caused the observed variations in ice volume in the late Pliocene and early Pleistocene.

# Chapter 6

# Late Pliocene and Early Pleistocene Glacial Cycles

One of the strengths of the model developed in this study is its ability to perform long time integrations covering multiple cycles in precession, obliquity, and eccentricity. This chapter will investigate the physics governing the oscillations in ice volume observed in the proxy record, with emphasis on the glacial cycles of the late Pliocene and early Pleistocene. It should be kept in mind that the model experiments described are not attempts at simulating past climate, rather they are intended to test the sensitivity of the ice-atmosphere system to changes in orbital insolation. This is also why the model is kept simple, such that it is possible to understand the underlying physics.

Before describing the model experiments, the following section briefly discusses the origin of the large continental ice sheets believed to have played such a dominant role in the climate of the past 3 Ma. This topic was the motivation of a study on the influence of the Central American Seaway on changes in ocean circulation in the middle Miocene and early Pliocene (*Nisancioglu et al.*, 2003). A few of the conclusions from this study are discussed below, however the reader is referred to appendix B for further details.

## 6.1 Origin of Northern Hemisphere Ice Sheets

The $\delta^{18}O$ records of benthic and planktonic foraminifera indicate that temperatures in the ocean decreased by about $15°C$ during the Cenozoic ($67 - 0$ Ma BP) (*Miller and Fairbanks.*, 1985; *Crowley and North*, 1991, p. 183). The early Pliocene ($5.3 - 3.6$ Ma BP), frequently called the Pliocene warm period, can be seen as a pause in the general cooling trend, with high latitude sea surface temperatures $\sim 5 - 8°C$ warmer than today (*Dowsett et al.*, 1996; *Crowley*, 1996). The general cooling trend continued in the late Pliocene ($3.6 - 1.8$ Ma BP) from about $3$ Ma BP, and at about $2.8 - 2.6$ Ma BP there was a significant expansion of ice cover, in particular at high latitudes of the Northern Hemisphere (*Shackleton et al.*, 1984; *Jansen et al.*, 1988; *Raymo*, 1994).

So far, no satisfactory explanation has been found for the cause of expansion of ice cover in the late Pliocene, although it is one of the largest and most important changes in past climate (see review by *Raymo* (1994)). Two recent hypotheses are that the gradual Cenozoic cooling trend (*Philander and Fedorov*, 2003), or the closure of the Indonesian seaway $4 - 3$ Ma BP *Cane and Molnar* (2001) cooled the east equatorial Pacific and reduced atmospheric heat transport from the tropics to higher latitudes, stimulating global cooling and the eventual growth of ice sheets. Another school of thought is that the expansion of ice is related to the closure of the Central American Seaway (CAS) about $5 - 3$ Ma BP (*Kaneps*, 1979; *Keigwin*, 1982; *Stanley*, 1995; *Haug and Tiedemann*, 1998; *Driscoll and Haug*, 1998). Before this time, the CAS was open, connecting the Pacific and Atlantic basins with a seaway at about $10°N$. This allowed for flow of relatively low salinity surface water from the Pacific to the Atlantic, freshening the surface of the North Atlantic, and inhibiting the production of deep water.

According to *Haug and Tiedemann* (1998), the closure of the CAS strengthened the Gulf Stream and the transport of warm saline water to high latitudes of the North Atlantic. This increased the production of North Atlantic Deep Water (NADW), leading to greater evaporative cooling of surface waters at high latitudes, and increased atmospheric moisture content. Combined with favorable orbital obliquity, the enhanced moisture content would facilitate a buildup of ice sheets in the Northern Hemisphere. *Driscoll and Haug* (1998) propose a similar mechanism, involving en-

hanced freshwater delivery to the Arctic via Siberian rivers and formation of sea ice. An increase in sea ice cover would have increased surface albedo, and insulated the high heat capacity of the ocean from the atmosphere. Thus, the insulating effect of sea ice would have reduced the warming expected at high latitudes from the increase in poleward heat transport by the ocean.

Early experiments with an ocean GCM suggest that the Atlantic meridional overturning circulation is severely reduced, or non existent when the CAS is open (*Maier-Reimer et al.*, 1990). As the CAS closes, the flow of relatively fresh water from the Pacific to Atlantic is cut-off, and the modern overturning circulation is established with formation of NADW at rates comparable to present. Similar experiments with the MIT ocean GCM indicate that significant amounts of NADW are formed even when the CAS is open, and that the modern overturning circulation is established at the time the CAS shoals to a depth of about $1000$ m in the middle Miocene (*Nisancioglu et al.*, 2003; appendix B). At the time of the final closure of the CAS, the meridional overturning circulation is strengthened. As a result, total global poleward ocean heat transport is enhanced by about $10\%$, due mostly to a $30\%$ increase in heat transport by the North Atlantic.

The predicted increase in heat transport by the North Atlantic at the time of the final closure of the CAS is in agreement with the studies of *Haug and Tiedemann* (1998) and *Driscoll and Haug* (1998). However, whether this event is related to enhanced growth of ice in the Northern Hemisphere is not clear. The hypotheses of *Haug and Tiedemann* (1998) and *Driscoll and Haug* (1998) imply that an increase in sea surface temperatures in the northern latitudes of the Atlantic basin, produce an increase in precipitation and accumulation of snow on high latitude land surfaces. As has been shown in this study, accumulation is not simply related to local temperature. Instead, accumulation is governed by the poleward flux of moisture by the atmosphere, which is related to both the local temperature and the strength of the meridional temperature gradient.

Further, if the climate system is at equilibrium, and planetary albedo and orbital configuration remains unchanged, an increase in poleward heat transport by the ocean would imply a reduction in poleward heat transport by the atmosphere (*Stone*, 1978). If this is the case, an increase in heat transport by the North Atlantic as the CAS closed, would cause a reduction in heat transport by the

atmosphere (*Nakamura et al.*, 1994). As a result, transport of moisture by the atmosphere would decrease, thereby reducing accumulation, and the potential for growth of ice sheets.

Following these arguments it is unlikely that the closure of the CAS caused the onset of enhanced glaciation. As suggested by *Berger and Wefer* (1996), the predicted increase in poleward ocean heat transport may have delayed the onset of Northern Hemisphere glaciation by several million years. In effect, the shoaling of the CAS probably had a profound effect on ocean circulation in the Miocene, and the eventual closure could have been the cause of the early Pliocene warm period ($\sim 5 - 3$ Ma BP). However, another explanation has to be found for the cause of the observed expansion of ice cover $\sim 2.8 - 2.6$ Ma BP.

## 6.2 Late Pliocene to Early Pleistocene Ice Volume

From the beginning of the period with enhanced glaciation in the late Pliocene, oscillations in benthic $\delta^{18}O$ followed cycles with a period of $41$ Ka, and an amplitude about one third to one half of the $\sim 100$ Ka cycles observed in the late Pleistocene (figure 2-4 on page 19). Numerous studies have tried to understand the large $\sim 100$ Ka cycles in global ice volume (e.g. *Weertman* (1976); *Oerlemans* (1980); *Pollard* (1982); *Hyde and Peltier* (1987); *Gildor and Tziperman* (2001)). However, very few have investigated the dynamics of the $41$ Ka cycles discussed in this study. When constructing model experiments which are to be run on orbital time scales ($> 10$ Ka) GCMs are too slow, and it is necessary to parameterize several of the physical processes involved. In most studies including a representation of ice sheets, the hydrological cycle is very crude and variations in accumulation are only influenced by local temperature (e.g. *Gallee et al.* (1992); *Deblonde et al.* (1992); *Berger et al.* (1999); *Huybrechts and de Wolde* (1999)). The model used in this study is highly simplified, making it extremely efficient and capable of running experiments spanning several million years. At the same time, a physical representation of the dependence of accumulation on atmospheric moisture transport is included.

In the following experiment, named ICE600 (table 6.1), the coupled atmosphere-ice model is

| Name | Description |
|---|---|
| ICE600 | Control experiment with an active ice sheet and no snow |
| ACC600 | Temperature dependent accumulation |
| COLD600 | Cold climate with a large ice sheet |
| SNOW600 | Temperature dependent snow cover and no ice |

Table 6.1: List of model experiments.

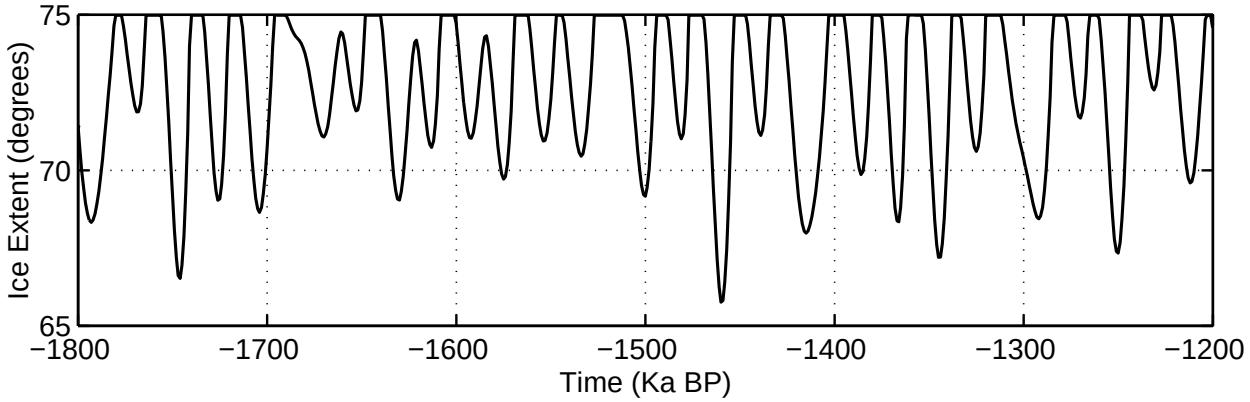


Figure 6-1: $600$ Ka of ice sheet extent ($1.8 - 1.2$ Ma BP) calculated by using the orbital solution of *Laskar et al.* (1993).

run for $600$ Ka forced with insolation for the period from $1.8$ to $1.2$ Ma BP, calculated using the orbital solution of *Laskar et al.* (1993). This period is taken to represent typical conditions of the late Pliocene to early Pleistocene, and insolation reconstructions for any other time period within the last $3$ Ma will give similar results. As before, the area north of $75°N$ is permanently covered by sea ice, and the ice sheet is restricted to land areas south of $75°N$. The standard parameters for the atmosphere and ice models are given in tables 3.1 (page 37) and 3.3 (page 50), respectively.

Figure 6-1 shows the change in meridional extent of the ice sheet with time. The latitude of the ice margin varies from about $66°N$ at its maximum to $75°N$, when it is completely melted. The model does not calculate the zonal extent of the ice sheet. However, at its maximum extent its meridional cross section is about $7 \times 10^8\, m^2$. If, for simplicity, it is assumed that the ice sheet has a fixed width of $6000\, km$, it's volume is approximately $4 \times 10^{15}\, m^3$. Using an ice density of $\rho_{ice} = 920\, kg/m^3$ and assuming that the total area of the Earth covered by ocean is about $3.6 \times 10^{14}\, m^2$ (71% of the Earth's surface), the maximum ice sheet extent calculated by the model

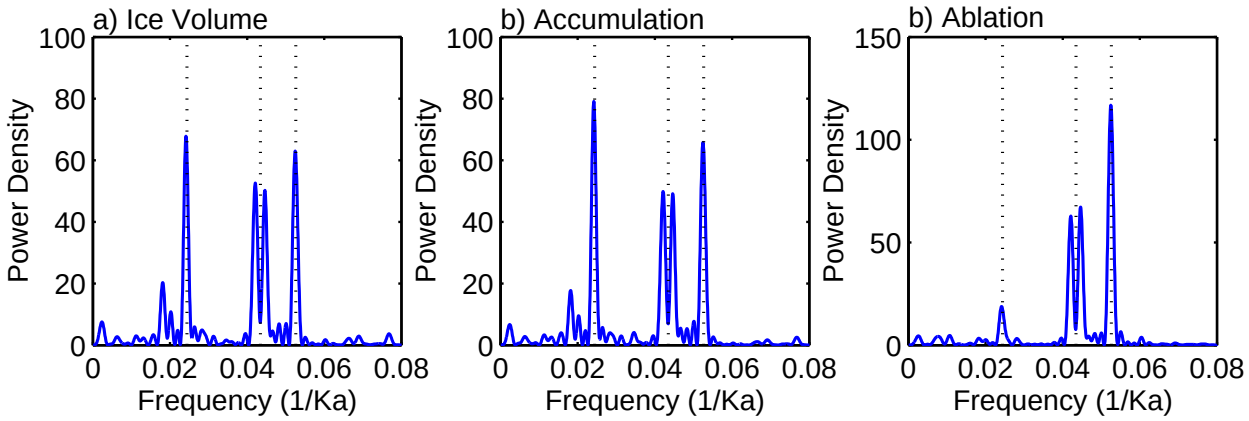


Figure 6-2: Power spectra of mean annual a) ice volume, b) accumulation, and c) ablation for the period $1.8 - 1.2$ Ma BP.

corresponds to a sea level lowering of about $10\,m$.

According to the $\delta^{18}O$ record (figure 2-4 on page 19), oscillations in late Pliocene to early Pleistocene ice volume could have contributed to a sea level change as large as $40$ to $60$ m. This is significantly larger than the amplitude of changes in ice volume estimated by the model. However, the model is highly simplified, and there are several important positive feedbacks in the climate system, such as $CO_2$, sea ice, and vegetation, which have not been included. It is conceivable that the amplitude of the oscillations in ice volume will be amplified in a model where these processes have been included.

At the same time, it is quite possible that the large amplitude oscillations in global ice volume observed in the proxy record cannot be explained as a direct response to variations in orbital insolation. Instead, it is likely that at least part of the oscillations in ice volume are a result of nonlinear self-sustained, or stochastic processes. Both of these options have been suggested as explanations for the larger amplitude $\sim 100$ Ka glacial cycles observed in the last $\sim 0.8$ Ma of the proxy record (e.g. *Kallen et al.* (1979); *Kominz and Pisias* (1979)).

However, it should be kept in mind that it is not possible to ascertain from the $\delta^{18}O$ ice volume record what portion of the variations in $\delta^{18}O$ observed in the period $\sim 2.8 - 0.8$ Ma BP are due to changes in temperature (see section 2.2 on page 17), or what portion is due to changes in ice volume on Antarctica. This issue will be discussed later in section 7.4.

Power spectra of mean annual ice volume, accumulation, and ablation calculated by the model for the period $1.8 - 1.2$ Ma BP are given in figure 6-2. As can be seen for ice volume, the strongest peak in the power spectrum is at the obliquity frequency ($1/41$ Ka). However, the difference between the strength of the obliquity and precession signals in the record is insignificant, and the response of ice volume to the two is approximately equal. As expected, there is no response of ice volume at the $100$ Ka eccentricity period, due to the negligible influence of eccentricity variations on insolation.

In the case of ablation, there is a clear dominance of precession frequencies ($1/19$ Ka, $1/23$ Ka), with a negligible contribution by obliquity. This is due to the strong dependence of surface melt on summer temperatures: melt only occurs during a few months in summer when temperatures on the surface of the ice are above freezing. Such a preference for a particular season rectifies the annual cycle and enhances the response to precession (*Schneider and Thompson*, 1979; *Kim et al.*, 1998; *Huybers and Wunsch*, 2003). If melt occurred at all times of the year, the response to precession would be small, as it's effect would cancel when averaged over an annual cycle.

The power spectrum of mean annual accumulation shows a slight dominance of obliquity, although precession frequencies are relatively strong. The influence of obliquity on accumulation is due to the control of the meridional temperature gradient on transport of moisture to the ice sheet. The precession signal in accumulation is introduced by the dependence of moisture transport on local temperature at the margin of the ice. Variations in local temperature are mostly due to changes in precession, amplified by the ice-albedo feedback. However, temperature changes at the ice margin are enhanced by the movement of the ice sheet. Therefore, any changes in latitude of the ice margin due to variations in ablation will have an impact on accumulation, and strengthen the precession signal.

In the experiments presented here the effect of an interactive sea ice cover is not considered, as it requires a representation of the thermal mass and circulation of the ocean. However, as a first test of the effect of sea ice, the parameterized sea ice cover described in section 4.3.3 on page 72 is adopted, and experiment ICE600 is rerun. In this case, the results of figure 6-1 and the amplitude of

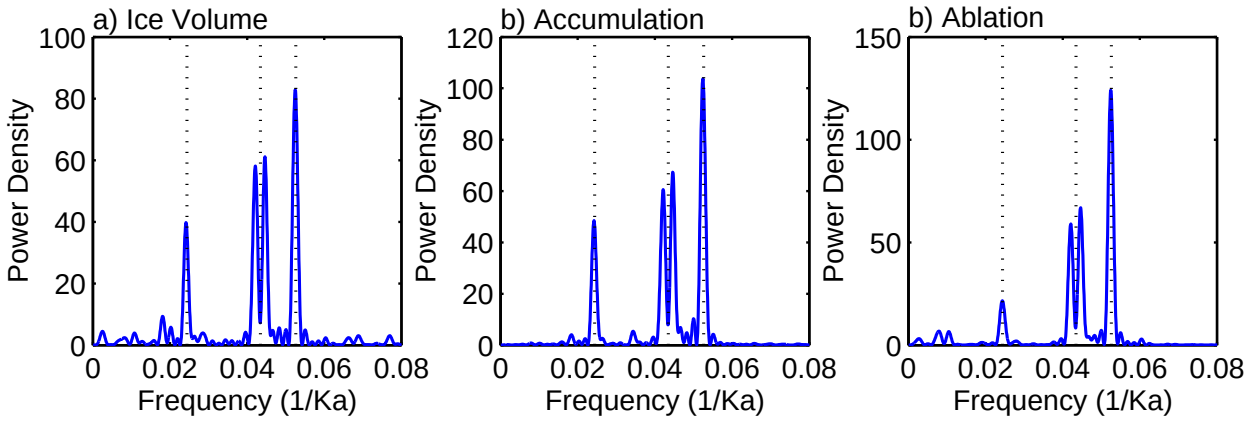


Figure 6-3: Power spectra of mean annual a) ice volume, b) accumulation, and c) ablation for the period $1.8 - 1.2$ Ma BP in an experiment where accumulation only depends on local temperature.

the response of the ice sheet remains unchanged. This indicates that an increased climate sensitivity, as defined by equation 4.1 on page 63, does not simply translate into an increased sensitivity of land based ice sheet extent in response to varying orbital insolation.

### 6.2.1 Temperature Dependent Accumulation

The results of the previous experiment (ICE600) suggest that the impact of obliquity on variations in ice volume are mostly a consequence of the dependence of accumulation on the meridional temperature gradient. In order to test this observation, the experiment is repeated with the relation between accumulation and temperature gradient removed. In this experiment, named ACC600, accumulation only depends on local temperature at the ice sheet margin, and the gradient term in equation 3.11 on page 45 is omitted. Except for the change in the parameterization of accumulation, the model configuration is unchanged.

Power spectra of mean annual ice volume, accumulation, and ablation for the period $1.8 - 1.2$ Ma BP are given in figure 6-3. The power spectrum of ablation is nearly identical to that found in experiment ICE600 (figure 6-2). However, in the case of accumulation, the influence of obliquity is significantly reduced. As a consequence, the impact of obliquity on variations in ice volume is also reduced.

Although the obliquity signal in the power spectrum of accumulation is weakened, it is still

significant. This suggests that there is an additional source of variability at the obliquity period in the accumulation record other than the meridional temperature gradient. This is most likely a result of accumulation occurring at all times of the year. In this case, when averaging over a full annual cycle, the response to precession cancels, enhancing the relative role of obliquity. Therefore, the strong precession signal in the power spectrum of accumulation is a result of variations in the ice margin imposed by changes in ablation.

### 6.2.2 Cold Climate with Large Ice Sheets

In the past $3$ Ma, ice volume increases slowly in response to the general cooling trend dominating throughout most of the Cenozoic, culminating at about $800$ Ka BP when large $\sim 100$ Ka oscillations in ice volume become dominant (figure 2-4 on page 19). The dynamics of these large ice sheets is likely to have been different from the smaller ice sheets present in the late Pliocene and early Pleistocene. In particular, deglaciations in the last part of the record are relatively rapid, suggesting that some strong non linear processes are involved in destabilizing an ice sheet when it has reached a certain maximum size.

Although it is not within the scope of this study to understand the dynamics of the large $\sim 100$ Ka oscillations in ice volume, it would be useful to understand how the surface mass balance depends on the size of the ice sheet. To investigate this, an experiment (COLD600) is constructed where the climate is colder, and the mean size of the ice sheet is comparable to reconstructions of the last glaciation maximum. To cool the climate, the value of the constant $A$ in the parameterization of outgoing thermal radiation (equation 3.3 on page 37) is increased to $A = 216\,W/m^2$. As before, the model is run for $600$ Ka using orbital insolation from *Laskar et al.* (1993) for the period $1.8$ to $1.2$ Ka BP.

Figure 6-4 shows the latitude of the ice margin with time. The ice sheet extends to a latitude of about $48°N$, as compared to $66°N$ in experiment ICE600 (figure 6-1), and the annual mean global temperature is reduced by about $5°C$. The amplitude of the oscillations in ice extent is relatively unchanged. However, the relative contribution by obliquity and precession is different. Power

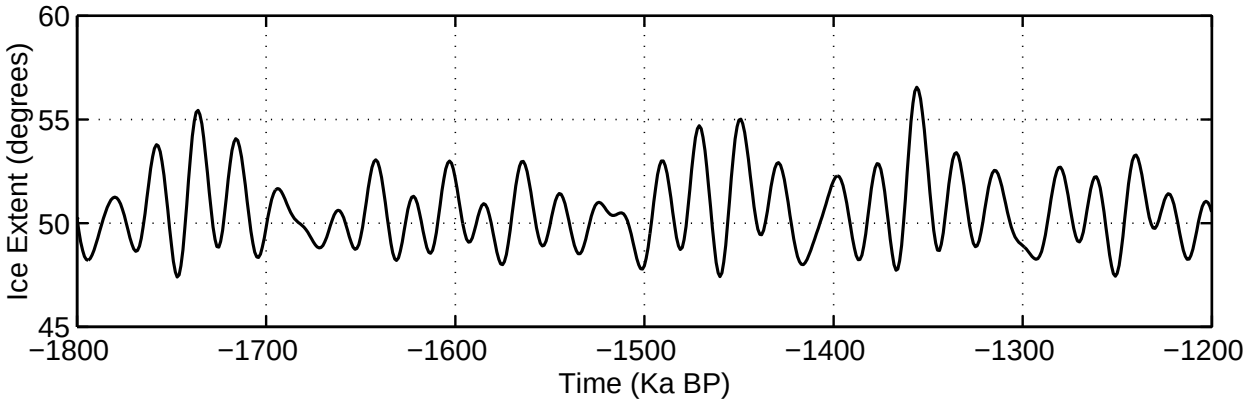


Figure 6-4: $600$ Ka of ice sheet extent ($1.8 - 1.2$ Ka BP) in an experiment with a colder climate and a larger mean ice sheet extent.

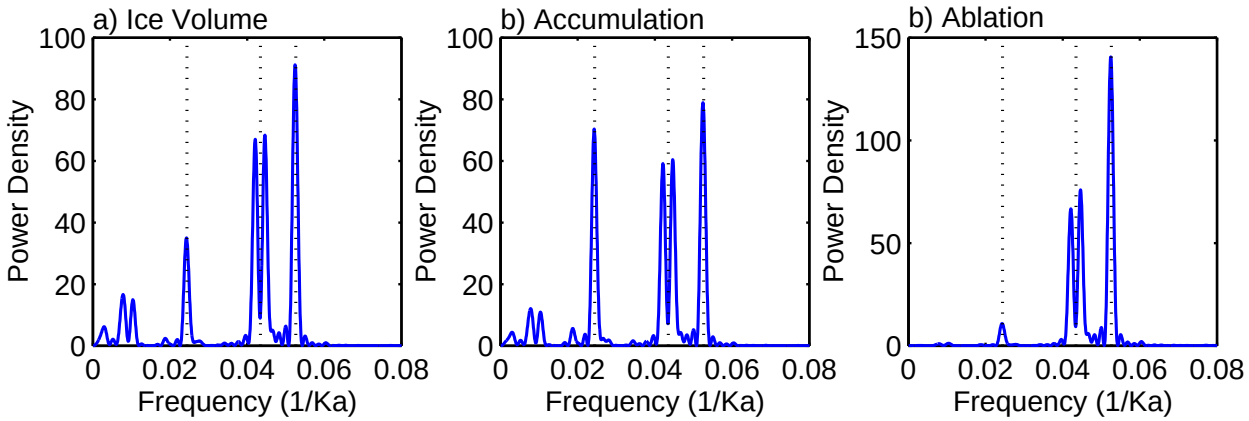


Figure 6-5: Power spectra of mean annual a) ice volume, b) accumulation, and c) ablation for the period $1.8 - 1.2$ Ma BP in an experiment with a colder climate and a larger mean ice sheet extent.

spectra of annual mean ice volume, accumulation, and ablation are given in figure 6-5. The relative strength of the obliquity signal in the power spectrum of accumulation is slightly reduced, whereas it is significantly reduced in ice volume.

One reason for the dominance of precession when the mean ice sheet extent is greater, is that temperature at the ice edge is higher. The mean annual temperature at the ice edge is $-2.9°C$, as compared to $-8.7°C$ for the small ice sheet in experiment ICE600. This results in a significantly larger ablation zone, and larger ablation oscillations dominating ice extent. Because ablation is dominated by precession, the precession signal in ice volume is enhanced relative to obliquity.

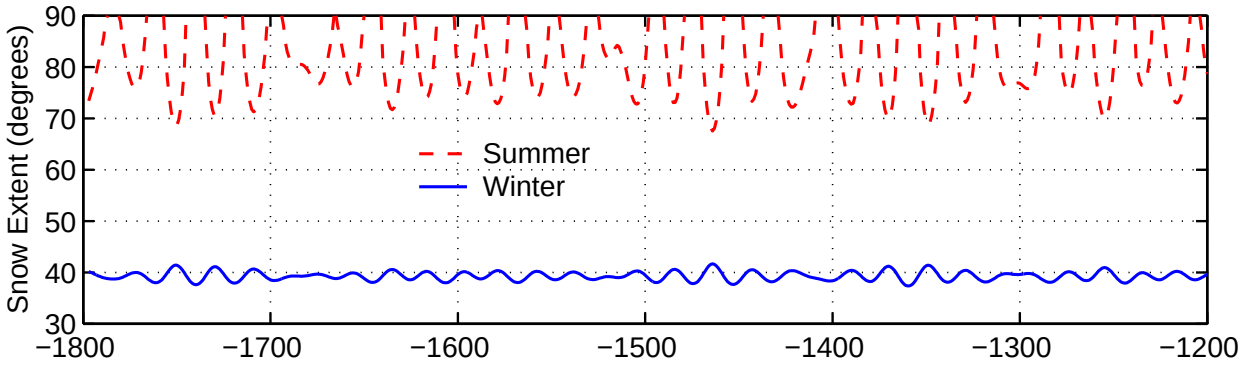


Figure 6-6: $600$ Ka of seasonal snow cover limits ($1.8 - 1.2$ Ma BP) calculated using the orbital solution of *Laskar et al.* (1993).

## 6.3 Late Pliocene to Early Pleistocene Snow Cover

As has been seen in chapters 4 and 5, the response of snow and ice cover to insolation variations differs significantly. In the following experiment (SNOW600), a version of the model without an active ice sheet, but with active snow cover is forced with insolation variations for the period $1.8$ to $1.2$ Ma BP. Climate is cooled slightly to allow for snow lasting through the summer season by setting $A = 212\,W/m^2$ in equation 3.3 on page 37, otherwise the standard parameters are used as in experiment ICE600 and given in table 3.1 on page 37.

Figure 6-6 shows the change in latitudinal extent of winter, and summer snow cover as estimated by the model. Winter snow extends to about $40°N$ and is less sensitive to insolation variations than summer snow, as discussed in section 4.3.1 on page 67. The extent of summer, or perennial snow cover varies between $90°N$ and $70°N$.

Variations in both winter and summer snow extents are dominated by precession, with very little influence by obliquity (figure 6-7). This is because snow cover depends on local seasonal temperature, which is governed by precession. The influence of obliquity only becomes important when averaging over a large part of the annual cycle, or when the system responds to latitudinal contrasts in insolation, as is the case when an interactive accumulation is included.

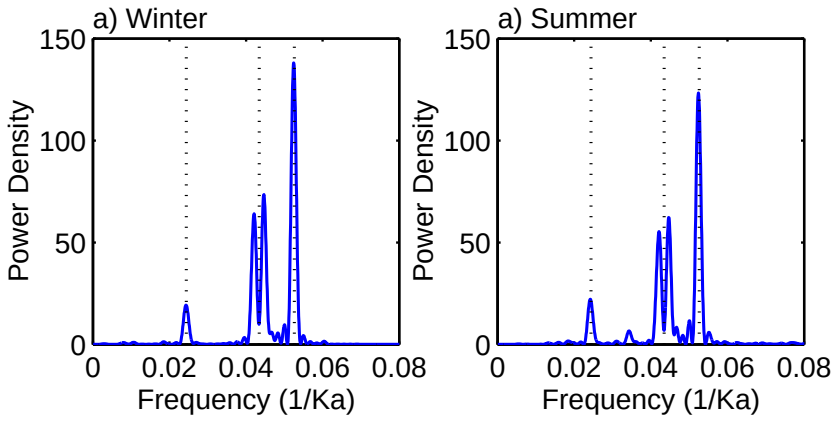


Figure 6-7: Power spectra of a) winter maximum, and b) summer minimum snow cover for the period $1.8 - 1.2$ Ma BP.

## 6.4 Summary

When investigating the mechanisms controlling the cycles in ice volume of the late Pliocene and early Pleistocene it would be useful to understand what caused the onset of enhanced glaciations $2.8-2.6$ Ma BP. One theory, often discussed in the literature, is the closure of the Central American Seaway which was completed $\sim$ 3 Ma BP. However, here it is argued that this event is more likely to have caused the early Pliocene warm period, perhaps even delaying the onset of enhanced glaciations.

In a model experiment forced with orbital insolation variations for the period $1.8 - 1.2$ Ma BP, oscillations in ice volume have a similar contribution by the main periods of precession and obliquity. Nearly all variability at the obliquity frequency is due to the influence of the meridional insolation gradient on accumulation, whereas the influence of precession is due to it's control of summer temperatures and surface melt.

All the experiments give an amplitude of oscillations in ice volume which is significantly lower than what is estimated from the benthic $\delta^{18}O$ record. However, there are several important positive feedbacks in the climate system which have not been included in the model, such as $CO_2$, vegetation, and sea ice. Further, it is likely that at least part of the variability observed in the ice volume record is a result of nonlinear self-sustained, or stochastic processes, which are not represented in

the model.

A model experiment where the ice sheet is removed and the ice-albedo feedback is represented by a temperature dependent snow line illustrates that the two approaches are significantly different. Assuming that the latitude of perennial snow cover is an indicator of changes in ice cover, as has been done in previous model studies (e.g. *Budyko* (1969); *Sellers* (1969); *North* (1975); *Schneider and Thompson* (1979); *Suarez and Held* (1979); *Short et al.* (1991)), is misleading. In such a simplified approach, perennial snow cover only depends on summer insolation and precession. Whereas in reality, snow and ice are influenced by accumulation of snow, which responds to the latitudinal insolation contrast and obliquity.

# Chapter 7

# Summary and Discussion

Interest in simple Energy Balance Models (EBMs) was invigorated by the early work of *Budyko* (1969) and *Sellers* (1969), who independently showed that the temperature-albedo feedback mechanism has the potential to greatly enhance the sensitivity of Earth's climate. According to their models, a decrease in the solar constant by only a few percent could trigger a transition to a completely ice covered planet. These early model results, combined with the concern for possible human induced climate changes, have led to a large research effort focused on understanding past as well as future climates.

However, some of the largest and most fundamental changes observed in the climate record are still not understood. A few examples are as follows: it is not known what triggered the onset of enhanced glaciations $\sim 2.8 - 2.6$ Ma BP; why the initial oscillations in ice volume were dominated by a period of $41$ Ka; or why larger oscillations in ice volume with a duration of approximately $100$ Ka dominated after $\sim 0.8$ Ma BP. Knowledge about these past events is crucial in the effort to understand the importance of different forcing and feedback mechanisms in determining the stability of the climate system, as well as its future response to man made forcing.

In this work EBMs have several advantages over comprehensive coupled General Circulation Models (GCMs): they are extremely efficient and can run multiple sensitivity experiments covering long time periods; and they are simple, making it possible to isolate individual feedback mechan-

isms and understand the underlying physics. In particular, EBMs are well suited to study problems where the spatial and temporal scales are large, compared with the spatial and temporal scales of weather systems. In this context, the response to variations in orbital insolation is a good candidate. As in most other studies with simple EBMs it is important to test the conclusions with a hierarchy of climate models with varying degrees of complexity, including Earth Models of Intermediate Complexity (EMICs) and GCMs. With this in mind, the results presented here will serve as a valuable guide for future experiments with more realistic models.

## 7.1 Summary

A summary of the main topics and results discussed in this study are as follows:

- Oscillations in ice volume before $\sim 0.8$ Ma BP are dominated by a period of $41$ Ka, which is the main period of orbital obliquity. After this time, the amplitude of ice volume oscillations increases by as much as $50\%$, the influence of precession increases, and there is a switch to a dominance of periods close to $100$ Ka.

- Based mainly on paleoclimate data from the last $0.8$ Ka, most researchers compare, or even tune, climate records to June or July $65^{\circ}N$ insolation. However, summer insolation at $65^{\circ}N$ is governed by precession, and is not a good candidate to explain the $41$ Ka period cycles dominating ice volume before $\sim 0.8$ Ma BP.

- As an alternative to current orbital theory, a hypothesis is tested, where obliquity dominated variations in the meridional insolation gradient influences the poleward flux of moisture and plays an important role in controlling high latitude ice volume before $\sim 0.8$ Ma BP.

- A simple atmosphere-ice process model is developed to test this hypothesis. Two of the most important differences between the new model and existing similar models is the inclusion of an explicit parameterization for calculating atmospheric moisture flux and accumulation on

the ice sheet, and the adjustment of the ice-albedo feedback for the influence of solar zenith angle and clouds.

- The model does a reasonable job at estimating the current seasonal cycle and atmospheric fluxes of sensible and latent heat. The sensitivity ($\beta$) to changes in the solar constant is $138^{\circ}$ with no snow or ice, $166^{\circ}$ with a temperature dependent snow cover, and $219^{\circ}$ with an active ice sheet. The sensitivity in the experiment with a temperature dependent snow cover is significantly lower than values found in the early EBM studies (*Budyko*, 1969; *Sellers*, 1969; *North*, 1975), due to the improved albedo parameterization used, as well as the increased strength of the negative dynamical flux feedback.

- Similarly, the multiple equilibria, observed in these previous model studies in response to a varying solar constant, are only observed when the strength of the snow-albedo feedback is increased to an unrealistically large value. However, it should be kept in mind that the experiments presented here only allow for snow or ice cover over land, taking no account for changes in sea ice.

- At equilibrium, changes in obliquity and precession have a relatively large impact on ice cover and high latitude climate. Between the extreme values of obliquity and precession, the ice sheet extent changes by as much as $15^{\circ}$ of latitude, and the change in high latitude summer temperatures is close to $6^{\circ}C$. In contrast, the response of a temperature dependent snow cover is small, and only significant in summer when the temperature gradient is relatively weak.

- In the model version with an active ice sheet, optimal conditions for ice growth are attained when: 1) obliquity is low; 2) eccentricity is high; and 3) perihelion coincides with winter solstice. Low obliquity strengthens the meridional temperature gradient, which in turn increases the flux of moisture to high latitudes and the accumulation of ice. At the same time, low obliquity cools high latitudes, reducing surface melt in summer. When perihelion coincides with winter solstice, the Earth is closest to the Sun in winter, resulting in relatively warm winter and cool summer seasons, in particular when eccentricity is large. As a result,

summer surface melt is reduced.

- In a model experiment forced with orbital insolation variations for the period $1.8 - 1.2$ Ma BP, oscillations in ice volume have a similar contribution by the main periods of precession and obliquity. Nearly all variability at the obliquity frequency is due to the influence of the meridional insolation gradient on accumulation, whereas the influence of precession is due to its control of summer temperatures and surface melt.

- The experiments forced with orbital insolation give an amplitude of ice volume oscillations ($\sim$ 10 m of mean sea level) which is significantly lower than what is estimated from the benthic $\delta^{18}O$ record of the late Pliocene to early Pleistocene ($\sim 40-60$ m of mean sea level). However, there are several important positive feedbacks which have not been included in the model, such as $CO_2$, vegetation, and sea ice. At the same time, it is likely that at least part of the variability observed in the ice volume record is a result of nonlinear self-sustained oscillations, or stochastic processes.

- Assuming that variations in the latitude of perennial snow cover is an indicator of changes in ice cover is misleading. In such a simplified approach, perennial snow cover only depends on summer insolation and precession. Whereas in reality, snow and ice are influenced by accumulation of snow, which responds to the latitudinal insolation contrast and obliquity.

## 7.2 Sea Ice

The main focus of this study is to understand processes related to atmospheric heat and moisture transports, as well as snow and ice cover on land surfaces. To achieve this, the model is kept as simple as possible, neglecting any influence by an interactive ocean. This implies that there is no active sea ice included in the model. Instead, it is assumed that the Arctic ocean is permanently covered by sea ice north of $75°N$, whereas all other ocean surfaces are free of sea ice.

In order to add an interactive sea ice component to the model, it is necessary to include an

appropriate representation of circulation and heat transports by the ocean. One alternative is to improve the mixed layer ocean, already existing in the model, by including a so-called $Q$-flux. This is a fixed meridional ocean heat transport, with a magnitude adjusted such that the model climate resembles the current observed climate. An alternative would be to use an ocean general circulation model where the thermal mass of the deep layers as well as ocean circulation are taken into account. However, it should be kept in mind that this would increase the computational cost of the model significantly.

Adding sea ice to the system will introduce an additional strong positive feedback mechanism. As high latitudes cool, sea ice expands, covering the surface ocean which has a relatively low albedo, and causes a further cooling. In effect, sea ice amplifies the response of the system to changes in high latitude insolation. The increased sensitivity of the system to a change in mean annual insolation, or to the solar constant $S$, is expected to be similar to the effect of increasing the strength of the snow-albedo feedback parameter ($\delta\alpha_{ice}$, see section 4.3.1 on page 67). However, there are several important differences between sea ice and snow cover. As opposed to snow cover, sea ice is affected by ocean circulation and atmospheric wind patterns. In turn, sea ice has an impact on surface salinity and the transfer of heat and water vapor between the atmosphere and ocean.

In the case of orbital forcing, there is another important distinction between sea ice and snow cover. This is due to the different seasonal cycles of sea surface temperature, as opposed to temperature over land. Because of the large thermal mass of the ocean, the seasonal cycle of sea surface temperature is significantly weaker than for surfaces temperatures on land. This implies that the seasonal variation in sea ice extent is smaller than the seasonal variation in snow cover. As has been discussed in the two previous chapters, a mean annual response to precession requires a strong seasonal response of a component in the climate system, such as surface albedo. However, the weak seasonal cycle in sea ice suggests that its response to precession should be weaker than that of snow cover over land.

Another important aspect of sea ice, is its effect on the atmospheric hydrological cycle. About $20\%$ of precipitation on Greenland today comes from local sources such as the Norwegian and

Greenland seas (*Charles et al.*, 1994), suggesting that a large change in sea ice cover could have an impact on the supply of moisture to the ice sheet. This link between sea ice cover and moisture supply to high latitude land surfaces is the basis of the so-called precipitation-temperature feedback (*Kallen et al.*, 1979; *Letreut and Ghil*, 1983; *Gildor and Tziperman*, 2001). The precipitation-temperature feedback implies that reduced sea ice cover and warm temperatures at high latitudes increase the amount of evaporation from the surface ocean, as well as the moisture holding capacity of the atmosphere. From this it is inferred that accumulation on land will increase.

The parameterization of atmospheric moisture transport used in this study takes into account the effect of variations in local temperature as given by the Clausius-Clapeyron relation (equation 3.11 on page 45). Therefore, any variations in high latitude temperature will have an impact on atmospheric moisture content. However, as has been shown in this study and discussed by *Nakamura et al.* (1994) and *Scott (1995)*, changes in meridional atmospheric temperature gradient dominate in controlling the atmospheric moisture transport and accumulation on land. Further, the empirical study by *Scott* (1995) (figure 4-5 on page 61), shows that the correlation between the observed seasonal atmospheric moisture transport and calculated transport using the parameterization adopted in this study is very good. Suggesting that for the range of temperature changes experienced in a seasonal cycle ($\sim 15^{\circ}C$), the assumption that the temperature gradient dominates in controlling moisture transport is valid. For reference, the estimated warming from average last glacial conditions to the Holocene is approximately $15^{\circ}C$ (*Cuffey et al.*, 1995; *Cuffey and Clow*, 1997), whereas during the late Pliocene, early Pleistocene the amplitude of the glacial cycles is smaller.

It should be noted, that an important assumption made in deriving the parameterized moisture flux is that relative humidity ($q_r$) remains constant. It is conceivable that large changes in sea ice, as might have occurred during the glacial cycles of the past, could have resulted in a change in relative humidity. Therefore, the possibility that accumulation on the Laurentide and Fennoscandian ice sheets is influenced by changes in sea ice cover should be thoroughly tested with an appropriate coupled atmosphere-ocean GCM with an interactive sea ice component. Although, existing model

studies indicate that the main moisture source regions for Greenland and Antarctica are tropical and mid-latitude ocean regions below $\sim 50^{\circ}$ of latitude (*Charles et al.*, 1994; *Werner et al.*, 2001), where there is thought to have been little sea ice even at the last glacial maximum (*Sarnthein et al.*, 2003).

There is very little data on accumulation rates in the past. However, a study of ice cores from central Greenland by *Cuffey and Clow* (1997) find that long-term averages ($0.5 - 1.0$ Ka) of estimated accumulation rates and temperature are negatively correlated during the past $7$ Ka of the Holocene. Whereas, on shorter time scales ($0.1$ Ka), accumulation rates and temperature are essentially uncorrelated. Based on these observations, the authors conclude that accumulation rate is not a reliable proxy for temperature, and that there is no evidence supporting the inference that a climatic warming results in increased precipitation over the Greenland ice sheet.

A study by *Kaspner et al.* (1995) find that atmospheric dynamics, not temperature, appears to have been the primary control on snow accumulation in central Greenland over the past $18$ Ka. The sensitivity of accumulation to temperature changes during both warm (Holocene) and cold (Younger Dryas, Last Glacial Maximum) periods is less than expected if the accumulation rate is only controlled by the ability of warmer air to deliver more moisture to the ice sheet. At the same time, accumulation during the transitions between these warm and cold periods varies more than can be explained thermodynamically.

Similarly, a multivariate regression analysis of Greenland accumulation rates by *van der Veen et al.* (2001) finds that about $80$% of the total variance in longer-term averaged accumulation can be explained by the large scale atmospheric circulation and its interaction with the geometry of the ice sheet. Further, *Bromwich and Robasky* (1993) show that accumulation in Antarctica is largely dominated by atmospheric circulation, with little influence of local temperature variations.

Interestingly, in the study of *Kaspner et al.* (1995) the sensitivity to temperature is found to be largest during transitions from cold to warm periods. This supports the suggestion that the sensitivity of surface melt ($\beta_{abl}$) to temperature is increased during times of ice sheet retreat (section 3.3.2 on page 51), due to the lower albedo of the snow free ice surface (*Braithwaite*, 1995;

*Braithwaite and Zhang*, 2000). A different ablation rate for growing and shrinking ice sheets could lead to asymmetric glacial cycles, as is observed for the $\sim 100$ Ka cycles of the past $\sim 0.8$ Ma.

To summarize, there is no historical evidence for a strong link between accumulation of snow and atmospheric temperature. Rather, the data suggests that accumulation is dominated by large scale atmospheric circulation. Hence, the assumption that accumulation is controlled solely by temperature, as used in model studies of changes in past, as well as future ice sheet mass balance (e.g. *Pollard* (1980); *Huybrechts* (1990); *Gallee et al.* (1992); *Deblonde et al.* (1992); *Tarasov and Peltier* (1997); *Huybrechts and de Wolde* (1999)), is questionable. However, it is possible that large variations in sea ice could have influenced atmospheric relative humidity and the supply of moisture to the ice sheets.

## 7.3 The Topographic Effect of an Ice Sheet

In the experiments described in this study the lower boundary of the atmosphere has been assumed to be flat. However, in reality the continental ice sheets represent a significant topographic feature once they advance to their maximum size. As an example, at the last glacial maximum, the dome of the Laurentide ice sheet reached a maximum altitude of about $3000$ m above sea level (*Peltier*, 1994). Although ice volume during the late Pliocene, early Pleistocene was significantly lower than at the last glacial maximum (figure 2-4 on page 19), the presence of the ice sheet could potentially have had an important effect on the thermal structure and circulation of the atmosphere.

Two possible mechanisms where the topography of an ice sheet might interact with the dynamics of atmospheric heat transport will be briefly discussed here. One mechanism involves the impact of a sloping lower boundary on the stability of baroclinic eddies, and the other relates to the topographic forcing of stationary eddies.

Under certain circumstances a sloping lower boundary can be compared to the $\beta$-effect which stabilizes the longer wavelengths (*Charney*, 1947). According to *Pedlosky* (1964a,b), the necessary condition for instability demands that at the lower boundary, the northward slope of the surfaces of

constant potential temperature exceed the northward slope of the boundary. Therefore, a sufficiently strong topographic slope can have a stabilizing effect. The relevance of this mechanism to the ice sheets of the late Pliocene, early Pleistocene requires that the surface slope is relatively steep, and that the meridional extent is large enough to have an affect on the baroclinic eddies.

To estimate the surface slope of a typical late Pliocene, early Pleistocene ice sheet, the maximum volume of ice contained in the Laurentide ice sheet is taken to be about $50\%$ of that estimated for the last glacial maximum. This gives a maximum ice thickness of $\sim 1800$ m (figure 3-9). Assuming that the density ratio of the ice and Earth's crust is about $2/3$ (*Weertman*, 1976), bedrock deflection under the load of the ice sheet results in a maximum altitude of $\sim 1500$ m above mean sea level. Together with a meridional extent ($L$) from the margin to the dome of the ice sheet on the order of $1500$ km, this gives a mean surface slope of approximately $0.001$ ($1:1000$).

In order for the northward slope of the ice sheet surface to have a stabilizing affect, it has to be larger than the slope of the surfaces of constant potential temperature. In the high latitudes of the Northern Hemisphere a typical northward slope of surfaces of constant potential temperature is $\sim 0.001$ (*Peixoto and Oort*, 1992), which is comparable to the estimated mean surface slope of the Laurentide ice sheet in the early Pliocene, late Pleistocene. This indicates that the surface slope of the ice sheet might have a weak stabilizing effect if it covers a large enough area to affect the baroclinic eddies.

However, it should be kept in mind that in the case of most ice sheets, such as the Laurentide, the increase in surface elevation with latitude is not constant. Instead, most of the increase in surface elevation is concentrated at its southern margin. When considering only the large interior surface of the ice sheet, the slope is smaller than the mean slope. According to a study by *Orlanski* (1969), the stabilizing effect of a steep marginal slope of a topographical feature is not great enough to oppose the increased instability caused by a weakly sloping interior. In the case of Antarctica, which is the closest modern analogue to the Laurentide ice sheet, the different surface slopes at the margin and in the vast interior result in a system which becomes more unstable overall (*Orlanski*, 1969).

Another important question is whether the horizontal extent of the ice sheet is large enough

to have an effect on the eddies. The ice sheet can only have a stabilizing effect if it grows to a meridional extent comparable to the scale of the baroclinic eddies. In the atmosphere, baroclinic eddies that transport heat have a typical north-south extent of about $3000$ km (*Stone et al.*, 1982). Therefore, if the horizontal extent of the ice sheet is small ($\sim 1000$ km or less) compared to the scale of the eddies, the stabilizing effect would be of less importance. As discussed above, the maximum horizontal extent of the ice sheets in the late Pliocene, early Pleistocene is smaller than the scale of typical baroclinic eddies. Indicating that their possible stabilizing effect on the growth of instabilities is relatively small.

Finally, even in the case when the size of the ice sheet is large compared to the scale of the eddies, and the arguments above suggest that the surface slope could have a stabilizing effect, it should be noted that in the fully equilibrated eddy regime, when the zonal mean flow is stable, the baroclinic eddies are still present (*Solomon and Stone*, 2001). In effect, the eddy heat transport parameterization used in this study does not depend critically on the nature and source of the eddies. Rather, the parameterization is based on scaling arguments such as the statement that: the radius of deformation which maximizes the release of eddy available potential energy is the characteristic meridional eddy scale; and that the eddy kinetic energy is comparable to the mean kinetic energy. The first statement is supported by the work of *Pedlosky* (1975), and the second statement is found to be robust in all seasons and throughout mid-latitudes for the current climate (*Lin*, 1980a,b). Further, a sloping bottom boundary impacts the transport by baroclinic eddies by modifying the height of the most unstable wave, as is the case for the $\grave{\beta}$-effect (*Held*, 1978). However, in the atmosphere much of the heat is transported by the longer planetary waves which extend throughout the troposphere and are not subject to this effect (*Stone and Miller*, 1980).

The second mechanism, involving the impact of ice sheet topography on atmospheric stationary waves is thought to be of more significance. As suggested by (*Roe and Lindzen*, 2001a,b) the presence of large continental ice sheets in the northern hemisphere is expected to have a significant impact on atmospheric circulation by forcing atmospheric stationary eddies. In the current climate these stationary eddies contribute significantly to the poleward transport of heat in Northern Hemi-

sphere winter, whereas the impact in the summer and in the Southern Hemisphere is negligible (*Peixoto and Oort*, 1992). The parameterization for heat transport used in this study does not explicitly include the effects of these stationary eddies. It is not known how a change to the stationary eddies, caused by the presence of the ice sheets, might have altered the meridional transport of heat and moisture. However, the studies of *Stone* (1978) as well as *Stone and Miller* (1980), indicate that there is a strong negative feedback between stationary and transient eddy fluxes of heat. Thus, a change in either transient, or stationary eddy heat flux might be compensated by the other, so as to maintain a constant total eddy heat transport.

## 7.4 The Role of Antarctic Ice Sheets

From the results of the model experiments, it is clear that surface melt on large land based ice sheets in the Northern Hemisphere is highly sensitive to variations in precession. As a consequence, simulated ice volume has a relatively strong precession signal, which is significantly larger than observed in the $\delta^{18}O$ ice volume record of the late Pliocene, early Pleistocene.

In Antarctica the situation is different. At present, the surface of the Antarctic ice sheet is too cold for any melt to occur, even in the summer season. Instead, ice volume is set by a balance of accumulation in the interior, and calving of ice into the Southern Ocean. If, as in the Northern Hemisphere, accumulation is governed by poleward transport of moisture by large scale baroclinic storm systems, long time period variations in accumulation will be dominated by obliquity. As surface melt is insignificant, the influence of precession on the mass balance will be significantly reduced.

Although calving accounts for almost all ablation in Antarctica, and roughly 40% in Greenland, it is not well understood. Empirical data suggest that there is a weak correlation between calving rate and water depth at the terminus of the ice sheet (*Brown et al.*, 1982). However, the correlation breaks down during rapid retreat of the ice, and there is no physical mechanism to explain why there should be any dependency of the calving rate on water depth (*Van der Veen*, 2002). On the

other hand, there is a good correlation between calving rate and flow speed of the ice (*Van der Veen*, 1996). Flow speed is governed by the dynamics and surface mass balance of the ice sheet. If the surface mass balance is dominated by accumulation, as is the case in Antarctica, variations in moisture flux will regulate the calving rate. In effect, this suggests that any long period oscillations in volume of the Antarctic ice sheet would be controlled by changes in obliquity.

From the benthic $\delta^{18}O$ record alone it is not possible to ascertain whether the observed variations in ice volume originate from the Northern Hemisphere, or from Antarctica. However, when comparing the $\delta^{18}O$ record with data on influx of IRD at core sites in the North Atlantic (figure 2-7), it is clear that there were continental ice sheets in the Northern Hemisphere with melting icebergs in the North Atlantic Ocean from at least $\sim 2.8 - 2.6$ Ma BP (*Jansen et al.*, 1988; *Raymo et al.*, 1989; *Jansen and Sjoholm*, 1991). The evolution of the Antarctic ice sheet is less clear. In the middle Pliocene ($\sim 3$ Ma BP), benthic $\delta^{18}O$ values are lower than in the Holocene, suggesting that a major deglaciation of Antarctica could have taken place. Alternatively, the low $\delta^{18}O$ values can be explained by warmer deep ocean temperatures.

A significant deglaciation of Antarctica in the middle Pliocene is supported by evidence of sea level being between 20 and 40 m higher than today (*Wardlaw and Quinn*, 1991; *Krantz*, 1991; *Dowsett et al.*, 1994). At present, the total volume of the Antarctic ice sheet corresponds to 61 m of sea level equivalent (*Huybrechts et al.*, 2000); implying that more than half the current ice sheet could have deglaciated in the middle Pliocene. Further, there is evidence from the terrestrial record of marine diatoms deposited at several locations on the Trans-antarctic Mountains (*Webb and Harwood*, 1991; *Barrett et al.*, 1992), suggesting the presence of marine conditions in the interior of East Antarctica in the past. The cyclic stratigraphy of these deposits indicates that the ice sheets on Antarctica could have undergone multiple glacial oscillations. Such major dynamic changes in ice volume during a period only slightly warmer than present, suggests that the Antarctic ice sheets are relatively unstable.

However, the evidence for a dynamic East Antarctic ice sheet that has undergone major deglaciations, is not universally accepted by the scientific community. According to the original theory

of *Kennett* (1977), the East Antarctic ice sheet formed in the middle Miocene ($\sim 14$ Ma BP) in response to a cooling of Antarctica. The cooling was caused by a progressive isolation of the Antarctic continent due to the opening of the Drake passage, and a strengthening of the Antarctic Circumpolar Current. Following the middle Miocene, polar climate cooled and the East Antarctic ice sheet is believed to have remained stable (*Denton et al.*, 1984; *Clapperton and Sugden*, 1990; *Kennett and Hodell*, 1993). On the other hand, the West Antarctic ice sheet, which is considerably smaller ($\sim 7$ m of sea level) and marine-based, is considered to be more vulnerable to changes in climate.

Although the glacial history of Antarctica is unclear and needs to be investigated further, the possibility of a dynamic Antarctic ice sheet capable of oscillating in size by more than 50% has serious implications for the understanding of early Pliocene and late Pleistocene glacial cycles. Presently, the Antarctic ice sheets cover an area about eight times the size of Greenland, and any significant change in their volume will have an impact on albedo. In the case of the marine-based West Antarctic ice sheet, a relatively small reduction in ice volume will result in a large decrease in area. Changes in surface albedo of the Antarctic continent will have an effect on global climate, and possibly influence the growth and decay of ice in the Northern Hemisphere.

The impact of changes in obliquity is synchronous between the two hemispheres, whereas the impact of changes in precession is asynchronous. As a result, changes in ice volume due to variations in obliquity will be in phase in both hemispheres, and could amplify the global ice volume signal. On the other hand, changes in ice volume due to variations in precession will be out of phase, and could cancel when calculating the global mean. In effect, obliquity dominated oscillations in Antarctic ice volume in the late Pliocene and early Pleistocene, could have been amplified by oscillations in ice volume of small versions of the Laurentide and Fennoscandian ice sheets.

The hypothesis of the $41$ Ka period glacial cycles being dominated by oscillations in Antarctic ice volume relies on the ice sheets in the Northern Hemisphere being relatively small. The benthic $\delta^{18}O$ record indicates that maximum global ice volume in the late Pliocene and early Pleistocene is about one third to one half that of the late Pleistocene. However, the gradual cooling of climate

from the Pliocene to the late Pleistocene is accompanied by a slow increase in global ice volume (figure 2-4 on page 19). The maximum size of the Antarctic ice sheets is constrained by the size of the continent. A similar constraint does not apply to the Laurentide ice sheet. Instead, the glacial size of the Laurentide ice sheet would have increased gradually until it became unstable. At this point, the rapid nonlinear deglaciations characteristic of the $100$ Ka glacial cycles would have commenced. The processes responsible for these rapid deglaciations are still unclear, but suggestions include: warm summers and high surface melt amplified by feedbacks related to ocean circulation (*Ruddiman and McIntyre*, 1981); catastrophic melt back of ice streams (*Hughes et al.*, 1977; *Hughes*, 1987); and enhanced calving into proglacial lakes formed in the bedrock depression at the margin of a retreating ice sheet (*Andrews*, 1973; *Pollard*, 1982).

In effect, the switch from the dominance of $41$ Ka to $\sim 100$ Ka period glacial cycles about $0.8$ Ma BP could have been the result of the emergence of large ice sheets in the Northern Hemisphere. After this time, the climate system switched from being controlled by the Southern Hemisphere to the Northern Hemisphere. During the glacial phase of the $\sim 100$ Ka cycles, ice volume is influenced by both obliquity and precession. The increase in the influence of precession at the time of the emergence of $\sim 100$ Ka ice volume cycles can be seen in figure 2-6 on page 22, and is most likely a result of an increased influence of surface melt on the large ice sheets of the Northern Hemisphere.

In a warmer climate, such as the early Pliocene, there could have been some surface melt in Antarctica. As seen in the model experiments presented in this study, surface melt is dominated by precession. However, the climate of the model is tuned to fit Northern Hemisphere climate. Due to the vicinity of the large thermal mass of the Southern Ocean, the seasonal cycle on Antarctica is significantly weaker than in the north. As the impact of precession relies on a strong preference for a particular season, a weak seasonal cycle reduces the influence of precession.

## 7.5 Further Work

As pointed out in the previous sections there are several aspects of the topics covered in this study which inspire further research. A few suggestions for questions which should be addressed in the future are as follows:

- How will an interactive sea ice component change the sensitivity of the model to variations in the solar constant, as well as orbital insolation?
- What is the impact of large changes in high latitude sea ice on relative humidity and the accumulation of ice on continental ice sheets such as the Laurentide and Fennoscandian?
- How will the inclusion of an active ocean circulation as well as the thermal mass of the deep ocean change the model results?
- What portion of the oscillations in benthic $\delta^{18}O$ in the late Pliocene, early Pleistocene is due to changes in temperature and Antarctic ice volume?
- How will the addition of an Antarctic ice sheet change the response of global ice volume to variations in orbital insolation?

# Appendix A

# The 41 Ka World: Milankovitch's Other Unsolved Mystery

PALEOCEANOGRAPHY, VOL. 18, NO. 1, 1011, doi:10.1029/2002PA000791, 2003

# The 41 kyr world: Milankovitch's other unsolved mystery

Maureen E. Raymo
Department of Earth Sciences, Boston University, Boston, Massachusetts, USA

Kerim Nisancioglu
Department of Earth, Atmospheric, and Planetary Sciences, Massachusetts Institute of Technology, Cambridge, Massachusetts, USA

Received 26 March 2002; revised 5 September 2002; accepted 19 September 2002; published 6 March 2003.

[1] For most of the Northern Hemisphere Ice Ages, from ~3.0 to 0.8 m.y., global ice volume varied predominantly at the 41,000 year period of Earth's orbital obliquity. However, summer (or summer caloric half year) insolation at high latitudes, which is widely believed to be the major influence on high-latitude climate and ice volume, is dominated by the 23,000 year precessional period. Thus the geologic record poses a challenge to our understanding of climate dynamics. Here we propose that variations in the insolation gradient between high and low latitudes control high-latitude climate and ice volume during the late Pliocene and early Pleistocene. The differential heating between high and low latitudes, driven by obliquity, controls the atmospheric meridional flux of heat, moisture, and latent energy, which may exert the dominant control on high-latitude climate on Milankovitch timescales. In the two-dimensional zonal energy balance models typically used to study the long-term evolution of climate, the meridional atmospheric moisture flux is usually kept fixed. The hypothesis that insolation gradients control the poleward energy fluxes, precipitation, and ice volume at high latitudes has never been directly examined within the context of an ice sheet model. In light of what we know about modern energy fluxes and their relative influence on high-latitude climate, this possibility should be examined. *INDEX TERMS:* 4267 Oceanography: General: Paleoceanography; 1620 Global Change: Climate dynamics (3309); 3344 Meteorology and Atmospheric Dynamics: Paleoclimatology; 3359 Meteorology and Atmospheric Dynamics: Radiative processes; *KEYWORDS:* Milankovitch, orbital variations, ice ages, Pleistocene, obliquity, paleoclimate

**Citation:** Raymo, M. E., and K. Nisancioglu, The 41 kyr world: Milankovitch's other unsolved mystery, *Paleoceanography*, *18*(1), 1011, doi:10.1029/2002PA000791, 2003.

## 1. Introduction

[2] All serious students of Earth's climate history have heard of the "100 kyr problem" of Milankovitch orbital theory, namely the lack of an obvious explanation of the dominant ~100 kyr periodicity in climate records of the last 800,000 years. However, few have considered an equally perplexing characteristic of Earth's climate, one that similarly defies simple physical explanation yet dominates the Earth's recent geologic record. We call this the "Milankovitch 41 kyr problem." For the time interval extending back to the Brunhes-Matuyama boundary (0.78 Ma), an interval in Earth's climate history dominated by the large (and largely unexplained) 100,000 year periodicity, *Imbrie et al.* [1992] definitively showed that the obliquity (41,000 year) and precessional (23,000 year) frequencies observed in climate records were direct linear responses, with physically appropriate lags, to high-latitude summer insolation forcing. However, during the previous two million years of Northern Hemisphere ice sheet growth, from ~3 million years ago to about 0.8 million years ago, global ice volume varied almost exclusively at the 41,000 year obliquity period. Because high-latitude summer insolation is always dominated by precession, we argue that these earlier climate variations cannot be understood within the current framework of the Milankovitch Hypothesis. Finding an explanation for late Pliocene to early Pleistocene global climate variations represents one of the most interesting and challenging problems facing climate modelers today.


0883-8305/03/2002PA000791$12.00

## 2. Ice Age Record

[3] The outlines of Earth's climate history for the last 3 million years have been known for nearly two decades. With an extremely low sedimentation rate piston core and then with longer Deep Sea Drilling Project cores, Nicholas Shackleton, and later William Ruddiman and others, measured oxygen isotopes in benthic foraminifera to derive a proxy for global ice volume over the last 3 million years. Many records generated since this time have confirmed their early observations, namely: (1) the main frequency of ice volume change from 3.0 to 0.8 m.y. was 41,000 years, the primary obliquity period; (2) after ~0.8 Ma, ice sheets varied predominately at the 100,000 year period and the amplitude of $\delta^{18}O$ variability increased implying growth of larger ice sheets.

[4] The double-cored and spliced benthic $\delta^{18}O$ record from DSDP607 nicely illustrates both these points (Figure 1). Note that the isotope record is plotted with a paleomagnetic time-

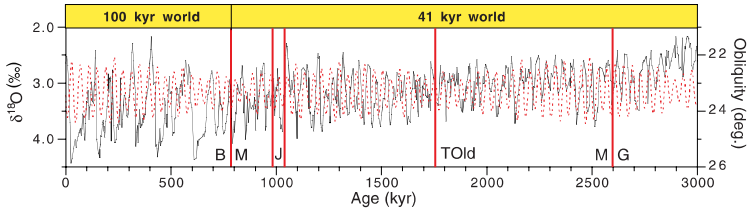


**Figure 1.** Benthic $\delta^{18}O$ record from DSDP Site 607 in the North Atlantic (solid line) plotted to a paleomagnetic timescale. The magnetic field reversals are marked, as well as the transition from a dominant 41 kyr to a 100 kyr world. B, Brunhes; M, Matuyama; J, Jaramillo; TOld, top of Olduvai; G, Gauss. Also shown is orbital obliquity (red dashed line).

scale (Table 1) determined by the depth of magnetic field reversals recorded by ferromagnetic grains in the sediment core [*Clement and Kent*, 1986]. Constant sedimentation rates are assumed between these magnetic reversal events (shown on Figure 1) which are dated by interpolating seafloor magnetic anomalies between fixed calibration points [*Cande and Kent*, 1992, 1995]. The two calibration points used in the post-3.0 Ma section of the record are independently derived by both radiometric and astronomic tuning techniques [*Berggren et al.*, 1995].

[5] Using this simple timescale, which is not biased by orbital "tuning," one can clearly observe the dominant 41,000 year periodicity of the Matuyama and Gauss intervals [see also *Imbrie et al.*, 1993a; *Tiedeman et al.*, 1994]. The obliquity periodicity can be further illustrated by statistically filtering the data at 41,000 years or by Fourier analysis (Figure 2a). Note the near complete lack of variance at the 23,000 year precessional and 100,000 year eccentricity frequencies. Indeed, over long parts of the record the $\delta^{18}O$ curve looks almost sinusoidal. Nearly identical results are seen in many other deep sea isotope records including benthic $\delta^{18}O$ records from the Pacific plotted either to paleomagnetic or orbitally tuned timescales (e.g., Figure 2b).

[6] Because Site 607 is located in the subpolar North Atlantic (41°N, 33°W, 3427 mbsl), it also contains a record of ice-rafted detritus (IRD) delivered to the open ocean over the Plio-Pleistocene. Over the entire length of the glacial record (>125 m), the input of IRD covaries with $\delta^{18}O$ [*Raymo et al.*, 1989; *Ruddiman et al.*, 1989]. The sedimentological data thus demonstrates that variability observed in benthic $\delta^{18}O$ must derive in part from the waxing and waning of ice sheets bounding the North Atlantic.

## 3. Current Milankovitch Theory

[7] Based mainly on climate proxy records of the last 0.5 Ma, a general scientific consensus has emerged that variations in summer insolation at high northern latitudes are the dominant influence on climate over tens of thousands of years. The logic behind nearly a century's worth of thought on this topic is that times of reduced summer insolation could allow some snow and ice to persist from year to year, lasting through the "meltback" season. A slight increase in accumulation from year to year, enhanced by a positive snow-albedo feedback, would eventually lead to full glacial conditions. At the same time, the cool summers are proposed to be accompanied by mild winters which, through the temperature-moisture feedback [*Kallen et al.*, 1979], would lead to enhanced winter accumulation of snow. Both effects, reduced spring-to-fall snowmelt and greater winter accumulation, seem to provide a logical and physically sound explanation for the waxing and waning of the ice sheets as high-latitude insolation changes [e.g., see *Hartmann*, 1994, p. 310]. However, in this model, the seasonal contrast, which is controlled by obliquity and varies systematically at the 41,000 year period, can dominate only if the precessional effects on insolation are assumed to cancel out over the course of the annual cycle. This assumption has generally not been made due to the presence of a strong precessional signal in late Pleistocene records, hence the greater relative importance accorded summer insolation versus seasonal contrast in controlling past climate.

[8] Over the last two decades, countless research papers have plotted (or tuned) climate records to June 65°N or July 65°N insolation. Using many of these records, *Imbrie et al.* [1992] showed that climate variance at precessional and obliquity frequencies appeared to be linearly forced by and was coherent with northern summer insolation. Only the 100,000 year cycle is left unexplained by this model (the familiar "100,000 year problem") and it, typically, is ascribed to non-linear variability arising internally within the climate system. A comprehensive summary of work on this subject is given by *Imbrie et al.* [1992, 1993b] [see also *Peltier and Marshall*, 1995; *Gildor and Tziperman*, 2000; *Muller and MacDonald*, 2000].

[9] In the late Pliocene and early Pleistocene, no significant variance at the 100 kyr period is observed in benthic

**Table 1.** Age Control Points Used for Paleomagnetic Timescale at DSDP Site 607

| Depth, mcd | Age, kyr | Magnetic Event |
|---|---|---|
| 0.0 | 0 | top of core |
| 31.84 | 780 | Brunhes/Matuyama |
| 40.345 | 984 | Jaramillo top |
| 43.965 | 1049 | Jaramillo bottom |
| 73.655 | 1757 | Olduvai top |
| 111.58 | 2600 | Matuyama/Gauss |
| 129.50 | 3054 | Kaena top |

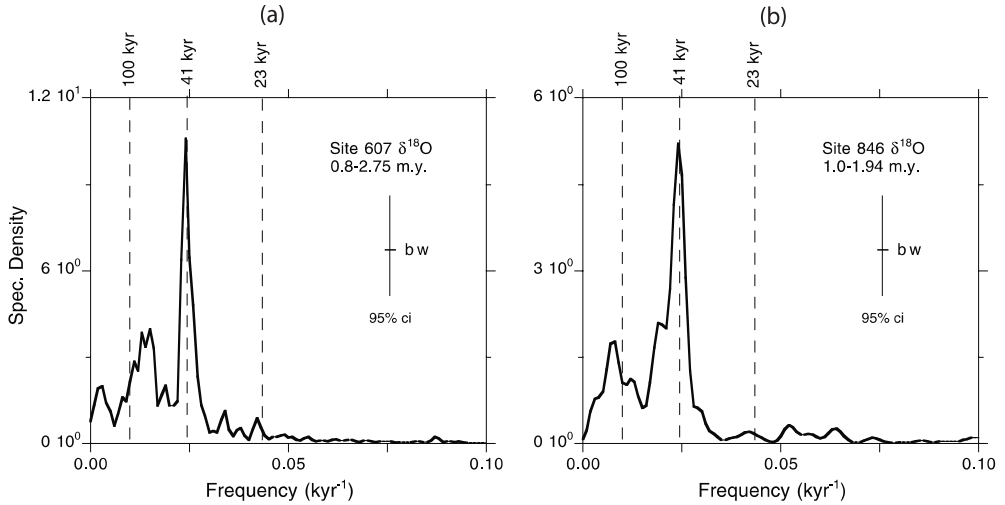


**Figure 2.** (a) Power spectra of Site 607 $\delta^{18}O$ plotted using timescale discussed in text (Table 1). The concentration of variance around 75–80 kyr is likely due to harmonics arising from the main obliquity frequency; (b) power spectra of the benthic $\delta^{18}O$ record of ODP Site 846 [*Mix et al.*, 1995] plotted to orbitally tuned timescale of *Shackleton et al.* [1990]. Bandwidths (bw) and confidence intervals (ci) shown on figure.

$\delta^{18}O$ records. Hence one might expect that the de facto implication of the "standard Milankovitch model" would be that global ice volume should vary linearly and coherently with high northern summer insolation. However, a comparison of $\delta^{18}O$ (ice volume; Figure 1) with various insolation records (Figure 3) clearly shows that while the ice volume proxies are dominated nearly exclusively by the 41,000 year obliquity periodicity, summer insolation is dominated, at nearly every latitude, by the 23,000 year period of precession. Any linear response to summer (or summer half year) insolation by high-latitude climate would require the strong presence of precession in the geologic record. In fact, this frequency is barely discernable in only a small stretch of the late Pliocene ice volume record and is absent over most (Figures 1 and 2). One must conclude that summer insolation at high northern latitudes does not exert a dominant (linear) influence on climate over most of the northern hemisphere Ice Ages.

## 4. The 41 kyr Problem

[10] While many investigators have attempted to model the 100 kyr world, few have focused their attention on the 41 kyr world. A notable exception is Andre Berger and colleagues who used a two dimensional ice sheet-climate model to try to simulate the growth and decay of ice sheets over the last 3 million years [e.g., *Berger et al.*, 1999]. While the obliquity period is present in the model output, precessional variance in ice sheet mass is also strongly present. In other words, although they successfully model the lack of the 100 kyr eccentricity cycle, they were not able to model an ice sheet that varies only at the obliquity frequency. This appears to be because the model is ultimately very sensitive to high-latitude summer insolation.

[11] Secondly, a discussion of the 41 kyr problem can be found in Richard Muller and Gordon MacDonald's book "Ice Ages and Astronomical Causes" [*Muller and MacDonald*, 2000]. Following *Kukla* [1968], they propose that northern latitude winter insolation (e.g., January 65°N) may drive late Pliocene/early Pleistocene climate cycles, even though the total insolation received in January is a factor of 20 less than summer insolation at the same latitude. However, they go on to say this proposition is speculative and that the geologic record is posing a problem that needs to be solved.

## 5. Insolation Gradients

[12] Given that summer insolation has too much precession and (one could argue) winter insolation appears too weak to drive anything, what is left? We propose that the gradient in insolation between high and low latitudes may, through its influence on the poleward flux of moisture which fuels ice sheet growth, play the dominant role in controlling climate from ~3 to 1 million years ago. Summer half-year insolation, for instance, is calculated as the mean of insolation received between the vernal (0°) and autumnal (180°) equinoxes as defined by the longitude of the sun in degrees. The gradient (or difference) in summer half-year insolation between 25° and 70°N (Figure 3) is almost completely dominated by obliquity (spectra shown in Figure 4). It is this temperature gradient that drives the poleward heat, moisture, and momentum fluxes in the atmosphere; the correlation between $\delta^{18}O$

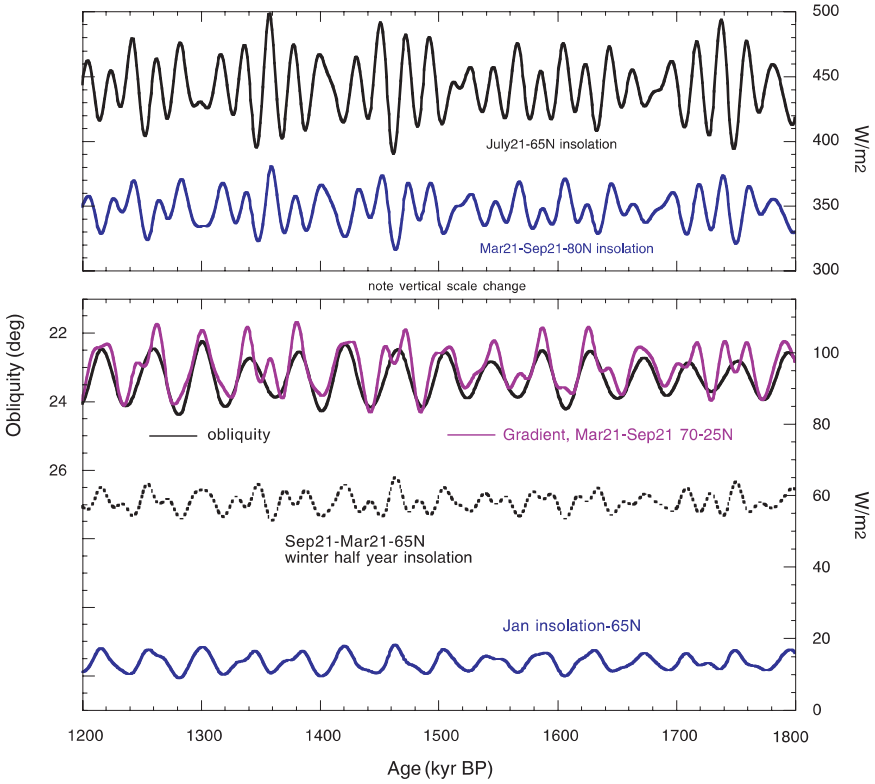


**Figure 3.** Various insolation and insolation gradient curves compared with obliquity. Curves derived using the *Laskar* [1990] orbital solution and Analyseries software of *Paillard et al.* [1996].

and the insolation gradient (Figure 5) suggests that increased gradients promote ice sheet growth (although given the uncertainties in the timescale we cannot definitively rule out other possibilities). Note that the oxygen isotope record in Figure 5 has been shifted to an older age by 8 kyr, a reasonable lag to assume for the climate response to obliquity and consistent with late Pleistocene observations [e.g., *Imbrie et al.*, 1992]. Of course the true lag of response after forcing would be almost impossible to determine directly in sediments of this age.

[13] The idea that insolation gradients could exert an important control on climate on Milankovitch timescales is not new; *Young and Bradley* [1984] proposed that hemispheric insolation gradients may have contributed to the growth and decay of continental ice sheets through their modulating influence on the poleward transport of moisture. They, and previously *Berger* [1976], suggest that times of rapid ice growth and decay correspond to especially pronounced deviations in latitudinal insolation gradients. *Johnson* [1991] similarly invokes a decrease in the insolation gradient, rather than direct summer insolation at high latitudes, as the immediate cause of the deglaciation at Termination 2, offering this mechanism as the explanation for paleoclimate data which suggest that deglaciation occurred prior to the increase in summer insolation. This perplexing mismatch in timing between the deglaciation at Termination 2 and the timing predicted by Milankovitch theory has also been discussed by *Winograd et al.* [1992] and more recently by *Gallup et al.* [2002].

[14] It may be that we are underestimating the influence of meridional fluxes of sensible and latent heat, driven by hemispheric temperature gradients, on continental ice sheet size. The mass balance of an ice sheet is set by the relative rates of accumulation and ablation. The rate of ablation is controlled by local incoming solar radiation and local atmospheric temperature. The rate of accumulation is controlled by the amount of moisture available for precipitation as well as the local temperature. As temperature and precipitation at high latitudes are strongly influenced by the magnitude of the atmospheric meridional heat and moisture fluxes, we would thus expect these fluxes to exert a strong influence on ice sheet mass balance. Today, annual mean poleward transports of heat by the atmosphere peak at about 5.0 PW in the mid-latitudes of both hemispheres

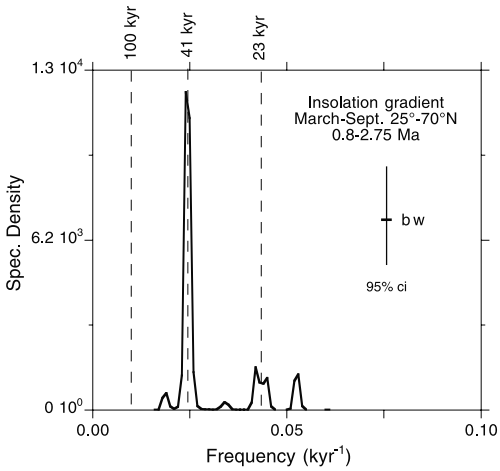


**Figure 4.** Power spectra of the gradient in insolation between 25° and 70°N for the summer half year between 0° (vernal equinox) and 180° (autumnal equinox). Bandwidth (bw) and confidence interval (ci) shown on figure.

[*Trenberth and Caron*, 2001], compensating the loss of heat to space from the polar regions. At high latitudes (>60°N) the Earth emits on an annual basis approximately twice as much energy (as long wave radiation) as it receives from absorbed solar radiation [*Hartmann*, 1994]; hence the meridional heat flux is comparable in magnitude to that received from high-latitude insolation. Lastly, recent studies suggest that a much greater portion of poleward energy transport occurs in the atmosphere, rather than the ocean which would be less directly affected by insolation gradients [*Trenberth and Caron*, 2001].

[15] All of the above observations suggest the possibility that variations in meridional heat and moisture fluxes (driven by orbital obliquity variations) could be large enough to override the effects of local insolation variations and imprint the dominant 41 kyr signal on the ice volume record. This seems especially plausible given the powerful ice-albedo feedback that would enhance the effects of insolation gradients on poleward energy transports. As the polar atmospheric temperature cooled at the onset of a glacial period, snow and ice would expand into regions previously covered by surfaces such as forests that have relatively low albedo. This increased snow/ice cover would raise the surface albedo dramatically, reflecting incoming radiation, and causing a further decrease in local temperature [e.g., *Bonan et al.*, 1992; *Kutzbach and Gallimore*, 1998]. Such an albedo change could have two effects: (1) act as a strong positive feedback on the meridional temperature gradients, further enhancing the poleward transport of the moisture that feeds ice sheet growth; and (2) act as a negative feedback by causing local cooling which decrease moisture availability through the temperature-precipitation feedback. Perhaps it is the interplay between these two feedbacks that determines the maximum ice sheet size (and perhaps the difference between the early and late Pleistocene climate behavior).

[16] Support for the idea that insolation gradients influence moisture flux to the ice sheets is found in the Antarctic deuterium excess record of the past 150 Ka which shows a strong correlation with the mean annual insolation gradient from 20°S to 60°S [*Vimeux et al.*, 1999]. As deuterium excess is a measure of the evaporative conditions of the oceanic source region for the moisture, this data indicates that there is a strong link between the insolation gradient and atmospheric moisture supply to the ice sheets. Note, that the deuterium excess values are high during glacial inception, a

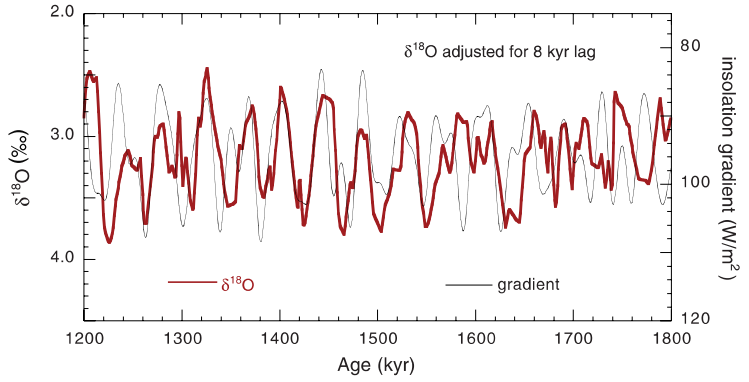


**Figure 5.** Site 607 benthic $\delta^{18}O$ record plotted versus the summer half-year gradient between 25° and 70°N. Isotope data is plotted to paleomagnetic timescale given in Table 1 and then shifted older by an assumed response lag of 8 kyr after the forcing [after *Imbrie et al.*, 1992] to better illustrate the correlation between the two parameters. The gradient in insolation is in phase with and shows a similar amplitude modulation as obliquity.

period characterized by low obliquity (cold high-latitude summers), and high meridional insolation gradient (e.g., a strong meridional atmospheric moisture flux).

[17] In most climate modeling studies of the long-term evolution of glacial-interglacial cycles (typically 2-D zonal energy balance models), the meridional atmospheric moisture flux has been kept fixed. Typically, models perturb the modern observed precipitation field according to changes in temperature. As a result, changes in atmospheric moisture flux have no impact on high-latitude precipitation and the accumulation of ice sheets. A notable exception is the study by *Gildor and Tziperman* [2000]. However, the hypothesis that insolation gradients as they control variations in poleward moisture fluxes and precipitation at high latitudes has never been directly examined within the context of an ice sheet model. In light of what we know about modern energy fluxes and their relative influence on high-latitude climate, this possibility should be examined.

## 6. Future Directions

[18] Above, we propose a ''gradient hypothesis'': that the strong obliquity signal imprinted on the Ice Age record is caused by the control meridional temperature gradients exert on the poleward transport of moisture. As obliquity decreases, cooling at high latitudes occurs and the gradient in solar heating between high and low latitude increases. Both effects, cooling polar regions and the enhanced delivery of moisture, promote ice sheet growth. The ice volume/temperature history of the last few million years is now well known and, as discussed above, poses a challenge both to climate modelers and paleoclimatologists. Ultimately, ocean circulation and ice volume are being controlled by atmospheric dynamics that must be sensitive to Milankovitch variations in incoming solar radiation. These are the same physical processes that will determine the response of Earth's climate to rising greenhouse gases. Building a model which can reproduce the first-order features of the Earth's Ice Age history over the Plio-Pleistocene would be an important step forward in the understanding of the dynamic processes that drive global climate change.

[19] **Acknowledgments.** The authors would like to thank Bill Ruddiman, Eli Tziperman, Peter Stone, Larry Peterson and an anonymous reviewer for comments, questions, and encouragement that significantly improved this manuscript as well as John Imbrie for his suggestions and his continued inspiration in thinking about Milankovitch. MER also thanks the NSF Marine Geology and Geophysics and Atmospheric Sciences Paleoclimate Programs for the support of this research.

## References

Berger, A., Long term variations of daily and monthly insolation during the last Ice Age, *Eos Trans AGU*, *57*(4), 254, 1976.

Berger, A., X. S. Li, and M. F. Loutre, Modeling northern hemisphere ice volume over the last 3 Ma, *Quat. Sci. Rev.*, *18*(1), 1–11, 1999.

Berggren, W., F. Hilgen, C. Langereis, D. Kent, J. Obradovich, I. Raffi, M. E. Raymo, and N. Shackleton, Late Neogene chronology: New perspectives in high resolution stratigraphy, *Geol. Soc. Am. Bull.*, *107*, 1272–1287, 1995.

Bonan, G. B., D. Pollard, and S. Thompson, Effects of boreal forest vegetation on global climate, *Nature*, *359*, 716–718, 1992.

Cande, S. C., and D. V. Kent, A new geomagnetic polarity time scale for the Late Cretaceous and Cenozoic, *J. Geophys. Res.*, *97*(B10), 13,917–13,951, 1992.

Cande, S. C., and D. V. Kent, Revised calibration of the geomagnetic polarity timescale for the late Cretaceous and Cenozoic, *J. Geophys. Res.*, *100*(B4), 6093–6095, 1995.

Clement, B. M., and D. V. Kent, Geomagnetic polarity transition records from five hydraulic piston core sites in the North Atlantic, *Init. Rep. Deep Sea Drill. Proj.*, *96*, 831–852, 1986.

Hartmann, D. L., *Global Physical Climatology*, 409 pp., Academic, San Diego, Calif., 1994.

Gallup, C. D., H. Cheng, F. W. Taylor, and R. L. Edwards, Direct determination of the timing of sea level change during Termination II, *Science*, *295*, 310–313, 2002.

Gildor, H., and E. Tziperman, Sea ice as the glacial cycles climate switch: Role of seasonal and orbital forcing, *Paleoceanography*, *15*, 605–615, 2000.

Imbrie, J., et al., On the structure and origin of major glaciation cycles, 1, Linear responses to Milankovitch forcing, *Paleoceanography*, *7*, 701–738, 1992.

Imbrie, J., A. Berger, and N. J. Shackleton, Role of orbital forcing: a two-million-year perspective, in *Global Changes in the Perspective of the Past*, edited by J. A. Eddy and H. Oeschger, pp. 263–277, John Wiley, New York, 1993a.

Imbrie, J., et al., On the structure and origin of major glaciation cycles, 2, The 100,000-year cycle, *Paleoceanography*, *8*, 699–736, 1993b.

Johnson, R. G., Major Northern Hemisphere deglaciation caused by a moisture deficit 140 ka, *Geology*, *19*, 686–689, 1991.

Kallen, E., C. Crafoord, and M. Ghil, Free oscillations in a climate model with ice-sheet dynamics, *J. Atmos. Sci.*, *36*(12), 2292–2303, 1979.

Kukla, J., The Pleistocene epoch and the evolution of man-A reply, *Curr. Anthropology*, *9*, 27–47, 1968.

Kutzbach, J. E., and R. G. Gallimore, Sensitivity of a coupled atmosphere/mixed layer ocean model to changes in orbital forcing at 9000 years B.P., *J. Geophys. Res.*, *93*, 803–821, 1998.

Laskar, J., The chaotic motion of the solar system: A numerical estimate of the chaotic zones, *Icarus*, *88*, 266–291, 1990.

Mix, A. C., J. Le, and N. J. Shackleton, Benthic foraminiferal stable isotope stratigraphy of Site 846: 0–1.8 Ma, *Proc. Ocean Drill. Prog. Sci. Results*, *138*, 839–854, 1995.

Muller, R. A., and G. J. MacDonald, *Ice Ages and Astronomical Causes*, 318 pp., Springer-Verlag, New York, 2000.

Paillard, D., L. Labeyrie, and P. Yiou, Macintosh program performs time-series analysis, *Eos Trans. AGU*, *77*, 379, 1996.

Peltier, W. R., and S. Marshall, Coupled energy-balance/ice-sheet model simulations of the glacial cycles: a possible connection between terminations and terrigenous dust, *J. Geophys. Res.*, *100*, 14,269–14,289, 1995.

Raymo, M. E., W. F. Ruddiman, J. Backman, B. M. Clement, and D. G. Martinson, Late Pliocene variation in Northern Hemisphere ice sheets and North Atlantic deep circulation, *Paleoceanography*, *4*, 413–446, 1989.

Ruddiman, W. F., M. E. Raymo, D. G. Martinson, B. M. Clement, and J. Backman, Mid-Pleistocene evolution of Northern Hemisphere climate, *Paleoceanography*, *4*, 353–412, 1989.

Shackleton, N. J., A. Berger, and W. R. Peltier, An alternative astronomical calibration of the lower Pleistocene time scale based on ODP site 677, *Trans. R. Soc. Edinburgh Earth Sci.*, *81*, 251–261, 1990.

Tiedeman, R., M. Sarnthein, and N. J. Shackleton, Astronomic timescale for the Pliocene Atlantic $\delta^{18}O$ and dust flux records of Ocean Drilling Program site 659, *Paleoceanography*, *9*, 619–638, 1994.

Trenberth, K. E., and J. Caron, Estimates of meridional atmosphere and ocean heat transports, *J. Clim.*, *14*, 3433–3443, 2001.

Vimeux, F., V. Masson, J. Jouzel, M. Stievenard, and J. R. Petit, Glacial-interglacial changes in ocean surface conditions in the Southern Hemisphere, *Nature*, *398*, 410–413, 1999.

Winograd, I. J., T. Coplen, J. Landwehr, A. Riggs, K. Ludwig, B. Szabo, P. Kolesar, and K. Revesz, Continuous 500,000-year climate record from vein calcite in Devil's Hole, Nevada, *Science*, *258*, 255–260, 1992.

Young, M. A., and R. S. Bradley, Insolation gradients and the paleoclimatic record, in *Milankovitch and Climate, Part 2*, edited by A. L. Berger et al., pp. 707–713, D. Reidel, Norwell, Mass., 1984.

K. H. Nisancioglu, Department of Earth, Atmospheric, and Planetary Sciences, Massachusetts Institute of Technology, Room 54-1715, Cambridge, MA 02139, USA.

M. E. Raymo, Department of Earth Sciences, Boston University, 685 Commonwealth Ave., Boston, MA 02215, USA. (raymo@bu.edu)

# Appendix B

# Reorganization of Miocene Deep Water Circulation in Response to the Shoaling of the Central American Seaway

PALEOCEANOGRAPHY, VOL. 18, NO. 1, 1006, doi:10.1029/2002PA000767, 2003

# Reorganization of Miocene deep water circulation in response to the shoaling of the Central American Seaway

Kerim H. Nisancioglu

Program in Atmospheres, Oceans, and Climate, Department of Earth, Atmospheric, and Planetary Sciences, Massachusetts Institute of Technology, Cambridge, Massachusetts, USA

Maureen E. Raymo

Department of Earth Sciences, Boston University, Boston, Massachusetts, USA

Peter H. Stone

Program in Atmospheres, Oceans, and Climate, Department of Earth, Atmospheric, and Planetary Sciences, Massachusetts Institute of Technology, Cambridge, Massachusetts, USA

Received 5 February 2002; revised 10 August 2002; accepted 26 August 2002; published 11 February 2003.

[1] The response of ocean circulation to the shoaling of the Central American Seaway (CAS) is investigated using the Massachusetts Institute of Technology (MIT) Ocean General Circulation Model (OGCM). In contrast to earlier model studies, it is found that significant amounts of deep water are formed in the North Atlantic prior to the closure of the CAS. However, the circulation pattern is fundamentally different from the modern ocean. In the upper layers of the CAS, there is a relatively strong geostrophic flow from the Pacific to the Atlantic, controlled by the pressure difference across the seaway. However, when the CAS is deeper than the level of North Atlantic Deep Water (NADW) outflow, a significant amount of NADW passes through the CAS to the Pacific Ocean. In the Pacific, the deep water traverses the basin from east to west in a relatively narrow zonal jet, and becomes a southward flowing western boundary current, before it joins with the Antarctic Circumpolar Current (ACC) to the south. This implies that deep sea sediment records from the Miocene Pacific Ocean could have been influenced by relatively young NADW and provides a new framework for the interpretation of geochemical tracer data. Diversification of benthic foraminifer fauna suggests that the CAS shoaled to a depth of about 1000 m toward the end of the middle Miocene. This would have prevented the passage of NADW to the Pacific and established the modern deep water circulation pattern at that time. *INDEX TERMS:* 1620 Global Change: Climate dynamics (3309); 3344 Meteorology and Atmospheric Dynamics: Paleoclimatology; 4255 Oceanography: General: Numerical modeling; 4267 Oceanography: General: Paleoceanography; *KEYWORDS:* paleoceanography, miocene, climate, model, deep water, world ocean

**Citation:** Nisancioglu, K. H., M. E. Raymo, and P. H. Stone, Reorganization of Miocene deep water circulation in response to the shoaling of the Central American Seaway, *Paleoceanography*, *18*(1), 1006, doi:10.1029/2002PA000767, 2003.

## 1. Introduction

[2] Some of the most important changes to past ocean circulation and climate have been connected with tectonic events involving the closure or opening of oceanic gateways. The most recent event of this nature was the closure of the Central American Seaway (CAS) between North and South America. The details of the tectonics in the region are complicated and not well constrained. However, the shoaling of the seaway is thought to have been gradual, beginning ~16 Ma at the early to middle Miocene boundary [*Keller and Barron*, 1983; *Duque-Caro*, 1990; *Droxler et al.*, 1998], with final closure at about 3 Ma in the middle Pliocene [*Keigwin*, 1982; *Marshall et al.*, 1982; *Coates et al.*, 1992].

[3] Before the closure of the CAS, water flowed between the Pacific and Atlantic Oceans at a latitude of about 10°N. Experiments with the Hamburg Ocean General Circulation Model (OGCM) suggest that North Atlantic Deep Water (NADW) production was severely reduced, or nonexistent when the CAS was open, due to a flow of relatively fresh Pacific water into the North Atlantic [*Maier-Reimer et al.*, 1990; *Mikolajewicz et al.*, 1993; *Mikolajewicz and Crowley*, 1997]. While some deep sea sediment core data indicate that the production of NADW increased in the early Pliocene as the CAS closed [*Tiedemann and Franz*, 1997; *Haug and Tiedemann*, 1998; *Billups et al.*, 1999], other data suggests that NADW production was significant in the Miocene when the CAS was open [*Keller and Barron*, 1983; *Miller and Fairbanks*, 1985; *Woodruff and Savin*, 1989; *Delaney*, 1990; *Wright et al.*, 1992].

[4] In this study, the structure of the meridional ocean circulation and its sensitivity to flow through the CAS at different depths is reexamined with the Massachusetts Institute of Technology (MIT) OGCM. It is important to note that the opening of the CAS is applied to the control run of the modern ocean, where modern values are used for


0883-8305/03/2002PA000767$12.00

**Table 1.** Common Parameters Used in Experiments With the MIT Ocean GCM

| Parameters | | Value |
|---|---|---|
| $A_h$ | Horizontal viscosity | $5 \times 10^5$ m$^2$/s |
| $A_z$ | Vertical viscosity | $10^{-3}$ m$^2$/s |
| $K_h$ | Horizontal diffusivity | 0 |
| $K_z$ | Vertical diffusivity | $5 \times 10^{-5}$ m$^2$/s |
| $\Delta T_{mom}$ | Momentum time step | 40 min |
| $\Delta T_{tracer}$ | Tracer time step | 1 day |
| $S_{max}$ | GM Maximum slope | 0.01 |
| $K_I$ | GM isopycnal diffusivity | $10^3$ m$^2$/s |
| $\Delta z$ | Thickness of model layers (m) | 50, 70, 100, 140, 190, 240, 290, 340, 390, 440, 540, 590, 640, and 690 |

the boundary conditions. Therefore, the results should be viewed as a sensitivity study of the meridional overturning circulation to an open CAS, with possible connections to ocean circulation before the closure, rather than as a simulation of climate before 3 Ma.

## 2. Description of the Model and Boundary Conditions

### 2.1. The MIT OGCM

[5] The MIT OGCM is based on the incompressible, Boussinesq form of the Navier–Stoke's equations. Full details of the equations and solution techniques are described by *Marshall et al.* [1997a, 1997b]. In this study the model is used in the hydrostatic limit, and the horizontal resolution is constant at about 2.8° × 2.8°. The maximum depth is 5200 m and there are 15 vertical levels, with the thickness of the layers gradually increasing from 50 m at the ocean surface to 690 m at the bottom (Table 1). As coarse resolution OGCMs are not capable of resolving mesoscale eddies, and ocean circulation is affected by mixing processes due to these eddies, it is necessary to apply a subgrid-scale parameterization for the advection of tracers (such as temperature and salinity). In this version of the model, the parameterization of *Gent and McWilliams* [1990], together with diffusion of tracers along isopycnals [*Redi*, 1982], is implemented as described by *Griffies* [1998].

### 2.2. Surface Boundary Conditions

[6] In the experiments, the model ocean is initialized with temperature and salinity fields from the studies of *Levitus and Boyer* [1994] and *Levitus et al.* [1994] at all depths for the month of March, when maximum convection takes place in the North Atlantic [*Marshall and Schott*, 1999]. Subsequently, the surface is forced with observed surface heat and freshwater fluxes, as well as sea surface temperature, i.e., mixed boundary conditions given by

$$K_z \frac{\partial S}{\partial z} = S_R F_W \tag{1}$$

$$K_z \frac{\partial T}{\partial z} = \frac{\Delta z}{\tau_T}(T_{obs} - T) + \frac{Q_{obs}}{\rho_0 C_P} \tag{2}$$

where $S_R$ is a reference salinity taken to be equal to 35 psu, $F_W$ is the net freshwater flux in m/s, due to evaporation, precipitation, and runoff (from rivers and ice discharge), $\rho_0$ is a reference density, $C_P$ is the specific heat capacity of seawater, and $Q_{obs}$ is the net heat flux into the oceans in W/m$^2$. The sea surface temperature relaxation time step $\tau_T$ is set to 75 days.

[7] Traditionally, when using mixed boundary conditions, the surface freshwater flux ($F_W$) and the heat flux ($Q_{obs}$) are diagnosed from a spin-up run using restoring boundary conditions [e.g., *Maier-Reimer et al.*, 1990]. In this study, the diagnosed fluxes are not used because they do not correspond to the observed atmospheric fluxes of heat and freshwater, and numerous model studies have found that GCMs forced with traditional mixed boundary conditions are unrealistically unstable to perturbations in the surface fresh water field [*Marotzke and Willebrand*, 1991; *Mikolajewicz and Maier-Reimer*, 1994; *Tziperman et al.*, 1994].

[8] The annual mean surface freshwater flux is based on precipitation minus evaporation data of *Schmitt et al.* [1989] for the Atlantic and *Baumgartner and Reichel* [1975] for the other oceans, combined with river runoff data of *Perry et al.* [1996], as well as Greenland ice-calving data of *Reeh* [1994] (Figure 1). It should be noted that the Arctic and its influence on the freshwater budget is not represented in the present version of the model. Monthly data for surface heat flux is compiled from an updated version of *Trenberth and Solomon* [1994] [see *Jiang et al.*, 1999]. Monthly wind stress fields are obtained from the data of the European Center for Medium-Range Weather Forecasts (ECMWF) for the years 1980–1986, as computed by *Trenberth et al.* [1989].

### 2.3. Experiment Implementation

[9] The time steps for the momentum and tracer equations are 40 min and 24 hours, respectively. Both time steps are constant with integration time, and the same values are used for all experiments. Note that the tracer time step is larger than the momentum time step by a factor of 36. This speeds up the relatively slow abyssal processes, and significantly accelerates the convergence of the model to equilibrium [*Bryan*, 1984]. The disadvantage is that it distorts the seasonal cycle [*Danabasoglu et al.*, 1996]. However, the annual mean conditions, which are discussed in this paper, are preserved [*Kamenkovich et al.*, 2002].

[10] The following three model experiments were undertaken to test the sensitivity of ocean circulation to the CAS:

1. CNTR: Control experiment with modern configuration of the continents and bathymetry,

2. CAS2700: Perturbed experiment with the bathymetry of the control experiment modified by introducing a three

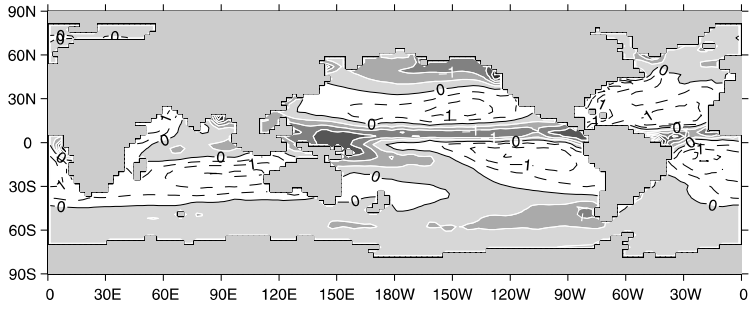


**Figure 1.** Annual mean surface freshwater flux ($F_W$) in m/yr equal to evaporation minus precipitation and runoff (from rivers and ice calving).

grid boxes wide and 2700 m deep channel, separating North and South America at latitudes of about 11°–19.5°N,

3. CAS1000: Same as CAS2700, but with a 1000 m deep channel.

The structure of the CAS chosen for experiment CAS2700 is similar to that used by *Maier-Reimer et al.* [1990]. The intermediate sill depth in experiment CAS1000 is chosen, because there is evidence from benthic foraminifera suggesting that the sill could have shoaled to about 1000 m by the end of the middle Miocene (~12.5 Ma) [*Duque-Caro*, 1990]. The same climatological data sets are used for the experiments with an open CAS as for the control experiment.

## 3. Model Results

### 3.1. Meridional Overturning Transport

[11] The Eulerian mean meridional overturning stream function, for the Global and Atlantic Oceans of the control experiment (CNTR), shows that the overturning circulation is dominated by the thermohaline cell, originating primarily in the North Atlantic (Figure 2a). This clockwise overturning consists of a warm, relatively saline northward flow in the upper branch, and a cold, southward return flow in the lower branch, recognized as NADW. The maximum strength of the cell is positioned at about 55°N and 1200 m depth in the North Atlantic with an overturning strength of 30 Sv. This is associated with 18 Sv of NADW transport southward across the equator, which agrees well with the modern value of 18 ± 3 Sv, estimated by *Ganachaud* [1999]. From the same figure it can be seen that there is very little Antarctic Bottom Water (AABW) produced in the Atlantic basin of the model. This is thought to be due partly to the lack of a representation of sea ice and the associated brine rejection in the present version of the model.

[12] A comparison of the control (CNTR) with the perturbed experiments (CAS2700 and CAS1000), reveals that the global meridional overturning circulation remains relatively unchanged when the CAS is open (Figures 2b and 2c). The maximum overturning in the Atlantic is reduced to 26 Sv in CAS2700 and CAS1000. Also, the deep southward transport of NADW across the equator in CAS1000 is reduced to 14 Sv. However, in experiment CAS2700 this transport decreases to 6 Sv, which is about one third of the value found in the control experiment. In other words, although the global meridional overturning is relatively strong, the influence of NADW in the South Atlantic appears to be greatly reduced when the CAS is deeper than about 1000 m.

### 3.2. Surface and Deep Currents

[13] The surface and deep circulation for experiment CNTR (Figures 3a and 4a) correspond reasonably well with the observed currents of the modern ocean. NADW originating in the Labrador and Greenland Seas, flows south as a western boundary current in the Atlantic, before it joins the Antarctic Circumpolar Current (ACC) and eventually upwells in the Pacific and Indian Oceans. A deep western boundary current is also observed in the southern Pacific, where a combination of AABW and NADW flows north from the ACC region.

[14] In experiment CAS2700, the surface circulation (Figures 3b and 3c) does not change much from that of the control experiment, except for a weakening of the western boundary current in the South Atlantic. However, a significant amount of water is shown flowing from the Pacific to the Atlantic. This flow increases in strength below the surface to a maximum at a depth of about 500 m (Figure 5).

[15] At depths below about 1000 m, the flow reverses, and a strong flow from the Atlantic through the CAS to the Pacific is observed. The result is a reduction in the amount of deep water crossing the equator from the North Atlantic to the South Atlantic compared to experiment CNTR, as was observed in the figures of the meridional overturning stream function (Figure 2b). In the same model run, it can be seen that the deep western boundary current in the southern Pacific reverses direction, and flows south toward the ACC region (Figures 4b and 4c). The reversal of the deep western boundary current is observed down to depths of about 3500 m, below which the circulation remains relatively unchanged (not shown).

[16] The deep flow from the Atlantic to the Pacific is caused by the disappearance of the E-W pressure gradient when the western boundary of the Atlantic basin is removed and replaced by the seaway. This allows the deep western boundary current in the Atlantic (which today consists

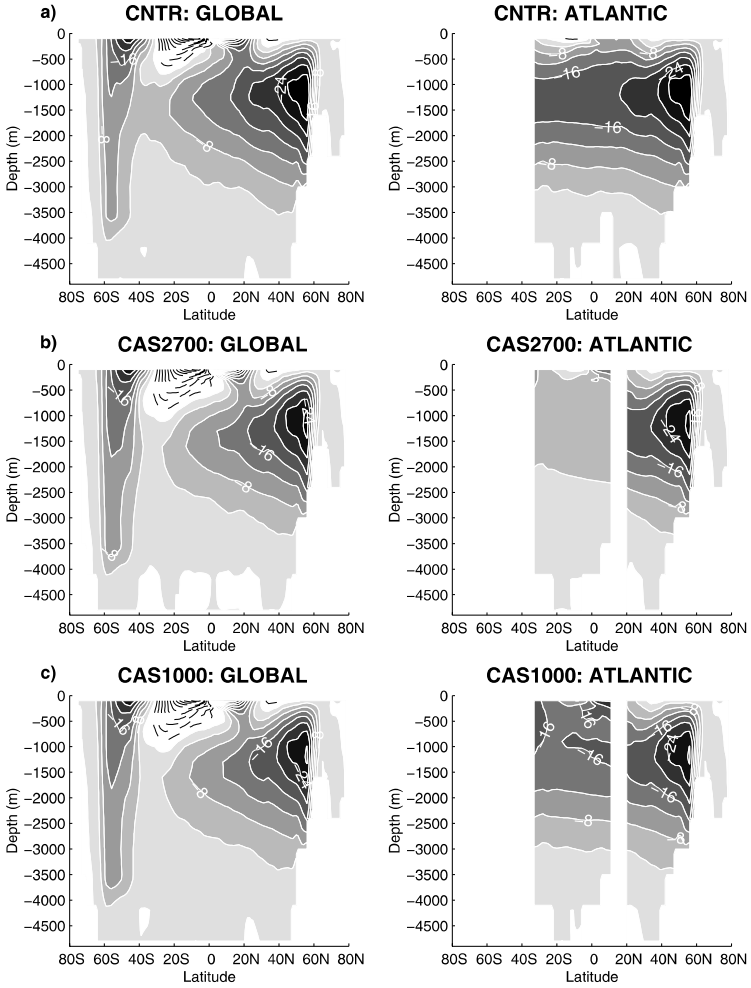


**Figure 2.** Eulerian mean Meridional Overturning Stream (MOS) function in units of Sv (Sv = $10^6$ $m^3/s$) for the Global and Atlantic oceans. The MOS is calculated from a 10-year mean of meridional velocity after 2000 years of model integration. Negative values (solid contours) imply clockwise overturning, and positive values (stippled contours) imply counterclockwise overturning. The contour interval is 4 Sv. (a) CNTR, (b) CAS2700, and (c) CAS1000.

mostly of NADW) to pass through the CAS to the Pacific, and reduces the southward flow to the South Atlantic. The total eastward and westward transports through the CAS with a sill depth of 2700 m are about 17 and 10 Sv, respectively (Figure 5).

[17] In experiment CAS1000, deep westward transport of NADW through the CAS is prevented by the shallow sill. This sill creates a boundary between the Atlantic and Pacific at depths below 1000 m, which supports the flow of the deep western boundary current to the South Atlantic. Therefore, the transport in the CAS is mainly eastward, with a strength of about 16 Sv (Figure 5).

### 3.3. Poleward Heat Transport (PHT)

[18] According to *Ganachaud and Wunsch* [2000], the estimated maximum modern PHT by the global ocean is $1.8 \pm 0.3$ and $-0.8 \pm 0.6$ PW for the Northern and Southern Hemispheres, respectively. These are relatively close to the values found for experiment CNTR, where the maximum PHTs are 1.7 and $-1.4$ PW (Figure 6a). In this experiment,

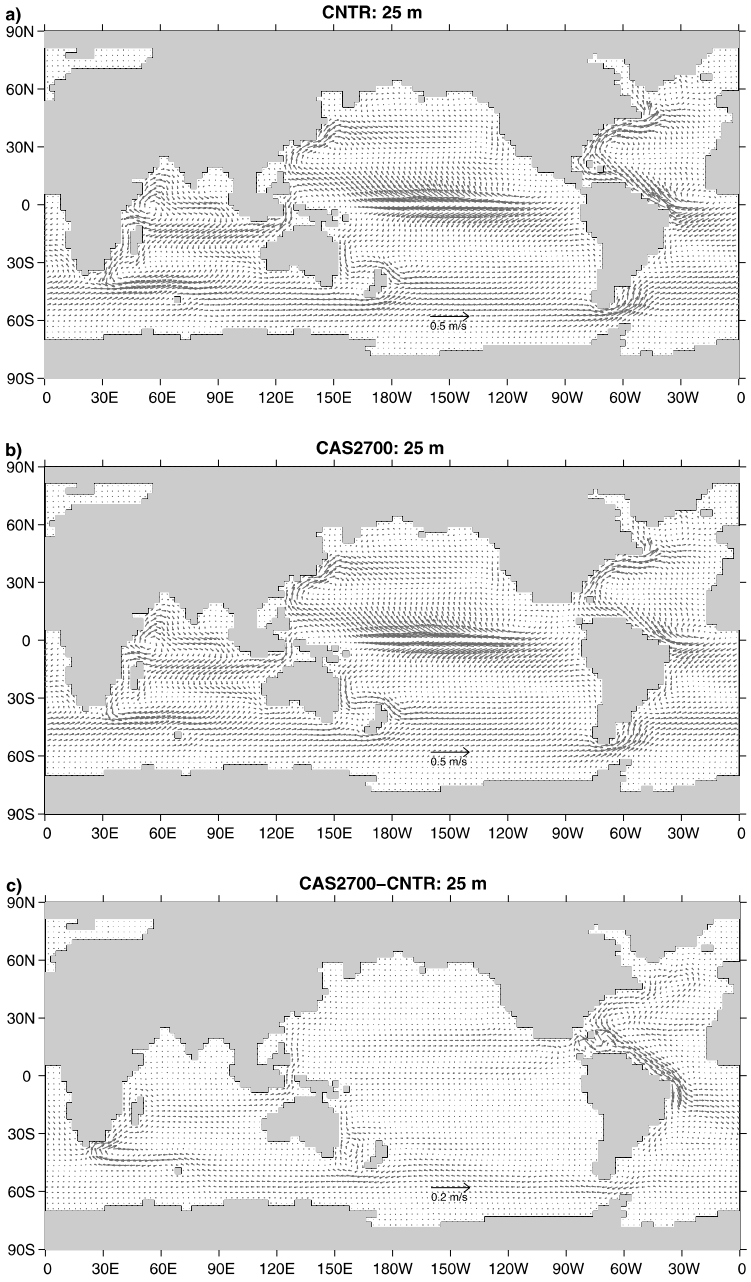


**Figure 3.** Ocean currents in m/s after 2000 years of model integration at a depth of 25 m for experiments (a) CNTR, (b) CAS2700, and (c) CAS2700 minus CNTR.

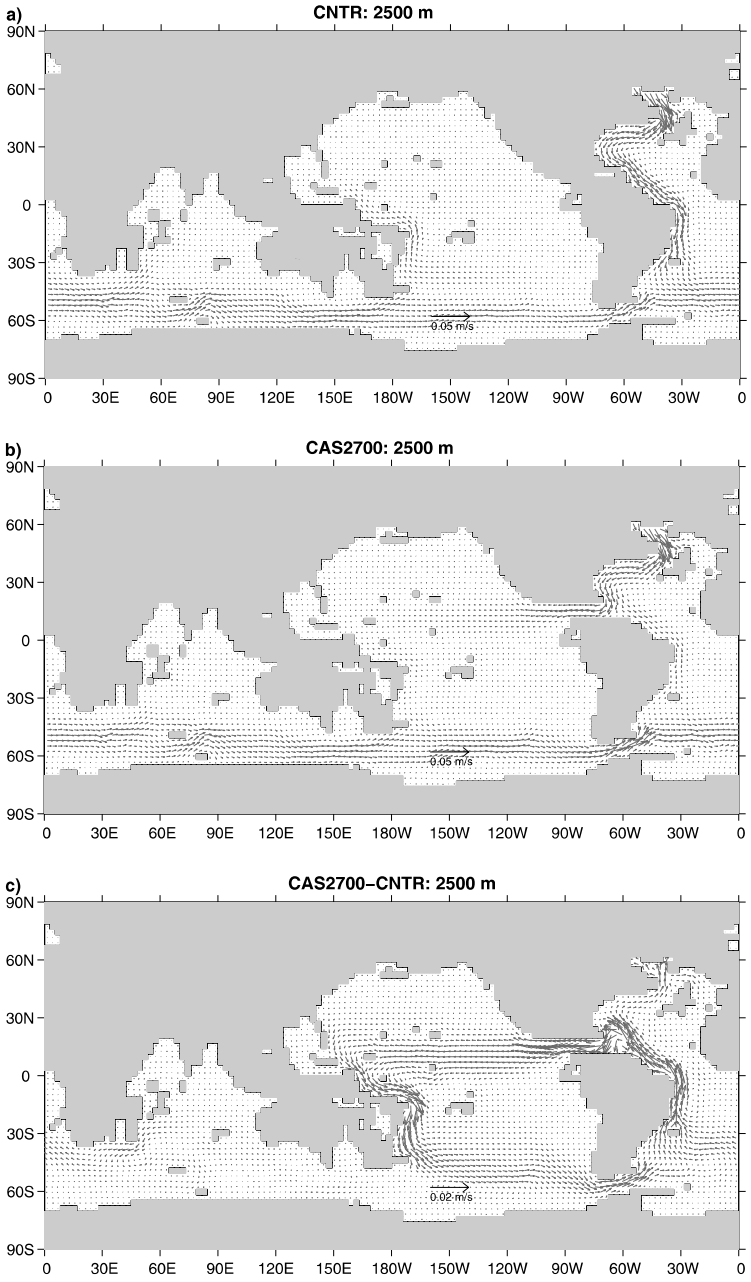


**Figure 4.** Ocean currents in m/s after 2000 years of model integration at a depth of 2500 m for experiments (a) CNTR, (b) CAS2700, and (c) CAS2700 minus CNTR.

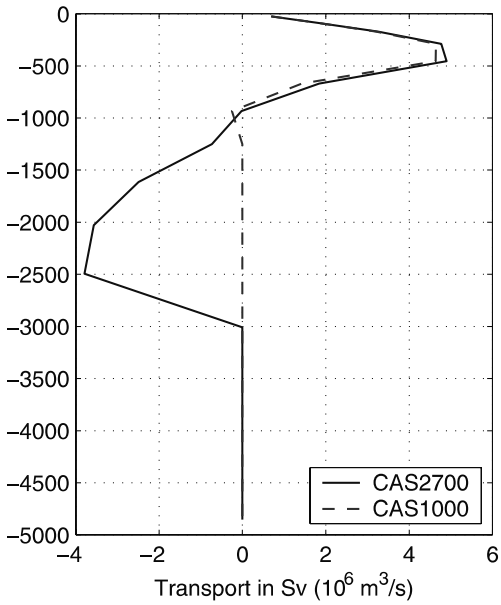


**Figure 5.** Transport through the CAS in Sv as a function of depth for experiments CAS2700 (solid blue line) and CAS1000 (dashed green line), with sill depths of 2700 and 1000 m, respectively. Positive and negative values imply eastward and westward transport, respectively.

transport by the Atlantic is northward at all latitudes, and dominates the PHT in the Northern Hemisphere, with a smaller northward contribution by the Indo-Pacific. In the Southern Hemisphere, the Indo-Pacific dominates with a strong southward transport.

[19] In experiments CAS2700 and CAS1000, the global PHT in the Northern Hemisphere is reduced by 14% and the global PHT in the Southern Hemisphere is enhanced by 13%, compared to the control experiment. The decrease in the Northern Hemisphere is due to a smaller Atlantic heat transport, whereas the contribution by the Indo-Pacific remains relatively unchanged.

[20] The observed increase in the heat transport in the Southern Hemisphere is linked to the reduced export of NADW south of the equator. In experiment CNTR, 18 Sv of NADW is exported southward across the equator. This has to be balanced by an import of surface waters from the South Atlantic. However, when the NADW export is reduced, as in CAS2700 (6 Sv) and CAS1000 (14 Sv), the import of South Atlantic surface water is reduced as well. The result is a warming of South Atlantic surface waters, and an increase in southward heat transport.

## 4. Discussion

[21] The model experiments suggest that the shoaling of the CAS had a significant impact on the circulation of the world's oceans. The most notable result is the strong flow through the CAS. This flow is found to vary in strength and direction with depth, and has a significant impact on the global overturning circulation; in particular the deep circulation of the Pacific Ocean.

[22] The experiments show that when the CAS is open, deep water forms in the high latitudes of the North Atlantic (NADW) and passes through the CAS to the Pacific. Once in the Pacific, the deep water flows westward in a relatively narrow zonal jet, and approaches the western boundary of the basin. At the western boundary, the water becomes a southward flowing boundary current, joining with the ACC to the south (see Figure 4b). In the Atlantic, part of the NADW produced flows past the CAS as a western boundary current even when it is open, however, the strength of the current is greatly reduced compared to the control experiment.

[23] These model results are in agreement with the dynamical framework of *Stommel and Arons* [1960a, 1960b] for the abyssal circulation. According to this theory, deep water produced at its source in the modern North Atlantic flows south to the Southern Ocean, where it combines with deep water produced in the Weddell Sea, and increases the transport of the ACC (Figure 7a). This in turn, feeds the northward flowing deep western boundary currents in the Indian and Pacific Oceans, and eventually upwells in the interior of the basins. The opening of the CAS (Figure 7b) is equivalent to introducing a source of deep water at the eastern boundary of the North Pacific, which connects to the western boundary of the basin through a zonal jet. This additional source of deep water in the Pacific results in a reversal of the deep western boundary current, which flows south and joins the ACC.

[24] It is further conceivable that part of the NADW could have continued from the Pacific through the Indonesian Passage and into the Indian Ocean, if the passage was sufficiently deep. However, an investigation of this idea requires further research as the depth of the Indonesian passage and its development through time is uncertain.

### 4.1. Comparisons With Earlier Model Studies

[25] The results from the experiments presented here differ from earlier model studies with the Hamburg OGCM [*Maier-Reimer et al.*, 1990]. According to the experiments with the Hamburg model, a CAS with a sill depth of about 2700 m, results in a flow of 10 Sv from the Pacific to the North Atlantic. This dilutes the surface salinity in the North Atlantic by >1.0 psu, with the largest changes seen in the subpolar North Atlantic (2.0–3.0 psu fresher). This decrease in salinity prevents the formation of NADW. Thus, no deep flow from the Atlantic to the Pacific is observed in these experiments, due to the negligible production of deep water in the North Atlantic, and the concomitant reduction in the strength of the deep western boundary current.

[26] In the experiments presented here, the North Atlantic is freshened by about 0.5 psu at latitudes above ~30°N, due to the eastward flow in the upper layers of the CAS. This

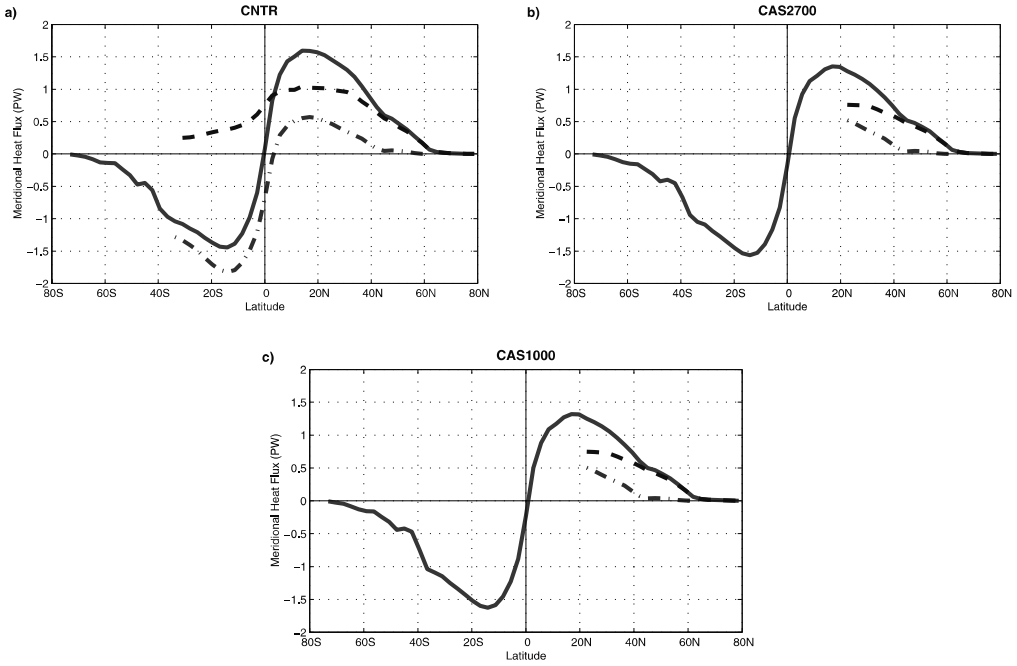


**Figure 6.** Total PHT in units of PW, where $10^{15}$ W = 1 PW for the Global (solid red line), Atlantic (dashed blue line), and Indo-Pacific (dash-dotted green line) basins. Positive and negative values imply northward and southward transport, respectively.

change is significantly smaller than that found by *Maier-Reimer et al.* [1990]. One reason for this is that the low surface salinity in the subpolar North Atlantic of the Hamburg model is not caused solely by the influx of Pacific water, which has a mean salinity about 1.5 psu lower than the Atlantic [*Broecker*, 1989]. The salinity is also reduced by the import of Arctic water, as the northeastward flow in the subpolar North Atlantic switches to southwestward. This effect is not observed in the experiments with the MIT OGCM, as the model does not include a representation of the Arctic Ocean. At the same time, the northward flowing Gulf Stream and North Atlantic Drift remain relatively strong when the CAS is open, preventing the southward flow of fresher water from the northernmost part of the basin.

[27] Earlier model studies, including studies with the Hamburg OGCM, suggest that more than one mode of meridional overturning circulation may exist in experiments with modern bathymetry and identical boundary conditions [e.g., *Broecker et al.*, 1985; *Manabe and Stouffer*, 1988; *Marotzke and Willebrand*, 1991; *Maier-Reimer et al.*, 1993]. To test whether the MIT OGCM can exhibit additional steady states, experiment CAS2700 is initialized with fields of homogeneous salinity and stratified, horizontally uniform temperature, instead of the full temperature and salinity fields of *Levitus and Boyer* [1994] and *Levitus et al.* [1994]. Except for these fields, all the boundary conditions remain the same. When integrated the model converges toward the same equilibrium state as the original experiment. Thus, the model gives the same solution with different initial conditions, and there are no indications of secondary modes of circulation.

[28] The test described above is not sufficient to rule out the possible existence of multiple steady states. However, during the course of this study, as well as numerous other experiments with the MIT OGCM, there is no evidence of multiple steady states of the ocean circulation. It is conceivable that the lack of a full Arctic basin in the present model configuration reduces the magnitude of the freshening in the North Atlantic as well as the change in deep water formation in response to an open CAS. However, it is unlikely that the circulation would switch to a steady state without NADW formation.

[29] The increased stability of the meridional overturning circulation in the MIT OGCM is believed to be mainly due to improvements in the surface boundary conditions and the parameterization of mixing due to subgrid-scale eddies. In the experiments with the Hamburg model, traditional mixed boundary conditions are used, where the freshwater flux is diagnosed from a control run with restoring of the surface fields to observed temperatures and salinities. The resulting freshwater flux does not agree well

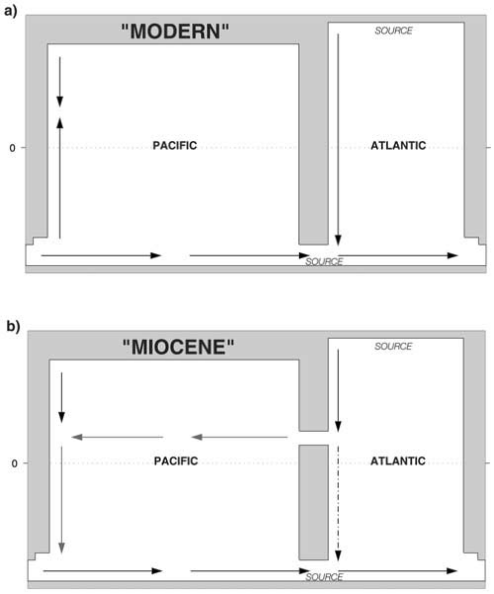


**Figure 7.** A simplified sketch of the reorganization of the abyssal circulation implied by the model experiments. The interior flow has not been drawn and the only sources of deep water are in the North Atlantic and Southern Ocean. (a) Control experiment with "modern" bathymetry. (b) Perturbed experiment with a CAS extending to depths below the core of NADW.

with observations, and leads to a meridional overturning circulation which is unrealistically sensitive to perturbations in surface salinity [e.g., *Marotzke and Willebrand*, 1991; *Mikolajewicz and Maier-Reimer*, 1994; *Tziperman et al.*, 1994].

### 4.2. Implications for Neogene Ocean Circulation and Climate

[30] The experiments described in this study employ modern continental configurations and atmospheric forcing. These conditions do not realistically represent the climate of the Miocene and Pliocene, and the results do not represent a simulation of ocean circulation during these periods. Instead, the results test the sensitivity of ocean circulation to a CAS with different depths. The model makes several physically based predictions which might lead to a better understanding of the role of the CAS in ocean circulation and climate. The following predictions can be compared with geochemical and sedimentological tracers from ocean sediment cores: (1) NADW was formed before the final closure of the CAS, (2) a sill depth greater than about 1000 m allows for the passage of a westward jet of NADW into the Pacific Ocean, thus greatly reducing the amount of NADW transported to the South Atlantic, (3) in the western Pacific relatively young NADW flows south as a deep western boundary current, and (4) a shallow sill prevents the flow of NADW to the Pacific and enhances the flow of NADW to the South Atlantic.

#### 4.2.1. Miocene Deep Water Circulation

[31] Data from deep sea sediment cores strongly suggests that NADW was being formed during parts of the middle Miocene (~17–11 Ma) [*Keller and Barron*, 1983; *Miller and Fairbanks*, 1985; *Woodruff and Savin*, 1989], and that the flux of NADW increased in the late Miocene (~11–5 Ma) [*Keller and Barron*, 1983; *Woodruff and Savin*, 1989; *Delaney*, 1990; *King et al.*, 1997], approaching modern values at the time of the final closure of the CAS in the early Pliocene (~5–3 Ma) [*Tiedemann and Franz*, 1997; *Haug and Tiedemann*, 1998; *Billups et al.*, 1999]. While these observations are consistent with this study, the model results also demonstrate that as the CAS shoaled it could have caused dramatic changes to the intermediate and deep circulation in the tropical Pacific, and along the western boundaries of the South Pacific and South Atlantic. It should be possible to test these findings with tracer data from deep sediment cores in these regions.

[32] A common procedure used to infer the relative influences of NADW and AABW in the Atlantic basin has been to compare paleo tracer data (such as $\delta^{13}C$ and *Cd*/*Ca*) from core sites in the Atlantic and Pacific. Convergence of tracer data between the two basins has typically been interpreted as evidence of NADW being replaced in the Atlantic basin by water of Southern Ocean (Pacific) origin [e.g., *Delaney*, 1990; *Wright et al.*, 1992]. However, the model experiments presented here (Figure 4b) suggest that cores in the western South Pacific and western Atlantic could have been influenced by a common water mass during the middle Miocene, with age and nutrient characteristics similar to modern NADW. In other words, convergence of geochemical tracers could indicate NADW in both basins, not water of Pacific or Southern Ocean origin.

[33] *Delaney* [1990], in a study of relative cadmium content (*Cd*/*Ca*) of Miocene benthic foraminifera from the deep South Atlantic (Site 289) and deep western equatorial Pacific (Site 525), showed that the difference in *Cd*/*Ca* ratio between the Atlantic and Pacific was negligible in the early Miocene, small in the middle Miocene, and relatively large in the late Miocene. This data can be interpreted to indicate that relatively young NADW from the CAS could have been present in the western equatorial Pacific during the early and middle Miocene. Similarly, a study comparing benthic foraminiferal $\delta^{13}C$ data from cores in the North Atlantic (Deep Sea Drilling Project (DSDP) 563) and western equatorial Pacific (DSDP 289) [*Wright et al.*, 1992], shows a negligible difference between North Atlantic and South Pacific $\delta^{13}C$ values during the early middle Miocene (15–13 Ma), again consistent with the model predictions.

[34] The sill depth is of great importance in controlling the flow in the CAS. A study of the foraminiferal biostra-

tigraphy of the Atrato Basin in northern South America during the Neogene (~24–2 Ma) [*Duque-Caro*, 1990], indicates that there was a major uplift of the sill to a depth of about 1000 m during the middle Miocene, at ~13–12 Ma, disrupting the exchange of deep water between the Atlantic and Pacific Oceans. This would be analogous to a transition from experiments CAS2700 to CAS1000, and would predict that relatively young NADW would no longer be entering the Pacific via the CAS.

[35] The proposed time for the shoaling of the CAS is close in time to observed increases in NADW formation [*Keller and Barron*, 1983; *Woodruff and Savin*, 1989; *Delaney*, 1990; *King et al.*, 1997], as well as the late Miocene ''carbonate crash.'' Studies from Leg 138 of the Ocean Drilling Program (ODP) find that the east equatorial Pacific was characterized by relatively high carbonate concentrations and accumulation rates before about 11 Ma. However, the accumulation rates declined between 11 and 9.8 Ma, and at about 9.5 Ma, an almost complete loss of carbonate was observed [*Lyle et al.*, 1995; *Farrell et al.*, 1995]. According to *Lyle et al.* [1995], the carbonate crash could not have been caused by an abrupt increase in productivity, or by loss of organic carbon from continental shelves. Instead, the authors conclude that the crash was probably caused by a relatively small reduction in deep water exchange between the Atlantic and Pacific Oceans through the CAS [*Lyle et al.*, 1995; *Farrell et al.*, 1995]. This interpretation is fully consistent with this study, and suggests that the CAS shoaled to less than 1000 m depth by the late Miocene. At this time, the deep water exchange was cut off and in the Pacific carbonate saturated NADW was replaced with older, carbonate undersaturated deep water from the Southern Ocean.

[36] Starting about 10.5 Ma, close in time to the east equatorial carbonate crash, ODP Leg 154 sites at Ceara Rise in the west equatorial Atlantic, experienced a permanent increase in carbonate preservation [*King et al.*, 1997]. Again, this agrees with the model results that predict an increased influence of less corrosive NADW in the South Atlantic as the CAS shoals to 1000 m depth.

#### 4.2.2. Pliocene Climate Change

[37] While the exact sequence of tectonic events leading to the shoaling of the CAS are uncertain [e.g., *Droxler et al.*, 1998; *Mann*, 1999], the timing of the final closure is better constrained. An early study by *Keigwin* [1982], compares $\delta^{18}O$ and $\delta^{13}C$ values of benthic and planktonic foraminifera from DSDP sites in the eastern Pacific and western Caribbean, covering a period ~8–2 Ma. From the $\delta^{18}O$ data it is found that the salinity of Caribbean surface waters started increasing ~4.6 Ma. Further, the $\delta^{13}C$ difference between the two basins increased at ~6 Ma and again at ~3 Ma, approaching modern values. From these data, *Keigwin* [1982] estimated that the final closure of the CAS took place about 3 Ma. Supporting these results are data presented by *Marshall et al.* [1982], which show that the exchange of marine organisms across the CAS was eliminated ~3 Ma, while the exchange of terrestrial biota between the two continents was enhanced.

[38] The proximity of the final closure of the CAS to the onset of enhanced northern hemisphere glaciation ~2.9–2.6 Ma [*Shackleton et al.*, 1984; *Raymo*, 1994; *Maslin et al.*, 1996; *Spielhagen et al.*, 1997] has prompted several authors to connect the two events [*Kaneps*, 1979; *Keigwin*, 1982; *Stanley*, 1995; *Haug and Tiedemann*, 1998; *Driscoll and Haug*, 1998]. According to the study by *Haug and Tiedemann* [1998], the closure of the CAS strengthened the Gulf Stream and the transport of warm saline water to high latitudes of the North Atlantic. This increased the production of NADW, leading to greater evaporative cooling of surface waters and increased atmospheric moisture content. Combined with favorable orbital obliquity, the enhanced moisture content facilitated a buildup of ice sheets in the Northern Hemisphere. The study by *Driscoll and Haug* [1998] proposes a similar mechanism, involving enhanced freshwater delivery to the Arctic via Siberian rivers and the formation of sea ice.

[39] The differences between experiments CAS1000 and CNTR imply that the production of NADW increased at the time of the final closure of the CAS, in agreement with the studies of *Haug and Tiedemann* [1998] and *Driscoll and Haug* [1998]. However, the increased strength of the meridional overturning circulation also implies that additional heat is transported to high latitudes of the North Atlantic (Figure 6). According to the model experiments, the total global PHT is enhanced by about 10% when the CAS is closed, due mostly to a 30% increase in the PHT by the North Atlantic. Indeed, *Berger and Wefer* [1996] have suggested that such an increase in PHT may have delayed the onset of Northern Hemisphere glaciation by several million years, and may possibly have been the cause of the early Pliocene warm period (~5–3) [e.g., *Dowsett et al.*, 1996; *Crowley*, 1996]. Both interpretations above are consistent with the model results: It is not clear whether the effect of the heat or the moisture fluxes dominates in controlling the growth of Northern Hemisphere ice sheets. To further investigate the effect of the final closure of the CAS on the onset of Northern Hemisphere glaciation, it will be necessary to include an atmospheric component to the ocean model. With such a coupled ocean–atmosphere model it will be possible to model changes to the heat and moisture transport by the atmosphere induced by the closure of the CAS.

## 5. Summary and Conclusions

[40] Experiments with the MIT OGCM were performed to investigate the response of ocean circulation to the shoaling and eventual closure of the CAS. Three model experiment were conducted: A control experiment with modern bathymetry, and two experiments with a CAS with sill depths of 2700 and 1000 m. The model experiments make several physically based predictions, providing a new framework with which to interpret Miocene geochemical tracer data:

1. Deep water is formed in the North Atlantic when the CAS is open, in agreement with Miocene and Pliocene geochemical tracer data. However, the formation rate is reduced by about 10% compared to the control experiment.
2. The reduced rate of NADW formation is due to a flow of relatively fresh water from the Pacific to the Atlantic in the

upper 1000 m of the CAS. The flow increases in strength below the surface to a maximum at a depth of about 500 m.

3. A sill depth greater than about 1000 m allows for the passage of a westward jet of NADW into the Pacific Ocean, thus greatly reducing the amount of NADW transported to the South Atlantic.

4. In the western Pacific, the NADW flows southward as a deep western boundary current, eventually joining the ACC. The presence of relatively young NADW in the western Pacific is consistent with records of $\delta^{13}C$ and *Cd*/*Ca*, which show similar values in the western Pacific and western Atlantic during the middle Miocene.

5. In response to the reduced export of NADW to the South Atlantic, the amount of imported South Atlantic surface water is reduced. The result is a warming of surface waters in the South Atlantic, and an increase in southward heat transport.

6. As the CAS shoals, the flow of NADW to the Pacific is prevented, and the flow of NADW to the South Atlantic is enhanced, creating the modern deep water circulation pattern. This change in the path of relatively young carbonate saturated NADW, is consistent with sediment core data. The data show a loss of carbonate in the east equatorial Pacific and an increase in carbonate preservation in the west equatorial Atlantic at the middle to late Miocene boundary, when the CAS is believed to have shoaled to intermediate depths.

[41] **Acknowledgments.** We are grateful to Veronique Bugnion, Baylor Fox-Kemper, Jeff Scott, John Marshall, Jochem Marotzke, and Ed Boyle for their encouragement and helpful comments. We would also like to thank Tom Crowley and Uwe Mikolajewicz for their valuable comments on an earlier version of this paper. Funding for M.E.R. was provided by MGG NSF grant OCE-0049011.

## References

Baumgartner, A., and E. Reichel, *The World Water Balance*, 179 pp., Elsevier Sci., New York, 1975.

Berger, H. W., and G. Wefer, Expedition into the past: Paleoceanographic studies in the South Atlantic, in *The South Atlantic: Present and Past Circulation*, edited by G. Wefer et al., pp. 363–410, Springer-Verlag, New York, 1996.

Bifllups, K., A. C. Ravelo, J. C. Zachos, and R. D. Norris, Link between oceanic heat transport, thermohaline circulation, and the Intertropical Convergence Zone in the early Pliocene Atlantic, *Geology*, *27*(4), 319–322, 1999.

Broecker, W. S., The salinity contrast between the Atlantic and Pacific Oceans during glacial time, *Paleoceanography*, *4*, 207–212, 1989.

Broecker, W. S., D. M. Peteet, and D. Rind, Does the ocean–atmosphere system have more than one stable mode of operation, *Nature*, *315*, 21–26, 1985.

Bryan, K., Accelerating the convergence to equilibrium of ocean climate models, *J. Phys. Oceanogr.*, *14*, 666–673, 1984.

Coates, A. G., J .B. C. Jackson, J. S. Collins, T. M. Cronin, H. J. Dowsett, L. M. Bybell, P. Jung, and J. A. Obando, Closure of the Isthmus of Panama: The near-shore marine record of Costa Rica and western Panama, *Geol. Soc. Am. Bull.*, *104*, 814–828, 1992.

Crowley, T. J., Pliocene climates: The nature of the problem, *Mar. Micropaleontol.*, *27*, 3–12, 1996.

Danabasoglu, G., J. C. McWilliams, and W. G. Large, Approach to equilibrium in accelerated global oceanic models, *J. Clim.*, *9*, 1092–1110, 1996.

Delaney, L. M., Miocene benthic foraminiferal Cd/Ca records: South Atlantic and western equatorial Pacific, *Paleoceanography*, *5*, 743–760, 1990.

Dowsett, H., J. Barron, and R. Poore, Middle Pliocene sea surface temperatures: A global reconstruction, *Mar. Micropaleontol.*, *27*, 13–25, 1996.

Driscoll, N. W., and G. H. Haug, A short circuit in thermohaline circulation: A cause for Northern Hemisphere glaciation?, *Science*, *282*, 436–438, 1998.

Droxler, A. W., K. C. Burke, A. D. Cunningham, A. C. Hine, E. Rosencrantz, D. S. Duncan, P. Hallock, and E. Robinson, Caribbean constraints on circulation between Atlantic and Pacific oceans over the past 40 million years, in *Tectonic Boundary Conditions for Climate Reconstructions*, edited by T. J. Crowley and K. C. Burke, pp. 169–191, Oxford Univ. Press, New York, 1998.

Duque-Caro, H., Neogene stratigraphy, paleoceanography and paleobiogeography in northwest South America and the evolution of the Panama Seaway, *Palaeogeogr. Palaeoclimatol. Palaeoecol.*, *77*, 203–234, 1990.

Farrell, J. W., I. Raffi, T. R. Janacek, D. W. Murray, M. Levitan, K. A. Dadey, K.-C. Emeis, M. Lyle, J.-A. Flores, and S. Hovan, Late Neogene sedimentation patterns in the eastern equatorial Pacific Ocean, in *Proc. Ocean Drill. Program Sci. Results*, vol. 138, edited by N. G. Pisias et al., pp. 717–756, Ocean Drill. Program, College Station, Tex., 1995.

Ganachaud, A. S., Large scale oceanic circulation and fluxes of freshwater, heat, nutrients and oxygen, doctoral dissertation thesis, Mass. Inst. of Technol., Cambridge, Mass., 1999.

Ganachaud, A. S., and C. Wunsch, Improved estimates of global ocean circulation, heat transport and mixing from hydrographic data, *Nature*, *408*, 453–456, 2000.

Gent, P. R., and J. C. McWilliams, Isopycnal mixing in ocean circulation models, *J. Phys. Oceanogr.*, *20*, 150–155, 1990.

Griffies, S. M., The Gent–McWilliams skew flux, *J. Phys. Oceanogr.*, *28*, 831–841, 1998.

Haug, G. H., and R. Tiedemann, Effect of the formation of the Isthmus of Panama on Atlantic Ocean thermohaline circulation, *Nature*, *393*, 673–676, 1998.

Jiang, S., P. H. Stone, and P. Malanotte-Rizzoli, An assessment of the Geophysical Fluid Dynamics Laboratory ocean model with coarse resolution: Annual-mean climatology, *J. Geophys. Res.*, *104*(C11), 25,623–25,645, 1999.

Kamenkovich, I. V., A. Sokolov, and P. H. Stone, An efficient climate model with a 30 ocean and statistical-dynamical atmosphere, *Clim. Dyn.*, *19*, 585–598, 2002.

Kaneps, A. G., Gulf Stream: Velocity fluctuations during the late Cenozoic, *Science*, *204*, 297–301, 1979.

Keigwin, L., Isotopic paleoceanography of the Caribbean and East Pacific: Role of Panama uplift in Late Neogene time, *Science*, *217*, 350–352, 1982.

Keller, G., and J. A. Barron, Paleoceanographic implications of the Miocene deep-sea hiatuses, *Geol. Soc. Am. Bull.*, *94*, 590–613, 1983.

King, T. A., W. G. Ellis Jr., D. W. Murray, N. J. Shackleton, and S. Harris, Miocene evolution of carbonate sedimentation at the Ceara rise: A multivariate data/proxy approach, in *Proc. Ocean Drill. Program Sci. Results*, edited by N. J. Shackleton et al., pp. 349–365, Ocean Drill. Program, College Station, Tex., 1997.

Levitus, S., and T. P. Boyer, *World Ocean Atlas 1994 Volume 4: Temperature*, 117 pp., U.S. Dept. of Commer., Washington, D. C., 1994.

Levitus, S., R. Burgett, and T. P. Boyer, *World Ocean Atlas 1994 Volume 3: Salinity*, 99 pp., U.S. Dept. of Commer., Washington, D. C., 1994.

Lyle, M., K. A. Dadey, and J. W. Farrell, The Late Miocene (11–8 Ma) eastern Pacific carbonate crash: Evidence for reorganization of deep-water circulation by the closure of the Panama gateway, in *Proc. Ocean Drill. Program Sci. Results*, edited by N. G. Pisias et al., pp. 821–838, Ocean Drill. Program, College Station, Tex., 1995.

Maier-Reimer, E., U. Mikolajewicz, and T. Crowley, Ocean general circulation model sensitivity experiment with an open Central American isthmus, *Paleoceanography*, *5*, 349–366, 1990.

Maier-Reimer, E., U. Mikolajewicz, and K. Hasselmann, Mean circulation of the Hamburg LSG OGCM and its sensitivity to the thermohaline surface forcing, *J. Phys. Oceanogr.*, *23*, 731–757, 1993.

Manabe, S., and R. J. Stouffer, Two stable equilibria of a coupled ocean–atmosphere model, *J. Clim.*, *1*, 841–866, 1988.

Mann, P., Caribbean sedimentary basins: Classification and tectonic setting from Jurassic to present, in *Caribbean Basins*, edited by P. Mann, pp. 3–31, Elsevier Sci., New York, 1999.

Marotzke, J., and J. Willebrand, Multiple equilibria of the global thermohaline circulation, *J. Phys. Oceanogr.*, *21*, 1372–1385, 1991.

Marshall, J., and F. Schott, Open-ocean convection: Observations, theory, and models, *Rev. Geophys.*, *37*(1), 1–64, 1999.

Marshall, J., A. Adcroft, C. Hill, L. Perelman, and C. Heisey, A finite-volume, incompressible Navier Stokes model for studies of the ocean on parallel computers, *J. Geophys. Res.*, *102*(C3), 5753–5766, 1997a.

Marshall, J., C. Hill, L. Perelman, and A. Adcroft, Hydrostatic, quasi-hydrostatic, and nonhydrostatic ocean modeling, *J. Geophys. Res.*, *102*(C3), 5733–5752, 1997b.

Marshall, L. G., S. D. Webb, J. J. Sepkoski, and D. M. Raup, Mammalian evolution and the great American interchange, *Science*, *215*, 1351–1357, 1982.

Maslin, M. A., G. H. Haug, M. Sarntheim, and R. Tiedemann, The progressive intensification of Northern Hemisphere glaciation as seen from the North Pacific, *Geol. Rundsch.*, *85*, 452–465, 1996.

Mikolajewicz, U., and T. J. Crowley, Response of a coupled ocean/energy balance model to restricted flow through the central American isthmus, *Paleoceanography*, *12*, 429–441, 1997.

Mikolajewicz, U., and E. Maier-Reimer, Mixed boundary-conditions in ocean general-circulation models and their influence on the stability of the models conveyor belt, *J. Geophys. Res.*, *99*(C11), 22,633–22,644, 1994.

Mikolajewicz, U., E. Maier-Reimer, T. J. Crowley, and K. Y. Kim, Effect of Drake and Panamanian Gateways on the circulation of an ocean model, *Paleoceanography*, *8*, 409–426, 1993.

Miller, K. G., and R. G. Fairbanks, Oligocene to Miocene carbon isotope cycles and abyssal circulation changes, in *The Carbon Cycle and Atmospheric CO2: Natural Variations Archean to Present*, edited by E. T. Sundquist and W. S. Broecker, pp. 469–486, AGU, Washington, D. C., 1985.

Perry, G. D., P. B. Duffy, and N. L. Miller, An extended data set of river discharges for validation of general circulation models, *J. Geophys. Res.*, *101*(D16), 21,339–21,349, 1996.

Raymo, M. E., The initiation of Northern Hemisphere glaciation, *Annu. Rev. Earth Planet. Sci.*, *22*, 353–383, 1994.

Redi, M. H., Oceanic isopycnal mixing by coordinate rotation, *J. Phys. Oceanogr.*, *12*, 1154–1158, 1982.

Reeh, N., Calving from Greenland glaciers: Observations, balance estimates of calving rate, calving laws, in *Workshop on the Calving Rate of West Greenland Glaciers in Response to Climate Change*, p. 171, Dan. Polar Cent., Copenhagen, 1994.

Schmitt, R. W., P. S. Bogden, and C. E. Dorman, Evaporation minus precipitation and density fluxes for the North Atlantic, *J. Phys. Oceanogr.*, *19*, 1208–1221, 1989.

Shackleton, N. J., et al., Oxygen isotope calibration of the onset of ice-rafting and history of glaciation in the North Atlantic region, *Nature*, *307*, 620–623, 1984.

Spielhagen, R. F., et al., Arctic ocean evidence for late Quaternary initiation of northern Eurasian ice sheets, *Geology*, *25*(9), 783–786, 1997.

Stanley, S. M., New horizons for paleontology with two examples: The rise and fall of the Cretaceous supertethys and the cause of the modern ice age, *J. Paleontol.*, *69*(6), 999–1007, 1995.

Stommel, H., and A. B. Arons, On the abyssal circulation of the world ocean, 1, Stationary planetary flow patterns on a sphere, *Deep Sea Res.*, *6*, 140–154, 1960a.

Stommel, H., and A. B. Arons, On the abyssal circulation of the world ocean, 2, An idealized model of the circulation pattern and amplitude in oceanic basins, *Deep Sea Res.*, *6*, 217–233, 1960b.

Tiedemann, R., and S. O. Franz, Deep-water circulation, chemistry, and terrigenous sediment supply in the equatorial Atlantic during the Pliocene, 3.3–2.6 Ma and 5–4.5 Ma, in *Proc. Ocean Drill. Program Sci. Results*, edited by N. J. Shackleton et al., pp. 299–318, Ocean Drill. Program, College Station, Tex., 1997.

Trenberth, K. E., and A. Solomon, The global heat-balance: Heat transports in the atmosphere and ocean, *Clim. Dyn.*, *10*(3), 107–134, 1994.

Trenberth, K. E., J. G. Olson, and W. G. Large, A global ocean wind stress climatology based on ECMWF analysis, *NCAR Tech. Note*, NCAR/TN-338+STR, Natl. Cent. for Atmos. Res., Boulder, Colo., 1989.

Tziperman, E., J. R. Toggweiler, Y. Feliks, and K. Bryan, Instability of the thermohaline circulation with respect to mixed boundary-conditions: Is it really a problem for realistic models, *J. Phys. Oceanogr.*, *24*, 217–232, 1994.

Woodruff, F., and S. Savin, Miocene deep-water oceanography, *Paleoceanography*, *4*, 87–140, 1989.

Wright, J. D., K. G. Miller, and R. G. Fairbanks, Early and middle Miocene stable isotopes: Implications for deepwater circulation and climate, *Paleoceanography*, *7*, 357–389, 1992.

---

K. H. Nisancioglu and P. H. Stone, Program in Atmosphere, Oceans, and Climate, Department of Earth, Atmospheric, and Planetary Sciences, Massachusetts Institute of Technology, Cambridge, MA 02141, USA. (kerim@mit.edu; phstone@mit.edu)

M. E. Raymo, Department of Earth Sciences, Boston University, 685 Commonwealth Avenue, Boston, MA 02215, USA. (raymo@bu.edu)

# Bibliography

Andrews, J. T., The Wisconsin Laurentide ice sheet: Dispersal centers, problems og rates of retreat, and climatic implications, *Arctic Alpine Research*, *5*, 185–199, 1973.

Barrett, P., C. Adams, W. McInstosh, C. Swisher, and G. Wilson, Geochronological evidence supporting Antarctic deglaciation 3 million years ago, *Nature*, *359*(6398), 816 – 818, 1992.

Berger, A., Long-term variation of the daily and monthly insolation during the Last Ice Age., *Transactions of the American Geophysical Union*, *57*, 254, 1976.

Berger, A., Long-term variations of daily insolation and quaternary climatic changes, *Journal of the Atmospheric Sciences*, *35*(12), 2362 – 2367, 1978a.

Berger, A., Long-term variations of caloric insolation resulting from earths orbital elements, *Quaternary Research*, *9*(2), 139 – 167, 1978b.

Berger, A., and M. Loutre, *Long-term climatic variations: data and modelling*, *NATO ASI series. Series I, Global environmental change*, vol. 22, chap. Precession, eccentricity, obliquity, insolation and paleocilmates, Springer-Verlag, Berlin, New York, proceedings of the NATO Advanced Study Institute on Long-Term Climatic Variations–Data and Modelling, Siena, Italy, September 27-October 11, 1992, 1994.

Berger, A., M. Loutre, and C. Tricot, Insolation and earths orbital periods, *Journal of Geophysical Research - Atmospheres*, *98*(D6), 10,341 – 10,362, 1993.

Berger, A., X. S. Li, and M. F. Loutre, Modelling northern hemisphere ice volume over the last 3 Ma, *Quaternary Science Reviews*, *18*(1), 1–11, 1999.

Berger, W. H., and G. Wefer, *Expedition into the Past: Paleoceanographic Studies in the South Atlantic*, pp. 363–410, Springer-Verlag, Berlin Heidelberg, 1996.

Berggren, W. A., F. J. Hilgen, C. G. Langereis, D. V. Kent, J. D. Obradovich, I. Raffi, M. E. Raymo, and N. J. Shackleton, Late Neogene Chronology - New Perspectives in High-Resolution Stratigraphy, *Geological Society of America Bulletin*, *107*(11), 1272–1287, 1995.

Birchfield, G., J. Weertman, and A. Lunde, A paleoclimate model of northern hemispheric ice sheets, *Quaternary Research*, *15*(126-142), 1981.

Birchfield, G., J. Weertman, and A. Lunde, A model study of the role of high-latitude topography in the climatic response to orbital insolation anomalies, *Journal of the Atmospheric Sciences*, *39*(1), 71 – 87, 1982.

Braithwaite, R., and Y. Zhang, Sensitivity of mass balance of five Swiss glaciers to temperature changes assessed by tuning a degree-day model, *Journal og Glaciology*, *46*(152), 7 – 14, 2000.

Braithwaite, R. J., Positive degree-day factors for ablation on the Greenland ice sheet studied by energy-balance modelling, *Journal of Glaciology*, *41*(137), 153–160, 1995.

Braithwaite, R. J., and O. B. Olesen, *Calculation of glacier ablation from temperature, West Greenland.*, pp. 219–223, Dordrecht, Kluwer Academic Publishers, 1989.

Bromwich, D., and F. Robasky, Recent precipitation trends over the polar ice sheets, *Meteorology and Atmospheric Physics*, *51*(3-4), 259 – 274, 1993.

Brown, C., M. Meier, and A. Post, Calving speed of Alaska tidewater glaciers, with application to Columbia Glacier, *Tech. Rep. 1258-C*, U.s. Geological Survey Professional Paper, 1982.

Budyko, M. I., The effect of solar radiation variations on the climate of the Earth, *Tellus*, *5*, 611–619, 1969.

Cande, S. C., and D. V. Kent, A New Geomagnetic Polarity Time Scale For the Late Cretaceous and Cenozoic, *Journal of Geophysical Research-Solid Earth*, *97*(B10), 13,917–13,951, 1992.

Cande, S. C., and D. V. Kent, Revised Calibration of the Geomagnetic Polarity Timescale For the Late Cretaceous and Cenozoic, *Journal of Geophysical Research-Solid Earth*, *100*(B4), 6093–6095, 1995.

Cane, M., and P. Molnar, Closing of the Indonesian seaway as a precursor to east African aridircation around 3-4 million years ago, *Nature*, *411*(6834), 157 – 162, 2001.

Cess, R., Climate change - appraisal of atmospheric feedback mechanisms emplying zonal climatology, *Journal of the Atmospheric Sciences*, *33*(10), 1831 – 1843, 1976.

Charles, C., D. Rind, J. JouzelL, R. Koster, and R. Fairbanks, Glacial-interglacial changes in moisture sources for Greenland - influences on the ice core record of climate, *Science*, *263*(5146), 508 – 511, 1994.

Charney, J., The dynamics of long waves in a baroclinic westerly current, *Journal of Meteorology*, 1947.

Clapperton, C., and D. Sugden, Late Cenozoic glacial history of the Ross embayment, Antarctica, *Quatenary Science Reviews*, *9*(2-3), 253 – 272, 1990.

Clark, P., and D. Pollard, Origin of the middle Pleistocene transition by ice sheet erosion of regolith, *Paleoceanography*, *13*(1), 1 – 9, 1998.

Clark, P. U., R. B. Alley, and D. Pollard, Climatology - Northern hemisphere ice-sheet influences on global climate change, *Science*, *286*(5442), 1104–1111, 1999.

Clement, B. M., and D. V. Kent, Geomagnetic Polarity Transition Records From 5 Hydraulic Piston Core Sites in the North-Atlantic, *Initial Reports of the Deep Sea Drilling Project*, *94*, 831–852, 1987.

Coakley, J., Study of climate sensitivity using a simple energy-balance model, *Journal of the Atmospheric Sciences*, *36*(2), 260 – 269, 1979.

Cortijo, E., S. Lehman, L. Keigwin, M. Chapman, D. Paillard, and L. Labeyrie, Changes in meridional temperature and salinity gradients in the North Atlantic Ocean (30 degrees-72 degrees N) during the last interglacial period, *Paleoceanography*, *14*(1), 23–33, 1999.

Croll, J., *Climate and Time*, Appleton, 1875.

Crowley, T. J., Pliocene climates: The nature of the problem, *Marine Micropaleontology*, *27*, 3–12, 1996.

Crowley, T. J., and G. R. North, *Paleoclimatology*, *Oxford Monographs on Geology and Geophysics*, vol. 18, 349 pp., Oxford University Press, New York, 1991.

Cubasch, U., and G. Meehl, *Projections of Future Climate Change*, chap. 9, p. 881, Cambridge University Press, Cambridge, UK, 2001.

Cuffey, K., and G. Clow, Temperature, accumulation, and ice sheet elevation in central Greenland through the last deglacial transition, *Journal of Geophysical Research-Oceans*, *102*(C12), 26,383 – 26,396, 1997.

Cuffey, K., G. Clow, R. Alley, M. Stuiver, E. Waddington, and R. Saltus, Large Arctic temperature-change at the Wisconsin-Holocene glacial transition, *Science*, *270*(5235), 455 – 458, 1995.

Dansgaard, W., The O18 abundance in fresh water, *Geochimica et Cosmochimica Acta*, *6*, 241–260, 1954.

Dansgaard, W., Stable isotopes in precipitation, *Tellus*, *16*, 436–468, 1964.

Deblonde, G., W. R. Peltier, and W. T. Hyde, Simulations of Continental Ice-Sheet Growth Over the Last Glacial Interglacial Cycle - Experiments With a One Level Seasonal Energy-Balance Model Including Seasonal Ice Albedo Feedback, *Global and Planetary Change*, *98*(1), 37–55, 1992.

Denton, G., M. Prentice, D. Kellogg, and T. Kellogg, Late Tertirary history of the Antarctic ice-sheet - evidence from the dry valleys, *Geology*, *12*(5), 263 – 267, 1984.

Dowsett, J. H, R. S. Thompson, J. A. Barron, T. M. Cronin, S. E. Ishman, R. Z. Poore, D. A. Willard, and J. T. R. Holtz, Joint investigation of the Middle Pliocene climate I: PRISM palaeoenvironmental reconstructions, *Palaeogeography Palaeoclimatology Palaeoecology*, *9*, 1994.

Dowsett, H., J. Barron, and R. Poore, Middle Pliocene sea surface temperatures: A global reconstruction, *Marine Micropaleontology*, *27*(1-4), 13–25, 1996.

Driscoll, N. W., and G. H. Haug, A short circuit in thermohaline circulation: A cause for northern hemisphere glaciation?, *Science*, *282*(5388), 436–438, 1998.

Ellis, J., and T. Vonder Haar, Zonal average earth radiation budget measurements from satellites for climate studies, *Tech. rep.*, Colorado State University, Fort Collins, 1976.

Emiliani, C., Pleistocene temperatures, *Journal of Geology*, *63*(6), 538–578, 1955.

Emiliani, C., The Pleistocene epoch and the evolution of man, *Current Anthropology*, *9*(1), 27–47, 1968.

Gallee, H., J. P. Vanypersele, T. Fichefet, C. Tricot, and A. Berger, Simulation of the Last Glacial Cycle By a Coupled, Sectorially Averaged Climate-Ice Sheet Model .1. the Climate Model, *Journal of Geophysical Research-Atmospheres*, *96*(D7), 13,139–13,161, 1991.

Gallee, H., J. P. Vanypersele, T. Fichefet, I. Marsiat, C. Tricot, and A. Berger, Simulation of the Last Glacial Cycle By a Coupled, Sectorially Averaged Climate-Ice Sheet Model .2. Response to Insolation and Co2 Variations, *Journal of Geophysical Research-Atmospheres*, *97*(D14), 15,713–15,740, 1992.

Gallimore, G. R, and J. E. Kutzbach, Snow cover and sea ice sensitivity to generic changes in Earh orbital parameters, *Journal of Geophysical Research*, *100*(D1), 1103–1120, 1995.

Gallup, C., H. Cheng, F. Taylor, and R. Edwards, Direct determination of the timing of sea level change during termination II, *Science*, *295*(5553), 310 – 313, 2002.

Ghil, M., Cryothermodynamics - the Chaotic Dynamics of Paleoclimate, *Physica D Nonlinear Phenomena*, *77*(1-3), 130–159, 1994.

Ghil, M., M. Allen, M. Dettinger, K. Ide, D. Kondrashov, M. Mann, A. Robertson, A. Saunders, Y. Tian, F. Varadi, and P. Yiou, Advanced spectral methods for climatic time series, *Rviews of Geophysics*, *40*(1), 2002.

Gildor, H., and E. Tziperman, Sea ice as the glacial cycles' climate switch: Role of seasonal and orbital forcing, *Paleoceanography*, *15*(6), 605–615, 2000.

Gildor, H., and E. Tziperman, A sea ice climate switch mechanism for the 100-kyr glacial cycles, *Journal of Geophysical Research-Oceans*, *106*(C5), 9117–9133, 2001.

Green, J. S. A., Transfer properties of the large-scale eddies and the general circulation of the atmosphere, *Quarterly Journal of the Royal Meteorological Society1*, *96*(408), 157–185, 1970.

Haney, R., Surface thermal boundary condition of ocean circulation model, *Journal of Physical Oceanography*, *1*, 145–167, 1971.

Hasselmann, K., *Construction and verification of stochastic climate models*, pp. 481–497, D. Reidel Publishing Company, 1981.

Haug, G. H., and R. Tiedemann, Effect of the formation of the Isthmus of Panama on Atlantic Ocean thermohaline circulation, *Nature*, *393*(6686), 673–676, 1998.

Hays, J. D., J. Imbrie, and N. J. Shackleton, Variations in the Earth's orbit: Pacemakers of the ice ages, *Science*, *194*(4270), 1121–1132, 1976.

Held, I., and M. Suarez, Simple albedo feedback models of ice-caps, *Tellus*, *26*(6), 613 – 629, 1974.

Held, I. M., The vertical scale of an unstable baroclinic wave and its importance for eddy heat flux parameterizations, *Journal of the Atmospheric Sciences*, *35*, 572–576, 1978.

Henderson, G., and N. Slowey, Evidence from U-Th dating against Northern Hemisphere forcing of the penultimate deglaciation, *Nature*, *404*(6773), 61 – 66, 2000.

Herbert, T. D., J. D. Schuffert, D. Andreasen, L. Heusser, M. Lyle, A. Mix, A. C. Ravelo, L. D. Stott, and J. C. Herguera, Collapse of the California Current during glacial maxima linked to climate change on land, *Science*, *293*(5527), 71–76, 2001.

Hughes, T., *North America and Adjacent Oceans During the Last Deglaciation, The Geology of North America*, vol. K-3, chap. Ice dynamics and deglaction models when ice sheets collapsed, pp. 183–220, Geological Society of America, Boulder, Colorado, 1987.

Hughes, T., G. Denton, and M. Grosswald, Was there a late-Wurm Arctic ice sheet?, *Nature*, *266*, 596–602, 1977.

Huybers, P., and C. Wunsch, Rectification and precession signals in the climate system, *Geophysical Research Letters*, *30*(19), 2003.

Huybrechts, A 3-D model for the Antarctic ice sheet:: a sensitivity study on the glacial-interglacial contrast, *Climate Dynamics*, *5*, 79–92, 1990.

Huybrechts, P., and J. de Wolde, The dynamic response of the Greenland and Antarctic ice sheets to multiple-century climatic warming, *Journal of Climate*, *12*(8), 2169 – 2188, 1999.

Huybrechts, P., A. Letreguilly, and N. Reeh, The Greenland Ice-Sheet and Greenhouse Warming, *Global and Planetary Change*, *89*(4), 399–412, 1991.

Huybrechts, P., D. Steinhage, F. Wilhelms, and J. Bamber, Balance velocities and measured properties of the Antarctic ice sheet from a new compilation of gridded data for modelling, *Annals of Glaciology*, *30*, 52 – 60, 2000.

Hyde, W., and W. Peltier, Sensitivity experiments with a model of the ice-age cycle - the response to Milankovich forcing, *Journal of the Atmospheric Sciences*, *44*(10), 1351 – 1374, 1987.

Imbrie, J., E. A. Boyle, S. C. Clemens, A. Duffy, W. R. Howard, G. Kukla, J. Kutzbach, D. G. Martinson, A. McIntyre, A. C. Mix, B. Molfino, J. J. Morley, L. C. Peterson, N. G. Pisias, W. L. Prell, M. E. Raymo, N. J. Shackleton, and J. R. Toggweiler, On the Structure and Origin of Major Glaciation Cycles .1. Linear Responses to Milankovitch Forcing, *Paleoceanography*, *7*(6), 701–738, 1992.

Imbrie, J., A. Berger, E. A. Boyle, S. C. Clemens, A. Duffy, W. R. Howard, G. Kukla, J. Kutzbach, D. G. Martinson, A. McIntyre, A. C. Mix, B. Molfino, J. J. Morley, L. C. Peterson, N. G. Pisias, W. L. Prell, M. E. Raymo, N. J. Shackleton, and J. R. Toggweiler, On the Structure and Origin of Major Glaciation Cycles .2. the 100,000-Year Cycle, *Paleoceanography*, *8*(6), 699–735, 1993.

Jansen, E., and J. Sjoholm, Reconstruction of glaciation over the past 6 myr from ice-borne deposits in the Norwegian Sea, *Nature*, *349*(6310), 600 – 603, 1991.

Jansen, E., U. Bleil, R. Henrich, L. Kringstad, and B. Slettemark, Paleoenvironmental changes in the Norwegian Sea and the northeast Atlantic during the last 2.8 m.y.: Deep Sea Drilling Project/Ocean Drilling Program sites 610, 642, 643, and 644, *Paleoceanography*, *3*, 563–581, 1988.

Johnson, R. G., Major Northern Hemisphere deglaciation caused by a moisture deficit 140 ka, *Geology*, *19*(7), 686 – 689, 1991.

Joussaume, S., and P. Braconnot, Sensitivity of paleoclimate simulation results to season definitions, *Journal of Geophysical Research-Atmospheres*, *102*(D2), 1943 – 1956, 1997.

Kageyama, M., F. D'Andrea, G. Ramstein, P. Valdes, and R. Vautard, Weather regimes in past climate atmospheric general circulation model simulations, *Climate Dynamics*, *15*(10), 773 – 793, 1999.

Kallen, E., C. Crafoord, and M. Ghil, Free Oscillations in a Climate Model With Ice-Sheet Dynamics, *Journal of the Atmospheric Sciences*, *36*(12), 2292–2303, 1979.

Kalnay, E., M. Kanamitsu, R. Kistler, W. Collins, D. Deaven, L. Gandin, M. Iredell, S. Saha, G. White, J. Woollen, Y. Zhu, M. Chelliah, W. Ebisuzaki, W. Higgins, J. Janowiak, K. Mo, C. Ropelewski, J. Wang, A. Leetmaa, R. Reynolds, R. Jenne, and D. Joseph, The NCEP/NCAR 40-year reanalysis project, *Bulletin of the American Meteorological Society*, *77*(3), 437 – 471, 1996.

Kaneps, A. G., Gulf Stream: Velocity fluctuations during the late Cenozoic., *Science*, *204*, 297–301, 1979.

Kaspner, W., R. Alley, C. Shuman, S. Anandakrishnan, and P. Grootes, Dominant influence of atmospheric circulation on snow accumulation in Greenland over the past 18,000 years, *Nature*, *373*(6509), 52 – 54, 1995.

Keigwin, L., Isotopic paleoceanography of the Caribbean and East Pacific: role of Panama uplift in Late Neogene time, *Science*, *217*, 350–352, 1982.

Kennett, J., Cenozoic evolution of Antarctic glaciation, cirum-Antarctic ocean, and their impacet on global paleoceanography, *Journal of Geophysical Research - Oceans and Atmospheres*, *82*(27), 3843 – 3860, 1977.

Kennett, J. P., and D. A. Hodell, Evidence for Relative Climatic Stability of Antarctica during the Early Pliocene: A Marine Perspective, *Geografiska Annaler. Series A. Physical Geography*, *75*(4), 205–220, 1993.

Khodri, M., Y. Leclainche, G. Ramstein, P. Braconnot, O. Marti, and E. Cortijo, Simulating the amplification of orbital forcing by ocean feedbacks in the last glaciation, *Nature*, *410*(6828), 570–574, 2001.

Kim, S., T. Crowley, and A. Stossel, Local orbital forcing of Antarctic climate change during the last interglacial, *Sciece*, *280*(5364), 728 – 730, 1998.

Kominz, M., and N. Pisias, Pleistocene climate - deterministic or stochastic, *Science*, *204*(4389), 171 – 173, 1979.

Köppen, W. P., and A. Wegener, *Die klimate der geologischen vorzeit*, Gebrüder Borntraeger, Berlin, 1924.

Krantz, D., A chronology of Pliocene sea-level flucturations - the United-Sates middle Atlantic coastal-plain record, *Quaternary Science Reviews*, *10*(2-3), 163 – 174, 1991.

Kukla, J., The Pleistocene epoch and the evolution of man - a reply, *Current Anthropology*, *9*, 27–47, 1968.

Kutzbach, J., R. Bryson, and W. Shen, An evaluation of the thermal Rossby number in the Pleistocene, *Meteorological Monographs*, *8*(3), 134–138, 1968.

Laskar, J., F. Joutel, and F. Boudin, Orbital, precessional, and insolation quantities for the earth from -20 myr to +10 myr, *Astronomy and Astrophysics*, *270*(1-2), 522 – 533, 1993.

Lee, W., and G. North, Small ice cap instability in the presence of fluctuations, *Climate Dynamics*, *11*(4), 242 – 246, 1995.

Leovy, C., Exchange of water vapor between atmosphere and surface of Mars, *Icarus*, *18*(1), 120 – 125, 1973.

Letreut, H., and M. Ghil, Orbital forcing, climatic interactions, and glaciation cycles, *Journal of Geophysical Research - Oceans and Atmospheres*, *88*(NC9), 5167 – 5190, 1983.

Li, Z., and H. Leighton, Global climatologies of solar-radiation budgets at the surface and in the atmosphere from 5 years of ERBE data, *Journal of Geophysical Research - Atmospheres*, *98*(D3), 4919 – 4930, 1993.

Lian, M., and R. Cess, Energy-balance climate models - reappraisal of ice-albedo feedback, *Journal of the Atmospheric Sciences*, *34*(7), 1058 – 1062, 1977.

Lin, C., Eddy heat fluxes and stability of planetary-waves .1., *Journal of the Atmospheric Sciences*, *37*(11), 2353 – 2372, 1980a.

Lin, C., Eddy heat fluxes and stability of planetary-waves .2., *Journal of the Atmospheric Sciences*, *37*(11), 2373 – 2380, 1980b.

Lorenz, E., Forced and free variations of weather and climate, *Journal of the Atmospheric Sciences*, *36*(8), 1367 – 1376, 1979.

Maier-Reimer, E., U. Mikolajewicz, and T. Crowley, Ocean general circulation model sensivity experiment with an open central american isthmus, *Paleoceanography*, *5*(3), 349–366, 1990.

Milankovitch, M., Kalorische Jahreszeiten und deren Anwendung im palaoklimalen Problem, *Bericht der konigl. serbischen Akademie, CIX*, 1923.

Milankovitch, M., *Handbuch der klimatologie (editors Koppen, W. , Geiger, R.)*, Gebruder Borntraeger, Berlin, 1936.

Milankovitch, M., Canon of insolation and the ice-age problem. K. Serb. Akad. Geogr., *Spececial Publication*, (132), 484, translated by Israel Program for Scientific Translations, Jerusalem, 1969, US. Depte of Commerce, 1941.

Miller, K. G., and R. G. Fairbanks., *Oligocene to Miocene carbon isotope cycles and abyssal circulation changes*, pp. 469–486, Geophysical Monograph Series, Washington D.C., 1985.

Myhre, G., E. Highwood, K. Shine, and F. Stordal, New estimates of radiative forcing due to well mixed greenhouse gases, *Geophysical Research Letters*, *25*(14), 2715 – 2718, 1998.

Nakamura, M., P. H. Stone, and J. Marotzke, Destabilization of the Thermohaline Circulation By Atmospheric Eddy Transports, *Journal of Climate*, *7*(12), 1870–1882, 1994.

Nisancioglu, K., M. Raymo, and P. Stone, Reorganization of Miocene deep water circulation in response to the shoaling of the Central American Seaway, *Paleoceanography*, *18*(1), art. no. – 1006, 2003.

North, G., The small ice cap instability in diffusive climate models, *Journal of the Atmospheric Sciences*, *41*(23), 3390 – 3395, 1984.

North, G., and J. Coakley, Differences between seasonal and mean annual energy-balance model calculations of climate and climate sensitivity, *Journal of the Atmospheric Sciences*, *36*(7), 1189 – 1204, 1979.

North, G., and T. Crowley, Application of a seasonal climate model to Cenozoic glaciation, *Journal of the Geological Society*, *142*, 475 – 482, 1985.

North, G., R. Cahalan, and J. Coakley, Energy-blance climate models, *Reviews of Geophysics*, *19*(1), 91 – 121, 1981.

North, G. R., Theory of energy-balance climate models, *Journal of the atmospheric sciences*, *32*(11), 2033–2041, 1975.

North, G. R., J. G. Mengel, and D. A. Short, Simple Energy-Balance Model Resolving the Seasons and the Continents - Application to the Astronomical Theory of the Ice Ages, *Journal of Geophysical Research-Oceans and Atmospheres*, *88*(C11), 6576–6586, 1983.

Nye, J. F., The flow of glaciers and ice-sheets as a problem in plasticity, *Proceedings of the Royal Society of London, Series A: Mathematical and Physical Sciences*, *207*(1091), 554–572, 1951.

Oerlemans, J., Model experiments of the 100,000-yr glacial cycle, *Nature*, *287*(5781), 430 – 432, 1980.

Ohmura, A., Physical basis for the temperature-based melt-index method, *Journal of Applied Meteorology*, *40*(4), 753 – 761, 2001.

Ohmura, A., M. Wild, and L. Bengtsson, A possible change in mass balance of Greenland and Antarctic ice sheets in the coming century, *Journal of Climate*, *9*(9), 2124 – 2135, 1996.

Oort, A., NOAA Professional Paper No. 14, *Tech. rep.*, U.S. Department of Commerce, Rockville, Md., 1983.

Orlanski, I., The influence of bottom topography on the stability of jets in a baroclinic fluid, *Journal of Atmospheric Sciences*, *26*, 1216–1232, 1969.

Orowan, E., and M. F. Perutz, The flow of ice and other solids, *Journal of Glaciology*, *1*(5), 231–240, 1949.

Owen, T., R. Cess, and V. Ramanathan, Enhanced CO2 greenhouse to compensate for reduced solar luminosity on early earth, *Nature*, *277*(5698), 640 – 642, 1979.

Paillard, D., Glacial cycles: Toward a new paradigm, *Reviews of Geophysics*, *39*(3), 325–346, 2001.

Patterson, W. S. B., *The physics of glaciers*, Pergamon, Oxford, UK, 1994.

Pedlosky, J., The stability of currents in the atmosphere and the ocean: Part I, *Journal of the Atmospheric Sciences*, *21*, 201–219, 1964a.

Pedlosky, J., The stability of currents in the atmosphere and the ocean: Part II, *Journal of the Atmospheric Sciences*, *21*, 342–353, 1964b.

Pedlosky, J., Secondary baroclinic instability and meridional scale of motion in ocean, *Journal of Physical Oceanography*, *5*(4), 603 – 607, 1975.

Peixoto, J. P., and A. H. Oort, *Physics of Climate*, American Institute of Physics, New York, 1992.

Peltier, W., Ice-age paleotopography, *Science*, *265*(5169), 195 – 201, 1994.

Percival, D., and A. Walden, *Spectral analysis for physical applications - Multitaper and conventional univariate techniques*, Cambridge University Press, 1993.

Philander, S., and A. Fedorov, Role of tropics in changing the response to Milankovich forcing some three million years ago, *Paleoceanography*, *18*(2), 2003.

Pisias, N. G., and J. Moore, T. C., The evolution of Pleistocene climate; a time series approach, *Earth and Planetary Science Letters*, *52*(2), 450–458, 1981.

Pollard, D., Investigation of astronomical theory of ice ages using a simple climate ice sheet model, *Nature*, *272*(5650), 233 – 235, 1978.

Pollard, D., A simple parameterization for ice-sheet ablation rate, *Tellus*, *32*(4), 384 – 388, 1980.

Pollard, D., A simple ice-sheet model yields realistic 100 kyr glacial cycles, *Nature*, *296*(5855), 334 – 338, 1982.

Pollard, D., A. Ingersoll, and J. Lockwood, Response of a zonal climate ice-sheet model to the orbital perturbations during the Quaternary ice ages, *Tellus*, *32*(4), 301 – 319, 1980.

Raymo, M., and K. Nisancioglu, The 41 kyr world: Milankovitch's other unsolved mystery, *Paleoceanography*, *18*(1), art. no. – 1011, 2003.

Raymo, M. E., The Initiation of Northern-Hemisphere Glaciation, *Annual Review of Earth and Planetary Sciences*, *22*, 353–383, 1994.

Raymo, M. E., W. F. Ruddiman, J. Backman, B. M. Clement, and D. G. Martinson, Late Pliocene variation in northern hemisphere ice sheets and North Atlantic deepwater circulation, *Paleoceanography*, *4*, 413–446, 1989.

Reeh, N., A plasticity theory approach to the steady-state shape of a 3-dimensional ice sheet, *Journal of Glaciology*, *28*(100), 431 – 455, 1982.

Reeh, N., Paramterization of melt rate and surface temperature on the Greenland ice sheet, *Polarforschung*, *59*(3), 113–128, 1989.

Rivin, I., and E. Tziperman, Linear versus self-sustained interdecadal thermohaline variability in a coupled box model, *Journal of Physical Oceanography*, *27*(7), 1216–1232, 1997.

Roe, G., and R. Lindzen, The mutual interaction between continental-scale ice sheets and atmospheric stationary waves, *Journal of Climate*, *14*(7), 1450 – 1465, 2001a.

Roe, G., and R. Lindzen, A one-dimensional model for the interaction between continental-scale ice sheets and atmospheric stationary waves, *Climate Dynamics*, *17*(5-6), 479 – 487, 2001b.

Ruddiman, W. F., and A. McIntyre, Oceanic Mechanisms For Amplification of the 23,000-Year Ice- Volume Cycle, *Science*, *212*(4495), 617–627, 1981.

Ruddiman, W. F., M. Raymo, and A. McIntyre, Matuyama 41,000-Year Cycles - North-Atlantic Ocean and Northern-Hemisphere Ice Sheets, *Earth and Planetary Science Letters*, *80*(1-2), 117–129, 1986.

Ruddiman, W. F., M. E. Raymo, D. G. Martinson, B. M. Clement, and J. Backman, Pleistocene evolution; Northern Hemisphere ice sheets and North Atlantic Ocean, *Paleoceanography*, *4*(4), 353–412, 1989.

Saltzman, B., and A. Sutera, A model of the internal feedback system involved in late Quaternary Climatic variations, *Journal of the Atmospheric Sciences*, *41*, 736–745, 1984.

Saltzman, B., A. R. Hansen, and K. A. Maasch, The Late Quaternary Glaciations As the Response of a 3- Component Feedback-System to Earth-Orbital Forcing, *Journal of the Atmospheric Sciences*, *41*(23), 3380–3389, 1984.

Sarnthein, M., U. Pflaumann, and M. Weinelt, Past extent of sea ice in the northern North Atlantic inferred from foraminiferal paleotemperature estimates, *Paleoceanography*, *18*(2), 2003.

Schneider, S., and S. Thompson, Ice ages and orbital variations - some simple theory and modeling, *Quaternary Research*, *12*(2), 188 – 203, 1979.

Scott, J., Simple parameterization of meridional sensible and latent heat eddy fluxes due to seasonal forcing, 1995.

Sellers, W. D., A global climatic model based on the energy balance of the earth-atmosphere system, *Journal of Applied Meteorology*, *8*, 392–400, 1969.

Shackleton, N., A. Berger, and W. Peltier, An alternative astronomical calibration of the lower pleistocene timescale based on ODP site 677, *Transactions of the Royal Society of Edinburgh - Earth Sciences*, *81*, 251 – 261, 1990.

Shackleton, N. J., and N. D. Opdyke, Oxygen Isotope and Palaeomagnetic Stratigraphy of Equatorial Pacific Core V28-238: Oxygen Isotope Temperatures and Ice Volumes on a 100,000 and 1,000,000 Year Scale (CLIMAP Program), *Quaternary Research (New York)*, *3*(1), 39–55, 1973.

Shackleton, N. J., M. A. Hall, and A. Boersma, Oxygen and Carbon Isotope Data From Leg-74 Foraminifers, *Initial Reports of the Deep Sea Drilling Project*, *74*, 599–612, 1984.

Short, D., J. Mengel, T. Crowley, W. Hyde, and G. North, Filtering of Milankovitch cycles by earths geography, *Quaternary Research*, *35*(2), 157 – 173, 1991.

Solomon, A., and P. Stone, Equilibration in an eddy resolving model with simplified physics, *Journal of the Atmospheric Sciences*, *58*(6), 561 – 574, 2001.

Stanley, S. M., New horizons for paleontology with two examples: The rise and fall of the Cretaceous supertethys and the cause of the modern ice age., *Journal of Paleontology*, *69*(6), 999–1007, 1995.

Stone, P., S. Ghan, D. Spiegel, and S. Rambaldi, Short-term fluctuations in the eddy heat-flux and baroclinic stability of the atmosphere, *Journal of the Atmospheric Sciences*, *39*(8), 1734 – 1746, 1982.

Stone, P. H., A simplified radiative-dynamical model for the static stability of rotating atmospheres, *Journal of the Atmospheric Sciences*, *29*(3), 405–418, 1972.

Stone, P. H., Constraints on dynamical transports of energy on a spherical planet, *Dynamics of Atmospheres and Oceans*, *2*, 123–139, 1978.

Stone, P. H., and D. A. Miller, Empirical relations between seasonal changes in meridional

temeprature gradients and meridional fluxes of heat, *Journal of the atmospheric sciences*, *37*, 1708–1721, 1980.

Stone, P. H., and M.-S. Yao, Development of a two-dimensional zonally averaged statistical-dynamical model. Part III: The parameterization of the eddy fluxes of heat and moisture., *Journal of Climate*, *3*, 726–740, 1990.

Suarez, M., and I. Held, Sensitivity of an energy-balance climate model to variations in the orbital parameters, *Journal of Geophysical Research-Oceans and atmospheres*, *84*(NC8), 4825 – 4836, 1979.

Tarasov, L., and W. R. Peltier, Terminating the 100 kyr ice age cycle, *Journal of Geophysical Research-Atmospheres*, *102*(D18), 21,665–21,693, 1997.

Thomson, D., Spectrum estimation and harmonic-analysis, *Proceedings of the IEEE*, *70*(9), 1055 – 1096, 1982.

Trenberth, K. E., and J. M. Caron, Estimates of meridional atmosphere and ocean heat transports, *Journal of Climate*, *14*(16), 3433–3443, 2001.

Trenberth, K. E., and D. P. Stepaniak, Co-variability of components of poleward atmospheric energy transports on seasonal and interannual timescales., 2003.

Urey, H. C., The thermodynamic propoerties of isotopic substances, *J. Chemical Society*, *1947*, 562–581, 1947.

Van der Veen, C., Tidewater calving, *Journal of Glaciology*, *42*(141), 375 – 385, 1996.

Van der Veen, C., Calving glaciers, *Progress in Physical Geography*, *26*(1), 96 – 122, 2002.

van der Veen, C., D. Bromwich, B. Csatho, and C. Kim, Trend surface analysis of Greenland accumulation, *Journal of Geophysical Research-Atmospheres*, *106*(D24), 33,909 – 33,918, 2001.

Vernekar, A. D., Long-period global variations of incoming solar radiation, *Meteorological Monographs*, *12*(34), 1, 1972.

Wang, W., and P. H. Stone, Effect of ice-albedo feedback on global sensitivity in a one-dimensional radiative-convective climate model, *Journal of the atmospheric sciences*, *37*, 545–552, 1980.

Wardlaw, B., and T. Quinn, The record of Pliocene sea-level change at Enewetak atoll, *Quaternary Science Reviews*, *10*(2-3), 247 – 258, 1991.

Webb, P., and D. Harwood, Late Cenozoic glacial history of the Ross embayment, Antarctica, *Quaternary Science Reviews*, *10*(2-3), 215 – 223, 1991.

Weertman, J., Rate of growth or shrinkage of nonequilibrium ice sheets, *Journal of Glaciology*, *5*(38), 145–158, 1964.

Weertman, J., Milankovitch solar radiation variations and ice age ice sheet sizes, *Nature*, *261*(5555), 17 – 20, 1976.

Werner, M., M. Heimann, and G. Hoffmann, Isotopic composition and origin of polar precipitation in present and glacial climate simulations, *Tellus Series B-Chemical and Physical Meteorology*, *53*(1), 53–71, 2001.

Wetherald, R., and S. Manabe, Effects of changing solar constant on climate of a general circulation model, *Journal of the Atmospheric Sciences*, *32*(11), 2044 – 2059, 1975.

Winograd, I. J., T. B. Coplen, J. M. Landwehr, A. C. Riggs, K. R. Ludwig, B. J. Szabo, P. T. Kolesar, and K. M. Revesz, Continuous 500,000-year climate record from vein calcite in Devils Hole, Nevada, *Science*, *258*(5080), 255 – 260, 1992.

Young, M. A., and R. S. Bradley, *Insolation gradients and the paleoclimate record*, pp. 707–713, D. Reidel Publishing Company, 1984.